The Dissertation Committee for Ying Lu Certifies that this is the approved version of the following dissertation:

Monte Carlo Studies of Polymer Chain Solubility in Water

Committee:

Isaac C. Sanchez, Supervisor

Benny D. Freeman

Peter F. Green

Keith P. Johnston

Peter J. Rossky

Monte Carlo Studies of Polymer Chain Solubility in Water

by

Ying Lu, B.S.; M.S.

Dissertation

Presented to the Faculty of the Graduate School of

The University of Texas at Austin

in Partial Fulfillment

of the Requirements

for the Degree of

Doctor of Philosophy

The University of Texas at Austin

December 2005

Dedication

For Mom, Dad, Yun and Timothy

Acknowledgements

First of all, I would like to thank Professor Isaac Sanchez for his guidance, financial support and patience. Both computer simulation and polymer solutions were new research areas to me when I joined his group, but his teaching, advices, inspiration and encouragement has helped me through. Without him this dissertation would not be possible.

I also thank my group members Matt Stone, Peter J. int' Veld, Xiaoyan Wang, Kenneth Lee, Frank Willmore and Xiaochu Wang, for insightful discussions and sharing ideas. Their brilliancy and team work spirit always made me proud of my group. Ms. Lydia Griffith, my graduate coordinator, is truly a friend to graduate students. I would like to thank her for her help.

My mother and father always encourage me to work hard and pursue my dream. The love and support from my parents, my husband and my son has always been the source of my strength.

Monte Carlo Studies of Polymer Chain Solubility in Water

Publication No._____

Ying Lu, Ph.D.

The University of Texas at Austin, 2005

Supervisor: Isaac C. Sanchez

Poly (Ethylene Oxide) (PEO, with a general formula $(CH_2\text{-}CH_2\text{-}O)_n$) is completely soluble in water at room temperature over an extremely wide molecular weight range and has been widely studied by experiment and theory. The objective of our work is to study the solubility behavior by the method of Monte Carlo simulation. The insertion factor lnB, which is equivalent to the infinite dilute Henry's Law Constant, is used to represent the solubility of various molecules in water.

Our research started with simple fluid and aqueous solutions of small molecules including hard spheres, inert gases, hydrocarbons and dimethyl ether (DME, as a precursor for PEO). Solubility consists of a favorable energy term and an unfavorable entropy term. Against the common belief of entropy-dominating-hydrophobicity effect, it is actually the ability of the solute to interact with solvent (or the energetic factor) that dominates solubility. The solubility minimum appearing for both hydrophobic and hydrophilic solutes along the water coexistence curve is the result of competition between the favorable energy contribution and the unfavorable entropy contribution.

Normal alkanes with carbon number from 1 to 20 have been modeled by LJ chains to study the solubility of non-polar polymer chains in water. Various constraints have been put on the LJ model to evaluate their effect on solubility. No significant difference was observed for LJ chain with or without fixed bond angles, but torsional interaction changed the chain solubility dramatically. The temperature and chain-length effect on chain solubility has been examined and it can be explained by the balancing between the intra-chain interaction and entropy penalty. By choosing the right torsional interaction parameters we may be able to reproduce by simulations the solubility minimum of normal alkanes at C_{11}.

PEO was modeled by united atom chains with length up to 30. The most probable distance between two nearest ether oxygens in both vacuum and aqueous solutions matches the hydrogen bond length in bulk water. Hydrogen bonding plays an important role in the unique water solubility behavior of PEO since the water-PEO interaction effectively increases the total number of hydrogen bonds and results in a favorable change in energy. A trans-gauche-trans conformation along the O-C-C-O bonds does enable hydrogen bond formation between one water molecule and two nearest or next nearest ether oxygens. A helix structure is not required for the PEO to have favorable interactions with water. Two polymers with similar structure as PEO but are insoluble in water: Poly (methylene oxide) (PMO) and Poly (propylene oxide) (PPO) have been studied to compare with PEO. Their difference in structure from PEO, though slight, reduces the chance of hydrogen bond forming between water and chains so as to decrease the solubility.

Table of Contents

List of Tables

List of Figures

Chapter 1 Introduction

Polyethylene oxide (PEO) is one of the most important hydrophilic polymers. Despite its simple chemical structure $(CH_2\text{-}CH_2\text{-}O)_n$, PEO has some extraordinary solubility behavior. At room temperature, PEO is completely miscible with water over a wide molecular weight range. However as shown in Table 1.1, other closely related polymers such as polymethylene oxide (PMO), polypropylene oxide (PPO) and polyacetaldehyde are insoluble in water under ordinary conditions.[1] PEO is also soluble in many organic solvents such as chloroform, acetic acid, and acetonitrile.

Due to its unique solubility behavior and non-ionic character, PEO has found use in separation, pharmaceutical and cosmetic industries.[2] It can serve as the electrolyte solvent in lithium polymer batteries[3] and also as drag reducer in the flow of fluids in pipes.[4] PEO also has important biological application since it is non-toxic and compatible with human tissue and blood.[5]

The temperature-concentration phase diagram of PEO-water solution is a closed loop, and it has both UCST (Upper Critical Solution Temperature) and LCST (Lower Critical Solution Temperature).[6,7,8,9] This miscibility gap appears at temperatures above the boiling point of water, and shifts to higher temperatures as the molecular weight decreases as shown in Figure 1.1. The immiscibility loop eventually vanishes when the PEO chain has less than 48 units.

Many experimental works have been done to study PEO in crystalline and molten states (the melting temperature of bulk PEO is 323K[10]) as well as in solvents. X-ray analysis has shown PEO adopts a 7-2 helix conformation in the crystalline state.[11] In the molten state a highly disordered conformation is favored.[12,13,14] It has been assumed that some helical structure of PEO in the crystalline state is retained in aqueous solutions.[15,16]

Some experimentalists claimed they have found helical structure in the aqueous solutions of PEO.[17,18] However, others have different opinions: Brown and Stilbs measured (through self-diffusion coefficients) frictional coefficients for short chain PEO

Table 1.1: Solubility of some polyethers in water at 25 ºC.

Polymer	Structure	Solubility in water at 25 °C
Poly(methylene oxide)	$(\text{-CH}_2\text{-O-})_n$	insoluble
Poly(ethylene oxide)	$(\text{-CH}_2\text{-CH}_2\text{-O-})_n$	soluble
Poly(acetaldehyde)	$(-CH_2-O-)_n$ $\vert$ CH_3	insoluble
Poly(propylene oxide)	$(-CH_2-CH_2-O-)_n$ $\vert$ CH_3	insoluble
Poly(trimethylene oxide)	$(\text{-CH}_2\text{- CH}_2\text{- CH}_2\text{-O-})_n$	insoluble
Poly(tetrahydrofuran)	$(\text{-(CH}_2)_4\text{-O-})_n$	insoluble
Poly(vinyl methyl ether)	$(-CH_2-CH-)_n$ $\vert$ $O-CH_3$	soluble
Poly(vinyl ethyl ether)	$(-CH_2-CH-)_n$ $\vert$ $O-CH_2-CH_3$	insoluble
Poly(vinyl 2-methoxyethyl ether)	$(-CH_2-CH-)_n$ $\vert$ $CH_2-CH_2-O-CH_3$	soluble

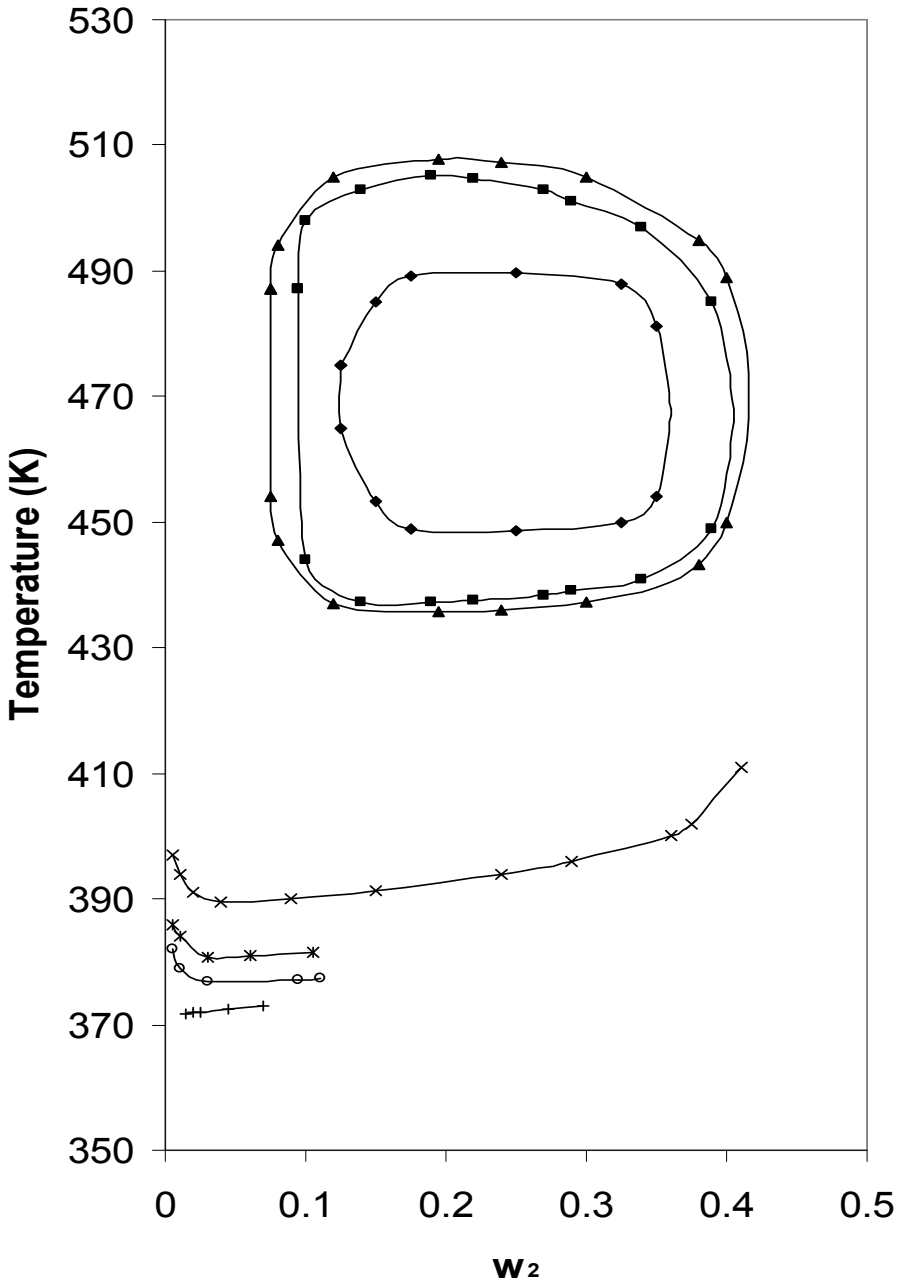

Figure 1.1: Temperature vs. weight fraction phase diagram for PEO samples in water at different viscosity average molecular weights[19]: •, $M_\eta = 2.18\times10^3$; •, $M_\eta = 2.27\times10^3$; •, $M_\eta = 2.29\times10^3$; ×, $M_\eta = 8.00\times10^3$; *, $M_\eta = 14.4\times10^3$; •, $M_\eta = 21.2\times10^3$; +, $M_\eta = 1020\times10^3$.

by spin-echo N.M.R. in chloroform, benzene, and water. Their result showed PEO has a common structure in all three solvents. In other words, water does not present any special feature compared with non-aqueous solvents.[20] Kawaguichi studied aqueous solution properties of PEO by static light scattering and intrinsic viscosity and found that PEO assumes an expanded random coil conformation in water at room temperature.[21] Some other researchers came to a similar conclusion that PEO conformation is relatively insensitive to solvents.[22,23] Koenig and Angood's Raman spectra results suggested that PEO in aqueous solutions have changed from helix conformation to a new, less ordered but not completely disordered structure.[24] Branca et al found that PEO has a more ordered structure in H_2O than in D_2O, and also in aqueous phase than in melted phase.[25,26,27] Liu and Parsons's infrared and NMR results stated that the PEO conformation in aqueous solutions retains to a large degree of trans-gauche-trans structures of its crystalline state.[28]

Many theoretical works have made PEO their subject as well. Mean field theories have been developed to model PEO aqueous solution, and some of them predicted the closed loop in the phase diagram successfully.[29,30,31] Polymer reference interaction site model (PRISM) calculations have also been carried out for PEO liquids.[32]

Computer simulation has gained increased importance in many research areas during the past decades. A large amount of MD simulation results have been reported on PEO[33] and its aqueous solutions[16,34,35,36]. Various force fields have been developed for PEO.[37,38,39,40,41]

In the aqueous solution of PEO, the oxygen-oxygen distance in the PEO chain has been measured to be 2.85 • which matches the hydrogen bond length in bulk water. It has been thought that PEO's being soluble is mainly due to its ability of fitting itself into an unperturbed water structure.[42,43] However experimental results do not support this theory[44]

for neutron scattering showed no evidence of structured water at the water-PEO interface, neither does the hydration model of PEO in an unperturbed water lattice fit the distribution data from experiments.

Simulations on 1,2-dimethyloxyethane in water also proved that the molecule does not fit into water network, and the PEO solubility in water most likely has an energetic origin.[45] It have been noticed that PEO prefers a gauche conformation around the C-C bond,[46,47,48] because of the large favorable dipole moment between the chain and water.[49] The solubility of PEO in water has also been attributed to hydrogen bonding between water molecules and oxygen atoms on PEO chain.[50,51]

As stated above, although PEO and its aqueous solution have attracted experimental and theoretical interest, a clear understanding of this problem is still lacking. To find the mechanism of the PEO solubility in water is the ultimate goal of our research project, and we have performed computer simulations and studied the solubility behavior of aqueous solutions of polymer chains as well as small molecules. In the next chapter we described the simulation details including molecular models, solubility measuring techniques, methods that help chain moves and error analysis.

To achieve a better understanding of water and its solutions, we started our work with aqueous solutions of both hydrophobic and hydrophilic small molecules. Non-polar gases (inert gases, hydrocarbons) were modeled by LJ particles and dimethyl ether which is a hydrophilic molecule with the simplest structure that resembles a PEO unit was modeled by a united atom model with LJ sites and partial electrical charges. Energetic and entropic effects on solubility have been assessed. The ability of the solute to interact with water (or the energetic factor) dominates solubility. The solubility minimum along the water coexistence curve is the result of competition between the favorable energy term and the unfavorable entropy term.

Research of chain solubility behavior has been done with alkane chains in water. Normal alkane chains with carbon number up to 20 have been modeled with LJ chains having various chain constraints to test their effects on solubilities. Fixed bond angle on a LJ chain model does not affect the solubility significantly, however the torsional interaction on the chain changes the solubility behavior. The temperature and chain-length effect on chain solubility has been examined and it can be explained by the balancing between the intra-chain interaction and entropy.

Finally PEO and its aqueous solution have been studied by both Monte Carlo and molecular dynamics simulations. The chain conformation in vacuum and in water and the hydrogen bonding effect have been examined. Some work on other polymers with similar structure but being insoluble in water has been conducted to shed some light on the unique solubility behavior of PEO. The distance between two nearest oxygen atoms on PEO chain matches the hydrogen bond distance in bulk water and hydrogen bonding plays an important role in PEO's solubility. Although a trans-gauche-trans conformation along the O-C-C-O bond of PEO chain is favored, a helical structure is not required for its solubility in aqueous solutions.

In the last chapter we summarized our work and suggested future research.

---

[1] F. E. Bailey, Jr., and R. W. Callard, Journal of Applied Polymer Science, 1, 56 (1959).
[2] Water-Soluble Polymers, edited by N. B. Bikales (Plenum, New York, 1973).
[3] J. A. Johnson, M. L. Saboungi, D. L. Price, S. Ansell, T. P. Russell, J. W. Halley and B. Nielsen, J. Chem. Phys. 109, 7005 (1998).
[4] J. L. Lumley, Ann. Rev. Fluid Mech. , 367 (1969).
[5] J. M. Harris, editor. Poly(ethylene glycol) Chemistry: Biotechnical and Biomedical applications. New York, Plenum Press (1992).
[6] H. L. Cox and L. H. Cretcher, J. Am. Chem. Soc. 48, 451 (1926).
[7] G. N. Malcolm and J. S. Rowlinson, Trans. Faraday Soc. 53, 921 (1957).
[8] S. Saeki, N. Kuwahara, M. Nakata, and M. Kaneko, Polymer 17, 685 (1976).
[9] Y. C. Bae, J. J. Shim, D. S. Soane, and J. M. Prausnitz, J. Appl. Polym. Sci. 47, 1193 (1993).
[10] V. Kuppa and E. Manias, J. Chem. Phys. 118, 3421 (2003).
[11] H. Tadokoro, Y. Chatani, T. Yoshihara, S. Tahara and S. Murahashi, Makromol. Chem. 73, 109 (1964).
[12] C Branca, S Magazu, G Maisano, P Migliardo and V Villari, J. Phys.: Condens. Matter, 10, 10141 (1998)
[13] J. L. Koenig and A. C. Angood, J. Polym. Sci. A 8, 1787 (1970).
[14] F. E. Bailey and J. V. Koleske, Poly(Ethylene Oxide), Academic Press, New York (1976).
[15] R. Kjellander and E. Florin, J. Chem. Soc. Faraday Trans. l. 77, 2053, (1981).

[16] Kenzabu Tasaki, J. Am. Chem. Soc. 118, 8459 (1996).
[17] Roksana Begum and Hiroatsu Matsuura, J. Chem. Soc., Faraday Trans., 93, 3839(1997).
[18] F Oesterhelt, M Rief and H E Gaub, New J. Phys. 1, 6 (1999).
[19] Susumu Saeki, Nobuhiro Kuwahara, Mitsuo Nakata, and Motoxo Kaneko, Polymer 17, 685 (1976).
[20] Wyn Brown and Peter Stilbs, Polymer, 23, 1780 (1982).
[21] Seigou Kawaguchi, Genji Imai, Junto Suzuki, Akira Miyahara, Toshiaki Kitano and Kiochi Ito, Polymer 38, 2885 (1997).
[22] Tanner, J.E., Liu, K.J. and Anderson, J.E., Macromolecules 4, 586 (1971).
[23] Molyneaux, P. in 'Water, A Comprehensive Treatise' (Ed. Felix Franks, Plenum Press, New York, 1974).
[24] J. L. Koenig and A. C. Angood, Journal of Polymer Science: Part A-2 8, 1787 (1970).
[25] C Branca, S Magazu, G Maisano, P Migliardo and V Villari, J. Phys.: Condens. Matter, 10, 10141 (1998).
[26] C Branca, A Faraone, G Maisano, S Magazu, P Migliardo, A Triolo, RTriolo and V Villari, J. Phys.: Condens. Matter, 11, 6079 (1999)
[27] C. Branca, A. Faraone, S. Magazu, etc., Physica B, 276-278, 332 (2000)
[28] K. Liu and J. L. Parsons, Macromolecules 2, 529 (1969).
[29] Elena E. Dormidontova, Macromolecules 35, 987 (2002).
[30] Stefan Bekiranov, Robijn Bruinsma and Philip Pincus, Physical Review E 55, 577 (1997).
[31] A. Matsuyama and F. Tanaka, Phys. Rev. Lett. 65, 341 (1990).
[32] John G. Curro and Amalie L. Frischknecht, Polymer 46, 6500 (2005).
[33] Haitao Dong, Jin-Kee Hyun, Curtis Durham, Ralph A. Wheeler, Polymer 42, 7809 (2001).
[34] Beatriz A. Ferreira, Hélio F. Dos Santos, Américo T. Bernardes, Glaura G. Silva, Wagner B. De Almeida, Chemical Physics Letters 307, 95 (1999).
[35] Grant D. Smith, Dmitry Bedrov, Oleg Borodin, J. Am. Chem. Soc. 172, 9548 (2000).
[36] Grant D. Smith, Dmitry Bedrov, Oleg Borodin, Physical Review Letters 85, 5583 (2000).
[37] Bin Lin, P. T. Bionske, and J. W. Halley, J. Chem. Phys. 105, 1668 (1996).
[38] Grant D. Smith, R. L. Jaffe, D. Y. Yoon, J. Phys. Chem. 97, 12752 (1993).
[39] P. Ahlstrom, O. Borodin, G. Wahnstrom, E. J. W. Wensink, P. Carlsson and G. D. Smith, J. Chem. Phys. 112, 10669 (2000).
[40] G. D. Smith, O. Borodin,and D. Bedrov, J. Comp. Chem. 23, 1480 (2002).
[41] Sylvie Neyertz and David Brown, J. Chem. Phys. 102, 9725 (1995).
[42] M. J. Blandamer, M. F. Fox, E. Powell, J. W. Stafford, Makromol. Chem. 124, 222 (1967).
[43] R. Kjellander and E. J. Florin, J. Chem. Soc. , Faraday Trans. 1 77, 2053 (1981).
[44] T. W. N. Bieze, A.C. Barnes, C. J. M. Huige, J. E. Enderby and J. C. Leyte, J. Phys. Chem. 98, 6568 (1994).
[45] Dmitry Bedrov, Oleg Borodin and Grant D. Smith, J. Phys. Chem. B. 5683 (1998).
[46] Akihiro Abe, Kenzabu Tasaki and J. E. Mark, Polym. J. 17, 883 (1985).
[47] Kenzabu Tasaki and Akihiro Abe, Polym. J. 17, 641 (1985).
[48] H. Matsuura and K. Fukuhara, J. Polym. Sci. Part B: Polym. Phys. 24, 1383 (1986).
[49] Ola Engkvist and Gunnar Karlstrom, J. Phys. Chem. B 101, 1631 (1997).
[50] S. Bekiranov, R. Bruinsma and P. Pincus, Europhys. Lett., 24, 183 (1993).
[51] Stefan Bekiranov, Robijn Bruinsma and Philip Pincus, Physical Review E, 55, 577 (1997).

Chapter 2 Methodology

2.1 Monte Carlo Simulation

2.1.1 Monte Carlo Methods

The classical expression for the partition function of a *N* particle system is given by statistical mechanics[2,15]:

$$Z = c\int dp^N dr^N \exp\left[-\beta H\left(p^N, r^N\right)\right] \tag{2.1}$$

where $\beta = 1/k_B T$, r^N represents the coordinates of all the particles, and p^N for the momenta. $H\left(r^N p^N\right)$ is the Hamiltonian of the system and it is the sum of the kinetic energy and the potential energy of the system. *c* is a constant and for a system with *N* identical atoms

$$c = \frac{1}{h^{3N} N!} \tag{2.2}$$

An average of property *A* can be calculated by

$$\langle A \rangle = \frac{\int dp^N dr^N A(p^N, r^N) \exp\left[-\beta H(p^N, r^N)\right]}{\int dp^N dr^N \exp\left[-\beta H(p^N, r^N)\right]} \tag{2.3}$$

Averages of functions that depend on momenta (p^N) only are usually easy to evaluate[1,15] , since the integration over p^N can be done analytically. However a successful calculation of the averages depends on r^N requires some technique. Monte Carlo importance sampling method developed by Metropolis et al[2] is the technique that generally be used.

In canonical ensemble, the configurational part of the partition function is

$$Q \equiv \int dr^N \exp\left[-\beta U(r^N)\right] \tag{2.4}$$

and the probability density of finding the system in a configuration around r^N is

$$\rho(\mathrm{r}^{\mathrm{N}}) \equiv \frac{\exp\left[-\beta U(r^N)\right]}{Q} \tag{2.5}$$

so the average can be denoted as

$$\langle A \rangle = \int dr^N \rho(r^N) A(r^N) \tag{2.6}$$

The ratio of the probabilities of system at state *n* and state *m* is

$$\begin{aligned} \frac{\rho_n}{\rho_m} &= \frac{\exp\left[-\beta U_n\right]/Q}{\exp\left[-\beta U_m\right]/Q} \\ &= \frac{\exp\left[-\beta U_n\right]}{\exp\left[-\beta U_m\right]} \\ &= \exp\left[-\beta\left(U_n - U_m\right)\right] \\ &= \exp\left[-\beta \Delta U_{nm}\right] \end{aligned} \tag{2.7}$$

A move from state *m* to *n* will be accepted with the probability

$$acc(m->n) = \min\left[1, \exp(-\beta \Delta U_{nm})\right] \tag{2.8}$$

where $\min\left[1, \exp(-\beta \Delta U_{nm})\right]$ means the move is accepted with probability 1 if $\Delta U_{nm} < 0$ and $\exp(-\beta \Delta U_{nm}) > 1$; When $\Delta U_{nm} > 0$ the move is accepted with a probability of $\exp(-\beta \Delta U_{nm})$ which now is a number between 0 and 1. A random number which is generated uniformly on (0,1) is compared with $\exp(-\beta \Delta U_{nm})$. Apparently the probability that is less than $\exp(-\beta \Delta U_{nm})$ is equal to $\exp(-\beta \Delta U_{nm})$, so the move is accepted if is less than $\exp(-\beta \Delta U_{nm})$.

In simulation, we first randomly select a particle and calculate its energy U_m, then randomly displace it, and calculate the new energy U_n. The displacement is generated using random numbers on [-1,1]. For example the new *x* coordinate becomes:

$$x_n = x_m + random \times \delta_{\max} \tag{2.9}$$

where $\delta_{\max}$ is the maximum displacement. It can be tuned to get the desired acceptance ratio of moves in simulations.

The move is accepted with the probability acc(m->n) as stated above. A Markov chain is constructed and ensures the probability of visiting a particular state is proportional to the Boltzmann factor.

2.1.2 Periodic Boundary Conditions

While conducting Monte Carlo simulations, we put N particles in a cubic box of a length (L) according to the density. Since we are interested in the properties of bulk liquids, the simulation should be able to mimic the presence of infinite number of molecules around our N particles, so that the surface effect can be eliminated.

Periodic Boundary Conditions are applied to solve this problem. The primitive cubic box is replicated and forms an infinite periodic lattice.[3,15] Every particle interacts with all other particles in its own box and all particles in other boxes. When a particle moves to cross the boundary of its box, it enters the same box through the opposite side.

It is impractical to try to calculate interactions between an infinite number of molecules, and spherical cut-off is adopted so that we can truncate the interaction at a certain distance r_c. A long range correction term for $r > r_c$ is added to account for the system error created by the truncated. Assuming the pair distribution function $g(r) = 1$ for $r > r_c$, the total interaction energy U_{total} is:

$$U_{total} = U_c + \frac{N\rho}{2}\int_{r_c}^{\infty} 4\pi r^2 u(r) dr \qquad (2.10)$$

where U_c is interaction energy result from simulation using cut-off, is the average number density and $u(r)$ is the pair potential. The long range correction is explained more in Section 2.2, and the pair distribution function is addressed in Section 2.3.

2.1.3 Cell Lists

If we simulate a large system with N particles and apply cut-off in interaction calculations, some methods can be employed to save CPU time. Cell list is one of them[3,15]. It divides the simulation box into n_c cubic cells and the cell length has to be at least the cut-off distance. On average there are $N_c = N/n_c^2$ particles in each cell. Each cell has 26 neighboring cells in a 3-D system. An example in 2-D system is shown in Fig. 2.1.

Only particles in its own cell and all the neighboring cells need to be considered while we calculate interaction energy for any particle in system. There are approximately $27\mathrm{NN_c}$ pairs of interaction if we apply the cell list, comparing to $\frac{1}{2}N(N-1)$ pairs if we do not, so it saves computation time for large system.

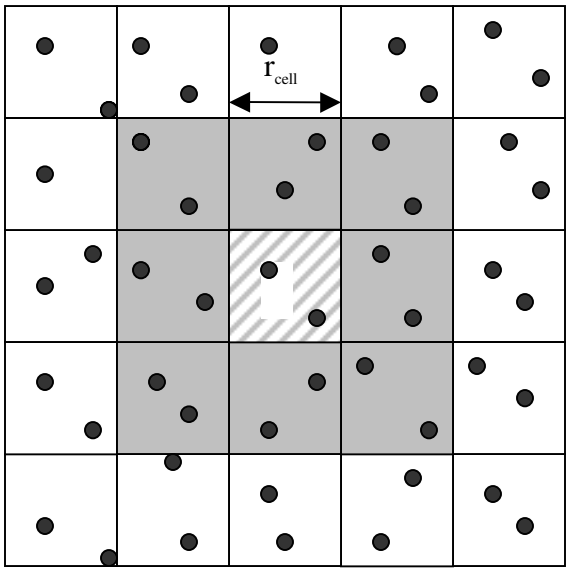

Figure 2.1: A simulation box is divided into cells with length r_{cell}. A particle (i) interacts with other particles in its own cell and all the neighboring cells. In 2-D each cell has 8 neighboring cells, and in 3-D, 26 cells).

If the N is not large enough (box length L < 4 times cut-off distance), there is no benefit in employing cell list. Actually the overhead of maintaining the cell list will slow down the simulation.

2.1.4 Reduced Units

In simulations, quantities are always reported in reduced units (denoted with *). For example:

distance	$r^* = r/\sigma$	(2.11)
pair potential	$u^* = u/\varepsilon$	(2.12)
density	$\rho^* = \rho\sigma^3$	(2.13)
temperature	$T^* = k_B T/\varepsilon$	(2.14)
pressure	$P^* = P\sigma^3/\varepsilon$	(2.15)

Reduced units are important in simulations because of the law of corresponding states, which means many combinations of , T, , in real systems correspond to the same state in reduced units.[15] It is also easier to spot errors by using reduced units since numbers in reduced units are usually close to unity and it is less likely to have overflow or underflow.

2.1.5 Error Analysis

It is important to provide error estimate along with the average value of a property calculated from computer simulations. While taking averages, sufficient time for equilibration should be allowed and then the average can only be calculated over the rest of the steps. How long the equilibration time is depends on the system and a preliminary run can be used to find it. The average of a property Y can be calculated over the N_{equil}

equilibrium configurations, and the N_{equil} equilibrium steps have to be divided into N_b blocks of m steps each. The average on block *i* is defined as,

$$Y_i^b = \frac{\sum_{j=(i-1)m+1}^{mi} Y(j)}{m} \tag{2.16}$$

These sub-block means are uncorrelated so the overall average can be calculated,

$$\langle Y \rangle = \frac{\sum_{i=1}^{N_b} Y_i^b}{N_b} \tag{2.17}$$

The error of $\langle Y \rangle$ is[4]

$$\sigma^2 = \frac{\sum_{i=1}^{N_b} \left(Y_i^b - \langle Y \rangle \right)^2}{N_b \left(N_b - 1 \right)} \tag{2.18}$$

2.2 Molecular Models

2.2.1 Lennard-Jones Model

The Lennard-Jones (LJ) potential is a simple, very commonly used pair potential, and it has been used extensively to model hydrophobic molecules such as noble gases and alkanes. It models interaction energy between two particles *r* apart as

$$u_{LJ}(r) = 4\varepsilon \left[\left(\frac{\sigma}{r} \right)^{12} - \left(\frac{\sigma}{r} \right)^{6} \right] \tag{2.19}$$

σ and ε are the empirical parameters for the LJ interaction. σ describes the repulsive wall since the energy rises steeply as *r* gets less than σ; ε defines the well-depth. The $1/r^{12}$ term models the repulsive interaction which dominates at short distance, and the $1/r^{6}$ term models the attractive interaction which dominates at long distance. The potential minimizes at distance $\sqrt[6]{2}\sigma$.

The Lorentz-Berthelot mixing rule can be applied to the parameters when two particles are different:

$$\sigma_{ij} = \frac{\sigma_i + \sigma_j}{2}; \quad \varepsilon_{ij} = \sqrt{\varepsilon_i \varepsilon_j} \tag{2.20}$$

As r increases, the LJ potential becomes very small and it saves computation time if we apply a spherical cut-off at distance r_c. The potential becomes

$$u_{LJ}^{cut-off}(r) = \begin{cases} u_{LJ}(r) & r \le r_c \\ 0 & r > r_c \end{cases} \tag{2.21}$$

The cut-off distance r_c has to be large enough to ensure that the introduction of cut-off only causes small system perturbation. Cut-off is also necessary if periodic boundary condition exists, and in that case r_c can be at most half of the box length to be consistent with the minimum image convention.

A long-range correction should be added back to the interaction at the end.

$$u^{LRC} = \frac{8}{3}\pi\rho\varepsilon\sigma^3\left[\frac{1}{3}\left(\frac{\sigma}{r_c}\right)^9 - \left(\frac{\sigma}{r_c}\right)^3\right] \tag{2.22}$$

Instead of simple truncate, a cut-and-shifted potential can be done as:

$$u_{LJ}^{cut-and-shift}(r) = \begin{cases} u_{LJ}(r) - u_{LJ}(r_c) & r \le r_c \\ 0 & r > r_c \end{cases} \tag{2.23}$$

This way there will be no discontinuities in the potential.

2.2.2 Columbic Interaction

For systems with electrical charges, the columbic interaction is the model chosen,

$$u(r_{ij}) = \frac{q_i q_j}{4\pi\varepsilon_0 r_{ij}} \tag{2.23}$$

where q_i, q_j are the charges on particle i and j, ε_0 is the permittivity of free space, and r_{ij} is the distance between the two particles.

Usually an Ewald sum is used to handle the long range correction for charge-charge interactions. However, in this work no Ewald sum was used. We did a molecular based cut-off and it has been shown that it does not affect the free energy which we are interested in.[5, 6, 21]

Potential cut-offs on a molecule with multiple interaction sites is more complicated than on simple LJ potentials. The system has to keep neutral on electrical charges, so it is necessary to keep all the atoms of a molecule "together" while apply cut-offs. If the reference site of a molecule is within the cut-off distance of the reference site of another molecule, all interactions between these two molecules will be calculated, even if the distance between some pairs might be larger than the cut-off distance. On the other hand no interaction will be calculated between the two molecules if the distance between the two reference sites exceeds the cut-off distance. Oxygen is chosen as the reference site for both water and DME, the two models which will be mentioned later in this chapter. The cut-off distance is 3 times the LJ parameter σ of the oxygen particle for SPC/E water, and 3 times the LJ parameter σ of the CH3 group for DME.

2.2.3 SPC/E Water

Among many available water models[7,8,9,10], the extended simple point charge model (SPC/E) developed by Berendsen[11] is the one we have chosen for simulating bulk water as well as water in aqueous solutions, because it gives good representation of real water[12,13]. This model is based on single point charge model (SPC) but adds a constant polarization energy term to the total interaction to better fit the behavior of real water over a wide density and temperature range. SPC/E is a three site model. On oxygen there is a LJ site ($\sigma = 3.16556\,\text{Å}$, $\varepsilon/k_B = 78.24K$) with fixed point charge (-0.8476*e*); on the

two hydrogen sites there is only a fixed point charge of 0.4238*e* on each. The O-H bond length is 1Å, and the H-O-H bond angle equals to tetrahedral angle which is 109.5º.

2.2.4 Dimethyl Ether

Dimethyl Ether is colorless gas at room temperature. It is a hydrophilic molecule and its simple structure (CH_3-O-CH_3) resembles the unit of PEO. B. Lin's model is used[14] in our simulation. This is a three site model. Each CH_3 group is treated as one particle. On each particle there is a LJ site and a point charge. The parameters are listed below in Table 2.1.

Table 2.1: Parameters for the DME model

σ_{CH3} = 2.851 Å	ε_O/k_B = 47.80 K
σ_{CH3} = 3.5636 Å	ε_{CH3}/k_B = 75.48 K
q_O = -0.342 e	q_{CH3} = 0.171 e
$l_{O\text{-}C}$ = 1.417 Å	$\theta_{C\text{-}O\text{-}C}$ = 111.7º

2.3 Pair Distribution Function

Pair distribution function $g(r)$ is the simplest yet the most notable distribution function that characterizes the local structure of a fluid. It is the probability of finding a pair of atoms a distance *r* apart, relative to the probability expected for a completely random distribution at the same density.[3] It is important in both experimental and theoretical views: neutron and X-ray scattering and light scattering gave information

about $g(r)$; the ensemble average of any pair function can be expressed as function of $g(r)$ and numerical results of $g(r)$ can be compared with theoretical predictions.

In the canonical ensemble $g(r)$ is defined as:

$$g(r_1, r_2) = \frac{N(N-1)}{\rho^2 Z_{NVT}} \int dr_3 r_4 \cdots dr_N \exp(-\beta U(r_1, r_2, \cdots r_N)) \tag{2.25}$$

where N is the number of molecules, is density, Z is the configuration integral, U is the total potential energy and is the inverse temperature $1/k_B T$. In a system with identical particles, the choice of molecules 1 and 2 is obviously arbitrary. When taking the ensemble average over pairs, the definition can be written as:

$$g(r) = \rho^{-2} \left\langle \sum_i \sum_{j \neq i} \delta(r_i) \delta(r_j - r) \right\rangle = \frac{V}{N^2} \left\langle \sum_i \sum_{j \neq i} \delta(r - r_{ij}) \right\rangle \tag{2.26}$$

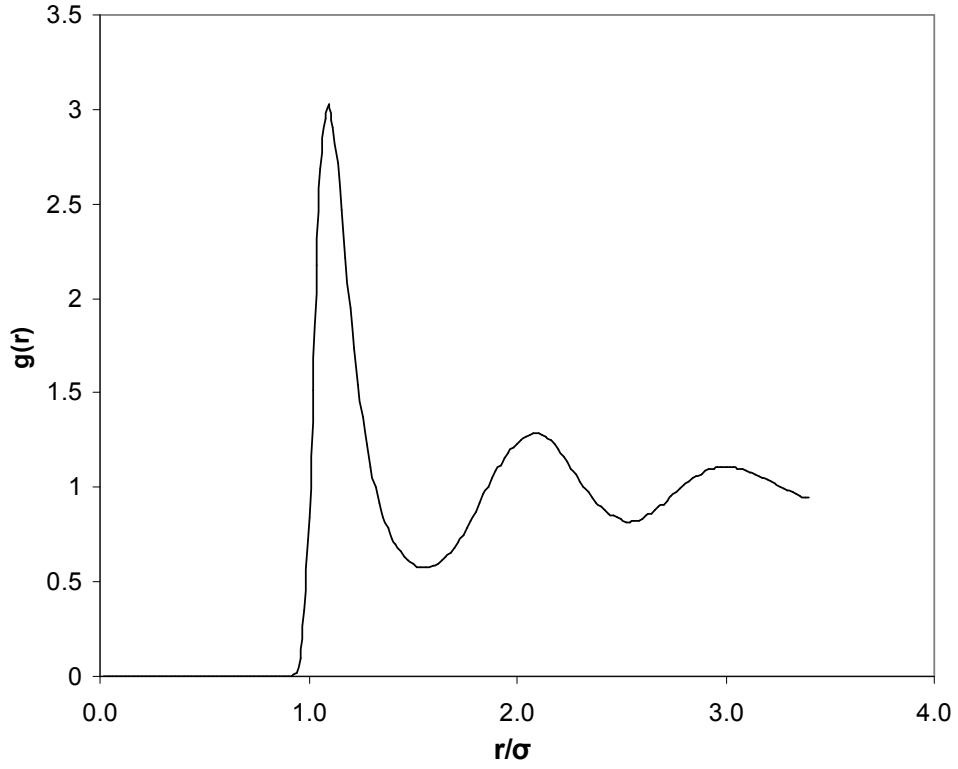

Figure 2.2: Pair distribution function $g(r)$ for the L-J fluid at T*=0.69, *=0.84.

Equation (2.26) can be used to calculate pair distribution function in a computer simulation. In a system with identical atoms, $g(r)$ in simulation is measured by the ratio between the average number density at a distance *r* from any given atom and the number density at a distance *r* from an atom in an ideal gas at the same overall density.[15] A pair distribution function for LJ fluid is shown in Figure 2.2.

The ensemble average of any pair function $a(r)$ can be calculated from the pair distribution function:[3]

$$\left\langle a(r_i, r_j) \right\rangle = \frac{1}{V^2} \int dr_i dr_j g(r_i, r_j) a(r_i, r_j) \tag{2.27}$$

2.4 Solubility

The classical partition function of a 3-dimensional system of *N* atoms in canonical ensemble is[15]:

$$Q(N,V,T) = \frac{V^N}{\Lambda^{3N} N!} \int ds^N \exp\left[-\beta U(s^N; L)\right] \tag{2.28}$$

It is assumed that the N atoms are in a cubic box with length L, and the volume $V = L^3$. The scaled coordinate $s^N = r^N / L$. The energy of the state U depends on the real coordinates instead of the scaled ones so the energy is denoted by $U(s^N; L)$. $\Lambda = \sqrt{h^2/(2\pi m k_B T)}$ is the de Broglie wavelength.

The Helmholtz free energy is,

$$\begin{aligned} F(N,V,T) &= -k_B T \ln Q \\ &= -k_B T \ln\left(\frac{V^N}{\Lambda^{3N} N!}\right) - k_B T \ln\left(\int ds^N \exp\left[-\beta U(s^N; L)\right]\right) \end{aligned} \tag{2.29}$$

The first term is the ideal gas contribution and the second term is the excess part.

The chemical potential can be defined as

$$\mu_i = \left(\frac{\partial F}{\partial N_i}\right)_{V,T,N_{j\neq i}} \tag{2.30}$$

When N is large enough, the chemical potential becomes

$$\begin{aligned}\mu &= -k_B T \ln(Q_{N+1}/Q_N) \\ &= -k_B T \ln\left(\frac{V/\Lambda^3}{N+1}\right) - k_B T \ln\left(\frac{\int ds^{N+1} \exp\left[-\beta U(s^{N+1})\right]}{\int ds^N \exp\left[-\beta U(s^N)\right]}\right) \\ &\equiv \mu_{id}(\rho) + \mu_{ex}\end{aligned} \tag{2.31}$$

and it is separated into an ideal gas part and an excess part. We can define energy difference $\Delta U \equiv U(s^{N+1}) - U(s^N)$, and it is the interaction energy between the *(N+1)*th particle with the rest of the system, so the excess chemical potential is

$$\mu_{ex} = -k_B T \ln\left\langle \exp(-\beta \Delta U)\right\rangle_N \tag{2.32}$$

This is an ensemble average so it can be sampled in simulation by the conventional Metroplis method.

Solubility can then be defined as[16,17]

$$B = \left\langle \exp\left(-\beta \Delta U\right)\right\rangle_N \tag{2.33}$$

so that

$$\mu_{ex} = -k_B T \ln B \tag{2.34}$$

B is called the insertion factor. It is also a dimensionless Henry's Law Constant. In our work this factor is used as a measure of solubility.

2.4.1 Widom Insertion

The Widom method[18] is a simple yet elegant method to calculate the chemical potential μ in pure fluid as well as mixtures. It is a particle insertion method, and one test particle is inserted into the solution in every move.

In the canonical ensemble, the excess chemical potential μ_{ex} can be expressed as:

$$\mu = -k_B T \ln\left\langle \exp(-\frac{\psi}{k_B T})\right\rangle_0 \tag{2.35}$$

or,

$$-\beta\mu = \ln\langle \exp(-\beta\psi) \rangle_0 \tag{2.36}$$

where ψ is the interaction energy between the test particle and the rest of the system. The subscript 0 means the test particle can not be seen or felt by other particles, so the test particle is also referred as a "ghost" particle.

The Widom method has been used extensively to calculate chemical potential s and it works well for fluid at low to medium density when it is relatively easy to find enough free space in the system for the test particle.

2.4.2 Expanded Ensemble

The expanded ensemble method[19,20] is a procedure that calculates effectively the free energy of solution even at high densities. It also provides information on intermediate states. As defined earlier in the solubility section, excess chemical potential, or solubility can be calculated from the ratio of the partition function of final state (m) and original state(0). The expanded ensemble defines a series of intermediate states, and modifies the partition function by adding a weighting factor η_k, so the partition function for the ensemble of all the states is:

$$Z = \sum_{k=0}^{m} Q_k \exp(\eta_k) \tag{2.37}$$

The probability of state k would be,

$$p_k = \frac{Q_k \exp(\eta_k)}{Z} \tag{2.38}$$

The solubility becomes,

$$\ln B = \ln\left(\frac{p_m}{p_0}\right) - \eta_m + \eta_0 \tag{2.39}$$

In simulation the expanded ensemble move can be conducted in the following steps (let's use NVT as an example):

1. Define a series of states, which 0 is the original state (solute doesn't exist), m is the final state (solute is fully coupled to the system), and there are (m-1) states in between. These states can be arbitrarily chosen but usually according to the system. For example, they can be correlated to the growing diameter of the solute particle, or increasing chain length of a polymer solute.

2. Choose weighting factors for each state. The weighting factors can be arbitrary, but should be chosen to obtain a evenly distributed histogram, i.e. encourage visits to energetically unfavorable states. Initially we don't know the chemical potential, so to find optimal weights, initial simulation can be run to set up the feedback loop:

$$\ln B = \ln\left(\frac{p_j}{p_i}\right)^{initial} - \eta_{ij}^{initial} = \ln\left(\frac{p_j}{p_i}\right) - \eta_{ij} \tag{2.40}$$

where $\eta_{ij} = \eta_j - \eta_i$. To get $\frac{p_j}{p_i}$ be approximately 1,

$$\eta_{ij} = -\ln\left(\frac{p_j}{p_i}\right)^{initial} + \eta_{ij}^{initial} \tag{2.41}$$

and the result can be used to further modify the weights.

3. Perform two kinds of Monte Carlo moves. The first is the traditional Metropolis move at a fixed state. The energy difference due to moving of one particle is used in the acceptance rule. Unlike in the Widom method where the solute is just a ghost particle, here the inserted solute is part of the system and the interaction of it with the solvent has to be taken into account. The second move is the transition of the solute between state i and state j, and the acceptance rule is:

$$acc(i \to j) = \min\left[1, \exp\left(-\beta\left(\psi_j - \psi_i\right) + \eta_j - \eta_i\right)\right] \tag{2.42}$$

where ψ is the interaction energy between the solute at that state with the rest of the system.

4. Keep a record of the number of times each state is visited (n_i), and use it to calculate the probability and then the solubility.

$$p_i = \frac{n_i}{\sum_{l=0}^{m} n_l} \tag{2.43}$$

The error of the solubility in expanded ensemble can be calculated as following[21]:

$$error(\ln B) = 2\sqrt{\frac{\sigma^2_{\ln B}}{N_{sampling}}}, \tag{2.44}$$

$$\sigma^2_{\ln B} = \frac{\sigma^2_{N_m}}{\langle N_m \rangle^2} + \frac{\sigma^2_{N_0}}{\langle N_0 \rangle^2} - 2\frac{\mathrm{cov}(N_m, N_0)}{\langle N_m \rangle \langle N_0 \rangle} \tag{2.45}$$

where $\mathrm{cov}(N_m, N_0) = \langle N_m N_0 \rangle - \langle N_m \rangle \langle N_0 \rangle$ is the covariance of N_m and N_0. The error analysis also shows the importance of optimizing the weighting factors to equally distribute the expanded ensemble moves to all states (from state 0 to m).

Although have not been tried in our simulations, worth mentioning here is the most recent development we have noticed in the expanded ensemble method. The probability density estimation was used to optimize the expanded ensemble parameters continuously in the expanded ensemble molecular dynamic simulation to get the solvation free energies[22]. This new method has proved to be much faster than the regular expanded ensemble MD move since the step of determining balancing factors is no longer necessary.

2.5 Polymer Chain

A chain model can be either highly simplified as in a united-atom model or a fully atomistic model. In most of our work, united atom models were used for polymer chains

because of its simplicity that reduces simulation time. In this kind of model, each molecular group or polymer unit can be treated as one particle with interaction sites such as LJ parameters and point charge on it. Simple examples include freely jointed chain and freely rotating chain. The freely jointed chain is defined here as a LJ chain with fixed bond length, and there is no other constraint on the chain. Freely rotating chain has one more constraint and it is fixed bond angles. More restrictions, such as torsional interactions, could be introduced to obtain a more realistic polymer chain.

In all-atom models, every atom in the chain is represented by a LJ sphere with a point charge. There are some widely used all-atom force fields such as Jorgensen's OPLS-AA[23,24,25], which has been used successfully for many organic molecules and ions.

COMPASS (Condensed-phase Optimized Molecular Potentials for Atomistic Simulation Studies)[26] is the force field used by Accelrys's Material Studio package. The intramolecular interaction includes bond stretching, angle bending, torsion, term for out-of-plane motion (or inversion), and crossterms. It appoints a 9-6 LJ interaction, and its non-bonded energy is calculated by:

$$u_{ij}(r) = \varepsilon_{ij}\left[2\left(\frac{\sigma_{ij}}{r}\right)^9 - 3\left(\frac{\sigma_{ij}}{r}\right)^6\right] + \frac{q_i q_j}{r} \tag{2.46}$$

2.5.1 Chain Coordinate System

In our work Flory's local coordinate system[27] is used for polymer chains. Bond ι connects particle (ι−1) and particle ι, and the bond length is l_i; the dihedral angle on bond ι (ϕ_i) is the angle formed by atom (ι−2), (ι−1), ι and (ι+1), and it is 0 when the chain is in trans conformation; the supplemental angle of the angle apex at ι is denoted by θ_i.

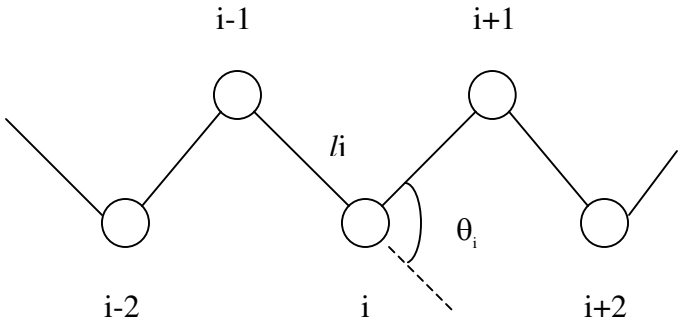

Figure 2.3: Flory's chain coordinate system.

Each bond can define a coordinate system with x axis in the direction of bond i, and y axis in the plane of the bond (i-1) and i, and forms an acute angle with bond (i-1) as shown in Fig. 2.3. A position vector (r_{i+1}) expressed in reference frame of bond (i+1) can be transformed to a vector r_i expressed in frame of bond i by the transformation matrix T_i,

$$r_i = T_i r_{i+1} \tag{2.47}$$

$$T_i = \begin{bmatrix} \cos\theta_i & \sin\theta_i & 0 \\ \sin\theta_i \cos\phi_i & -\cos\theta_i \cos\phi_i & \sin\phi_i \\ \sin\theta_i \sin\phi_i & -\cos\theta_i \sin\phi_i & -\cos\phi_i \end{bmatrix} \tag{2.48}$$

So given a chain with a unify bond length fixed to l, the bond vector l_i is $(l, 0, 0)^T$, and the position vector of the ith particle (r_i) is expressed in the laboratory-fixed coordinate system as,

$$r_i = (E + T_1 + T_1T_2 + \cdots + T_1T_2 \cdots T_{i-1})l_i \tag{2.49}$$

2.5.2 Continuum Configurational Bias Monte Carlo

Rosenbluth and Rosenbluth developed a scheme[28] to sample polymer configurations in 1955. Improvements have been made on this scheme to find a method that is able to properly simulate long polymer chains, and correctly generate chain

conformations according to the Boltzmann weight. Siepmann and Frenkel[29], de Pablo, Laso, and Suter[30] have developed configurational bias Monte Carlo and applied it on polymer systems in early 1990's, and this scheme has been used widely on polymer simulations since.

Our simulations are all carried on off-lattice system so only continuum configurational bias (CCB) Monte Carlo will be discussed here. For each polymer chain in the system, the CCB scheme consists of the following steps:

1. Pick randomly a point on the chain, and cut off one part. (Which part to be cut off is decided randomly for polymer chain with both ends free).
2. Regrow the chain segment by segment. For each segment, n trial positions are created, and for each trial position (i) the interaction energy with the rest of the system (u_i) is calculated. These trial positions can be created based on Boltzmann weight ($\exp(-\beta u_i)$), or uniformly, or even purely randomly, depend on the system. Among these trial positions, one is selected with a probability p:

$$p = \frac{\exp(-\beta u_i)}{\sum_i^n \exp(-\beta u_i)} \tag{2.50}$$

3. The probability of regrowing m segments on the chain would be,

$$W = \prod_j^m p_j \tag{2.51}$$

4. The probability of accepting this move is,

$$P_{old \to new} = \min(1, \frac{W_{old} P_{new}}{W_{new} P_{old}}) \tag{2.52}$$

where P_{new} and P_{old} are the probabilities of the trial and old configurations, $\frac{P_{new}}{P_{old}} = \exp(-\beta \Delta U_{old \to new})$, and W_{new} is the probability of generating the trial chain. W_{old} is the probability of generating the old chain, and it is obtained the same way as we did

W_{new}, except it is always the old configuration being selected, instead of according to the Boltzmann weights.

CCB only delete and regrow end segments, and it becomes inefficient when the chain gets long. Escobedo and de Pablo also developed ECCB, which is an extension of CCB[31] This scheme allows deleting and regrowing of the inner chain segments. Since the algorithm has to make sure the inner segments grow back together to complete the chain, jacobean of transformation is added to the acceptance rule in order to account for the unequal sampling. ECCB works well on freely jointed chains. However for chains with fixed bond angles, ECCB can not deal with this extra constraint. Concerted rotation method is developed for chains with more geometry constraints.

2.5.3 Concerted Rotation /Rebridging /End-Bridging

When simulating dense polymer systems using CCB algorithm, the configuration rearrangement is difficult since the inner chain segments moves rarely get accepted. As mentioned in the previous section, the ECCB method which works for freely jointed chain models is not capable of solving the problems for freely rotating chains because of the extra configurational constraint of the fixed bond angle. Concerted rotation (CONROT) was first developed in 1993 by Dodd, Boone and Theodorou[32] to alter a chain section in a coordinated way, and to keep unaffected the rest of the chain, as well as the bond length and angle. CONROT move can be implemented in following steps (Flory's local coordinate system is used for chain particles, bonds and angles):

On the chain select randomly a torsion angle as the driver angle (ϕ_0^m). If this driver angle is more than 8 bonds away from chain end, this is a full (7 bond) concerted rotation move.

1. Change the driver angle, make it $\phi_0^n = \phi_0^m + \Delta\phi_0$, where $\Delta\phi_0$ is picked randomly on $(-\Delta\phi_0^{\max}, \Delta\phi_0^{\max})$.

2. Solve the equation $F(\phi_1; \phi_0^n, f) = 0$ either geometrically or numerically to find all $\phi_1 \in (\phi_1^m - \pi, \phi_1^m + \pi)$. For a full CONROT move, the function is $F(\phi_1; r_5^{(1)}, u_6^{(1)}, \gamma_6) \equiv \left[u_6^{(1)}\right]^T T_1 T_2 T_3 T_4 e_1 - \cos\theta_5$, the superscript 1 means the position and the unit bond vector are in the frame of reference of bond 1.

3. If the equation has $N^{(n)}$ real roots ($N \geq 2$), select one from these roots. The selection can be based on uniform discrete distribution (random) with a probability $\alpha_{cr}(m \to n) = 1/N^{(n)}$, or based on Boltzmann factor of the potential energies with a probability,
$$\alpha_{cr}(m \to n) = \exp(-\psi(n)/k_B T) \Big/ \sum_{i=1}^{N^{(n)}} \exp(-\psi(i)/k_B T) \tag{2.53}$$

4. To satisfy detailed balance, the reverse CONROT move needs to be made. Start from the new ϕ_1^n, find all $\phi_1 \in (\phi_1^n - \pi, \phi_1^n + \pi)$. The original ϕ_1^m must be among these $N^{(m)}$ roots.

5. Calculate the Boltzmann factor for both the original (m) and the final (n) states, using the total potential energy of the system. Also calculate the Jacobian determinant of the chain in the original state (m) and the final state (n).

6. Accept the move with probability
$$P(m \to n) = \min\left[1, \frac{\alpha_{cr}(n \to m)\exp(-\psi(n)/k_B T)J(n)}{\alpha_{cr}(m \to n)\exp(-\psi(m)/k_B T)J(m)}\right] \tag{2.54}$$

Should this move be accepted, the positions of 4 inner particles, as well as the 7 torsion angles related to them, will be changed.

The algorithm was later generalized by Pant and Theodorou[33], and the formulation was called Intramolecular Rebridging or double driven CONROT. In Rebridging, an interior trimer is excised from a chain, and both particles neighboring the trimer will be displaced, or in other words, both torsion angles neighboring the trimer will be rotated by an amount selected randomly on $(-\Delta\phi_0^{\max}, \Delta\phi_0^{\max})$, and then the trimer will be reconstructed.

The equation is solved numerically by an iterative Newton-Raphson algorithm. If a viable root is found, the reverse move will be conducted using the identical algorithm. The move is only accepted if the reverse move produces the original position. This way although the Intramolecular Rebridging move here only locates one geometric solution, the microscopic reversibility is still ensured. The acceptance probability of the Rebridging move is

$$P(m \to n) = \min\left[1, \frac{\exp(-\psi(n)/k_B T) J(n)}{\exp(-\psi(m)/k_B T) J(m)}\right] \tag{2.55}$$

End-Bridging (EB) Monte Carlo[34] has a similar mathematical formulation as CONROT since these two algorithms solve the same geometric problem. However EB allows chain connectivity altering moves and it makes possible the simulation of polydisperse systems with fully controlled molecular weight distribution and increased efficiency of sampling chain configurations. In an EB move, two chains within certain distance from each other will be selected, then a trimer will be cutoff from the inner part of a chain, and a bridging trimer will be grown to connect the end of the other chain with one segment of the excised chain.

---

[1] W. W. Wood. Early history of computer simulation in statistical mechanics. In G. Ciccotti and W. G. Hoover, editors, Molecular Dynamics Simulations of Statistical Mechanics Systems, pages 2-14. Proceedings of the 97th Int. "Enrico Fermi" School of Physics, North Holland, Amsterdam, (1986).
[2] N. Metropolis, A. W. Rosenbluth, M. N. Rosenbluth, A. N. Teller, and E. Teller, J. Chem. Phys. 21, 1087 (1953)
[3] M. P. Allen, D. J. Tildesley, Computer Simulation of Liquids (Oxford Science Publications, 1987).

[4] Marvin Bishop and Sharon Frinks, J. Chem. Phys. 87, 3675 (1987).
[5] Matthew T. Stone, Pieter J. In 'T Veld, Ying Lu and Isaac C. Sanchez, Mol. Phys. 100, 27733 (2002).
[6] Y. V. Vorobjrv and J. Hermans, J. Phys. Chem. B 103, 10234 (1999).
[7] Frank H. Stillinger, Aneesur Rahman, J. Chem. Phys. 60,1545 (1974).
[8] H. J. C. Berendsen, J. P. M. Postma, W. F. van Gunsteren, and J. Hermans, Intermolecular Forces, edited by B. Pullmannn (Reidel, Dordrecht, 1981), pp331-8.
[9] W. L. Jorgensen, J. Chandrasekhar, J. D. Madura, R. W. Impey, and M. L. Klein, J. CHem. Phys. 79, 926 (1983).
[10] M. W. Mahoney and W. L. Jorgensen, J. Chem. Phys. 112, 8910 (2000).
[11] H. J. C. Berendsen, J. R. Grigera and T. P. Straastsma, J. Phys. Chem. 91, 6269(1987).
[12] B. Guillot and Y. Guissani, J. Chem. Phys. 99, 8075(1993).
[13] D. van der Spoel, P. J. van Maaren, and H. J. C. Berendsen, J. Chem. Phys. 108, 10220 (1998).
[14] B. Lin and J. W. Halley, J. Phys. Chem. 99, 16474 (1995).
[15] Daan Frenkel and Berend Smit, Understanding Molecular Simulation (Academic Press, 1996)
[16] I. C. Sanchez and M. T. Stone, Statistical Thermodynamics of Polymer Solutions and Blends. Polymer Blends, Vol. 1. D. R. Paul, C. Bucknall (John Wiley and Sons, Inc.; New York, 2000) Chapter 1, pages 15-53.
[17] Kenneth Michael Lee, Exploring Solvent Properties of High Pressure Carbon Dioxide via Computer Simulation, The University of Texas at Austin, 2003.
[18] B. Widom, J. Chem. Phys., 39, 2802 (1963).
[19] A. P. Lyubartsev, A. A. Martsinovskii, S. V. Shevkunov and others, J. Chem. Phys. 96, 1776 (1992).
[20] P. N. Vorontsov-Velyaminov, A. V. Broukhno, T. V. Kuznetsova and A. P. Lyubartsev, J. Phys. Chem. 100, 1153 (1996).
[21] Matthew T. Stone, Mente Carlo Approaches to the Protein Folding Problem, The University of Texas at Austin, 2002.
[22] Aberg K. Magnus, Alexander P. Lyubartsev, Sven P. Jacobsson and Aatto Laaksonen, J. Chem. Phys. 120, 3770 (2004).
[23] George Kaminski, William L. Jorgensen, J. Phys. Chem., 100, 18010 (1996).
[24] Erin M. Duffy, William J. Jorgensen, Journal of the American Chemical Society, 122, 2878 (2000).
[25] William L. Jorgensen, Jokob P. Ulmschneider, Julian Tirado-Rives, J. Phys. Chem. B, 108. 16264 (2004).
[26] H. Sun, J. Phys. Chem. B, 102. 7338 (1998).
[27] Paul J. Flory, Statistical mechanics of chain molecules (Interscience Publishers, New York, 1969).
[28] M.N. Rosenbluth and A.W. Rosenbluth, J. Chem. Phys., 23, 356 (1955).
[29] J.I. Siepmann and Frenkel, Mol. Phys., 75, 59 (1992).
[30] J.J. de Pablo, M. Laso, and U.W. Suter, J. Chem. Phys., 96, 2395 (1992).
[31] F.A. Escobedo and J.J. de Pablo, J. Chem. Phys., 102, 2636 (1995).
[32] L. R. Dodd, T. D. Boone, and D. N. Theodorou, Molecular Physics, 78, 961 (1993).
[33] P. V. K. Pant, D. N. Theodorou, Macromolecules 28, 7224 (1995).
[34] Vlasis G. Mavrantzas, Travis D. Boone, Evangelia Zervopoulou, and Doros N. Theodorou, Macromolecules 32, 5072 (1999).

Chapter 3 Monte Carlo Studies of Gas Solubilities in Water

3.1 Introduction

Oil does not mix with water. People have known this phenomenon for thousands of years, yet a clear understanding of it is still the object of many scientists work. Hydrophobicity, which is associated with the poor solubility of non-polar gases (inert gases, hydrocarbons, etc), is very important in many areas such as environmental science (air and water pollutions) and biological science[1, 2,3,4] (protein folding and micellization).

Traditionally hydrophobic hydration has been attributed to the“ iceberg” structure, or, the clathrate structures forming around the nonpolar solutes[5]. However, the entropy gain/loss will be exactly cancelled by the enthalpy loss/gain, so the structure around the solute does not affect solubility[6].

Since Scaled Particle Theory (SPT)[7]used a small size for water, there exists a hypothesis that the small size of water causes small cavities is the origin of low solubilities of non-polar solutes in water[8,9,10]. However, the usage of SPT model for hydrophobic hydration has been criticized[11,12,13]. The small sized water hypothesis has been disputed by many scholars[6, 14, 15, 16]. Other theoretical approaches to hydrophobicity include integral equation techniques[17,18] and information theory approach[19, 20].

During the past decades, computer simulations have gain increasing importance in theoretical research. The development in statistical thermodynamic techniques, such as the Widom insertion[21,22] and expanded ensemble methods[29,30] made possible the comparison of calculated solubilities or free energies with experimental values.

Based on Monte Carlo simulation results, we will discuss two important problems related to hydrophobicity and hydrophilicity: Is hydrophobicity primarily an entropic effect? What is the origin of the gas solubility minimum in water?

3.2 Methodology

Extended simple point charge (SPC/E) model[23] has been used for water molecules in all of our simulations. Xenon is modeled with a LJ particle with parameters[24] $\sigma = 3.97\,\mathring{A}$ and $\varepsilon / k = 215K$. Lin's united atom model[25] has been used for dimethyl ether (DME). The solute and water cross interaction parameters are calculated from the Lorentz-Berthelot combining rules. The hard sphere used to compare solubility with xenon has the size of xenon LJ particle size (σ).

Long range corrections have been applied on LJ interactions and the cutoff distance was set to 2.5 σ. For Coulombic interactions a molecular based cut-off at 3σ was used, since no difference in free energy results have been noticed between results from simulations with Ewald sums and with this molecular based cut-off.[26, 27]

All of our simulations have been performed in the canonical ensemble along the water coexistence curve, unless mentioned otherwise in the text. The water coexistence data are from the experimental value or the data provided by Boulougouris, Economou, and Theodorou[28].

Solubilities (chemical potential) are calculated by simulations performed in the expanded canonical ensemble[29,30]. A system contains 256 or 512 SPC/E water molecules, and in each MC cycle one or two expanded ensemble moves are performed.

3.3 Results and Discussions

3.3.1 Second Osmotic Virial Coefficient

Potential mean force $\phi(r)$ is the potential of the average force between two molecules or atoms that are at a distance *r* apart. It is defined by the relationship:[31]

$$g(r) = \exp\left(-\frac{\phi(r)}{k_B T}\right) \tag{3.1}$$

$g(r)$ is the pair distribution function. For dilute gas $\phi(r) = u(r)$ where $u(r)$ is the pair potential energy, but generally there is:

$$g(r) = \exp\left(-\frac{u(r) + W(r)}{k_B T}\right) \tag{3.2}$$

$W(r)$ is the contribution from a third molecule.

The virial expansion of the equation of state is:

$$\frac{\pi}{c k_B T} = 1 + B_2 c + B_3 c^2 + \cdots \tag{3.3}$$

where B_2 is the second osmotic virial coefficient, is osmotic pressure, and *c* is the molar concentration of the polymer . B_2 is positive for a solute in a good solvent, and temperature can be found when B_2 equals to 0. B_2 can be calculated from the potential of mean force.

$$B_2 = 2\pi \int_0^\infty r^2 \left(1 - \exp(-\frac{\phi(r)}{k_B T})\right) dr \tag{3.4}$$

or simply,

$$B_2 = 2\pi \int_0^\infty r^2 \left(1 - g(r)\right) dr \tag{3.5}$$

Simulations have been run for two DME molecules in water at room temperature to measure the pair distribution function $g(r)$. Water is modeled explicitly. The second osmotic virial coefficient B_2 was calculated by integrating the function of $g(r)$ between 0 and 4 times the (LJ parameter of SPC/E water) using equation (3.5). B_2 for DME in water at 298 K is measured 6.39 which is reduced by σ^3. The positive second osmotic virial coefficient proves that the model we have chosen for DME indeed captures the hydrophilicity of DME at room temperature.

The second osmotic virial coefficient can not be measured experimentally for DME, however for polymers the osmotic-pressure measurement can be used to determine the number average molecular weights in the range 3×10^4 to 1×10^6.[32] The second osmotic virial coefficient of linear and star PEO has been measured. It is $(9.0\pm0.2)\times10^{-7}\ l\cdot mol/g^2$ for linear PEO with number molecular weight $7.2\times10^4\ g/mol$ in water at 33.8°C.[33] The equation they used was:

$$\frac{\pi}{c_2 RT}=\frac{1}{M_n}+B_{22}c_2+\cdots \tag{3.6}$$

where B_{22} is the second virial coefficient and c_2 is the polymer mass concentration.

To convert our calculated B_2 to the same unit, we can compare equation (3.3) and (3.6), so there are $c\equiv c_2/M_n$ and $B_{22}\equiv B_2 N_A\sigma^3/M_n{}^2$. The number $6.39/\sigma^3$ is equivalent to $5.8\times10^{-5}\ l\cdot mol/g^2$.

3.3.2 Hydrophobic vs. Hydrophilic Solute

Traditionally the low solubility of non-polar gases in aqueous solution is attributed to the large unfavorable hydration entropy[5,34,35], which is accompanied by favorable, but smaller hydration enthalpy. First we need a clear definition of solubility. The equilibrium condition of a solute between two phases is:

$$\frac{\rho_{aq}}{\rho_{vap}}=\frac{B_{aq}}{B_{vap}} \tag{3.7}$$

where *B* is the insertion factor, and it is the ensemble average of Boltzmann factor,

$$B=\left\langle \exp(-\beta\psi)\right\rangle_0 \tag{3.8}$$

ψ is the interaction energy between a test particle and all the other particles in the system. The ensemble average with a subscript 0 means the test particle is a "ghost" particle, or, the system cannot see the existence of the test particle. At low solute pressure, where the vapor phase can be considered ideal,

$$B_{vap} = 1 \tag{3.9}$$

so the equilibrium condition becomes,

$$\frac{\rho_{aq}}{\rho_{vap}} = B_{aq} \tag{3.10}$$

hence we can define a solute hydrophobic if $B_{aq} < 1$, and hydrophilic if $B_{aq} > 1$, as described in Figure 3.1.

The insertion factor can also be represented as an energy-entropy pair:

$$\ln B = -\beta \Delta u_{\text{int}} + \Delta s_{\text{int}} / k_B \tag{3.11}$$

k_B is the Boltzmann Constant; For interaction energy Δu_{int},

$$\Delta u_{\text{int}} \equiv \langle \psi \rangle \tag{3.12}$$

It is the same thing as the average interaction energy between solute and solvent. The interaction entropy Δs_{int} consists of two terms,

$$\Delta s_{\text{int}} / k_B = \ln P_{ins} - \ln \left\langle e^{\beta(\psi - \langle \psi \rangle)} \right\rangle_a \tag{3.13}$$

of which $\ln P_{ins}$ is the probability the solute finding a cavity large enough in the solvent to insert itself. The second term is the entropy fluctuation term, and it is the logarithm of an ensemble average only over those configurations where there is attractive interaction between solute and solvent. For hard sphere fluids, the fluctuation term is zero, and the interaction entropy equals to the insertion probability. However in solutions with attractive interactions between solute and solvent, the fluctuation term always contributes unfavorably to the interaction entropy.

Hydrophobic solute $B_{aq} < 1$

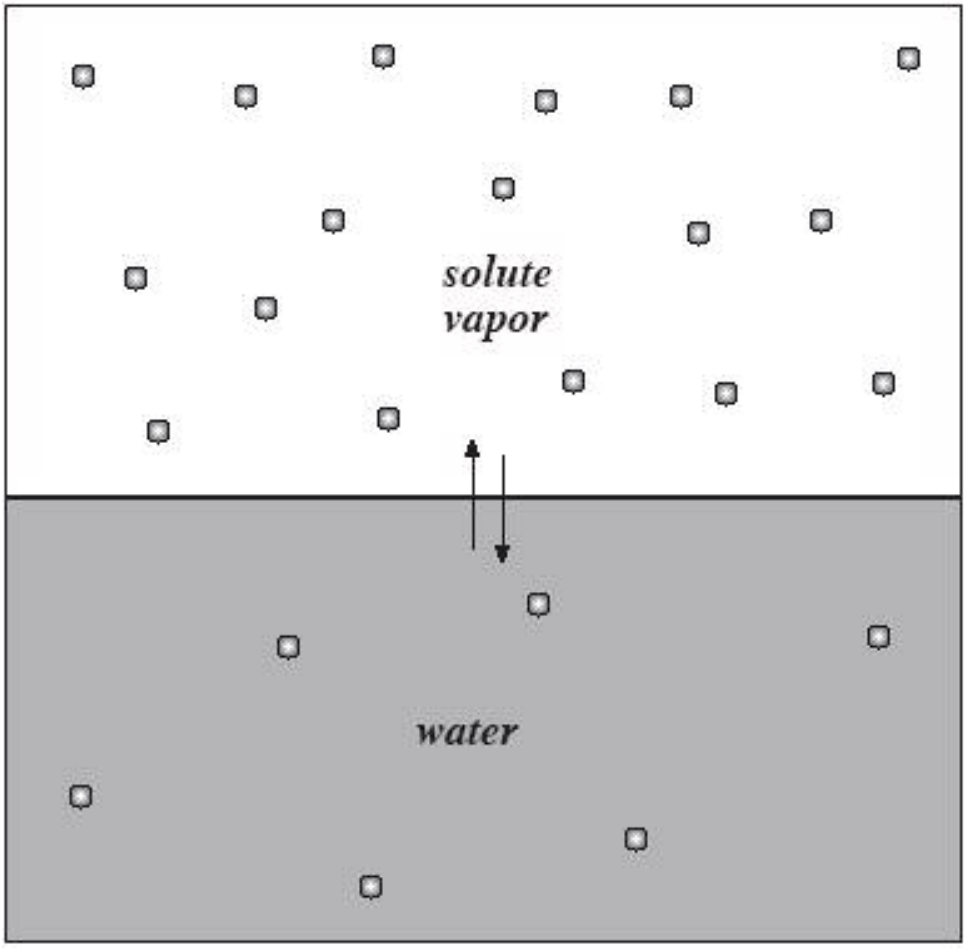

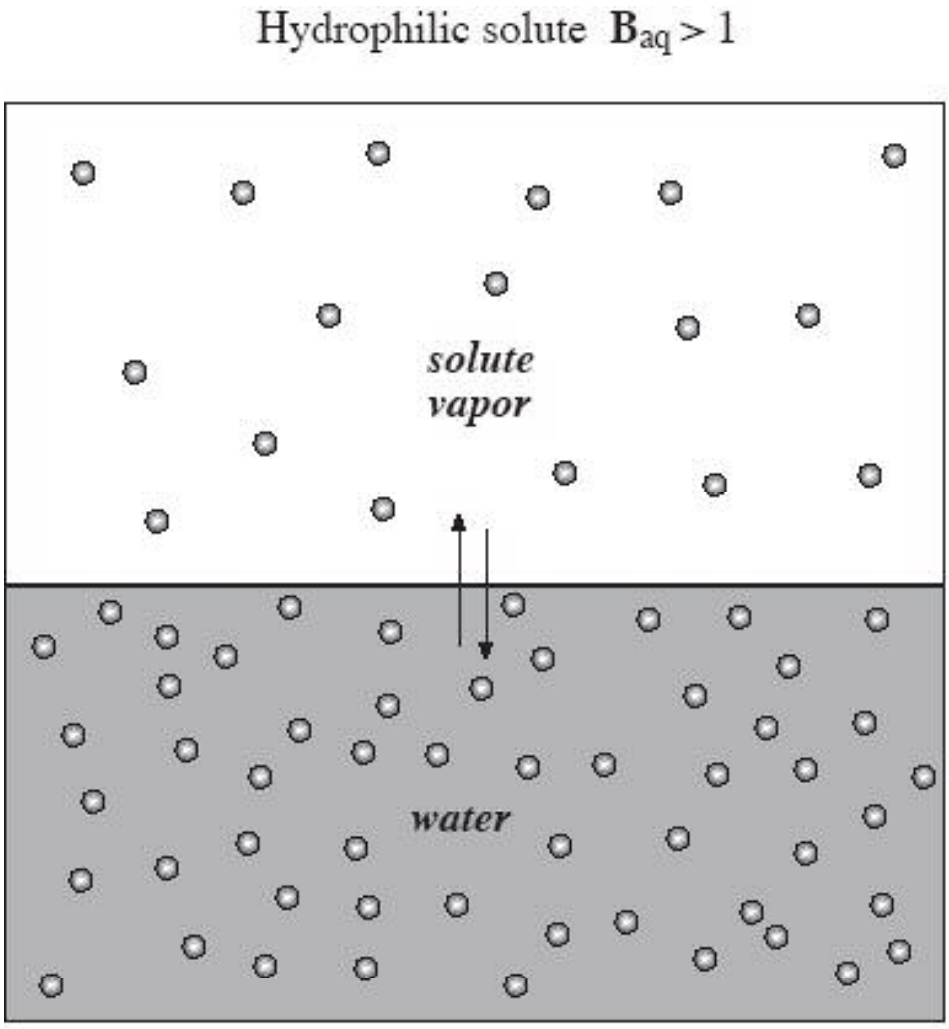

Figure 3.1: Insertion factor B is used to describe hydrophobic/hydrophilic solute in water.

Solubility of non-polar solutes in water is lower than in organic solvents, and at the same time solvation entropies of non-polar solutes are more unfavorable in water than in organic solvents. There appears to be a good correlation between solubility and solvation entropy. Another support for this entropy-dominate-solubility theory is for the normal alkanes with small carbon numbers (< C_{11}), the solubility in room temperature water decreases as the carbon number increases, while the solute size increases to make the solvation entropies more unfavorable.

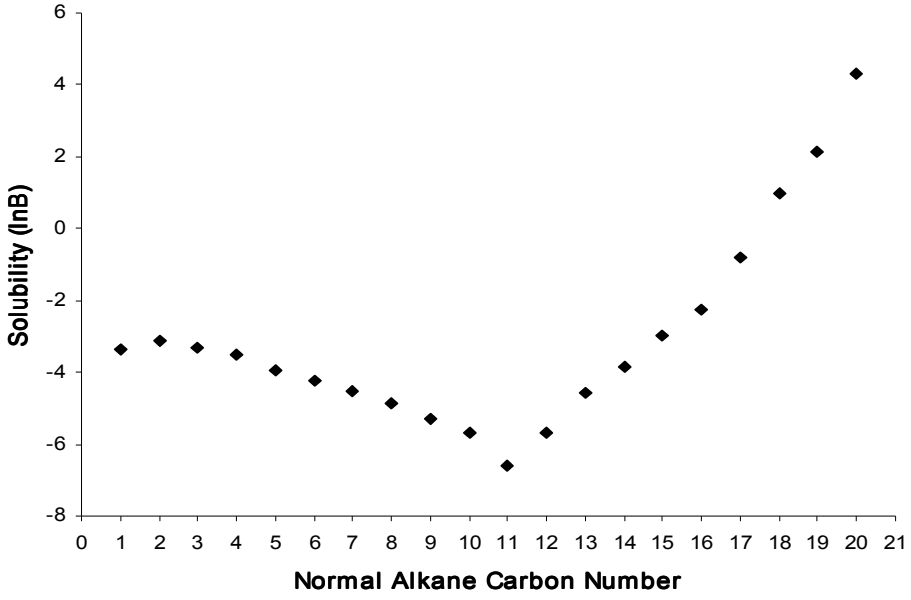

Figure 3.2: Room temperature solubilities of n-alkane pass through a minimum at carbon number 11. Solubility shown is the dimensionless Henry's Law solubility (lnB), and data are from the NIST database.[39]

However, if we look at the normal alkanes beyond C_{11} in Figure 3.2, the solubility in water starts to increases despite the entropy is still getting more unfavorable.

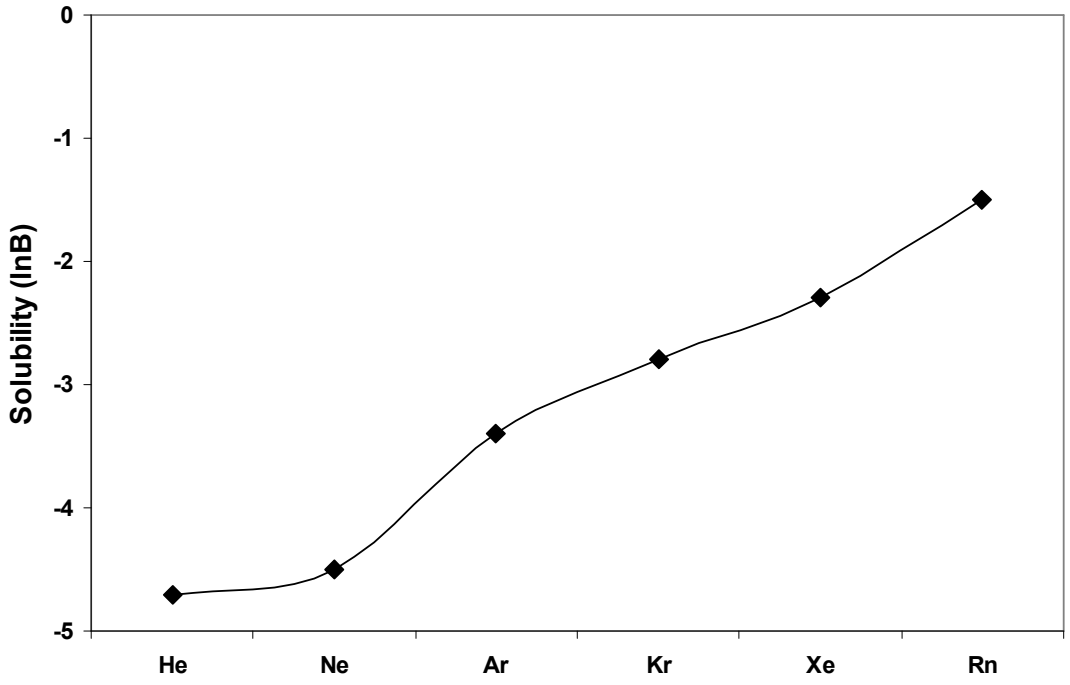

Figure 3.3: Solubility of inert gases in water at 298K. Experimental data is taken from NIST Chemistry webbook.[39]

The solubility of inert gases in water at 298 K is shown in Figure 3.3. The solute size is getting bigger from Helium to Radon, so it is getting harder to find a cavity in water large enough to accommodate the solute. However, the solubility rises up although the entropy penalty gets worse as the solute size increases.

In Figure 3.4, solvation entropy is plotted vs. van der Waals surface area for hydrophobic as well as hydrophilic solutes. Solvation entropy scales with solute size, i.e. the entropy gets more unfavorable as the van der Waals surface area of solute increases. This shows that solvation entropy does not determine solubility, since systematic difference can not be found here between hydrophobic and hydrophilic solutes. However, a linear correlation is observed between solubility and solvation enthalpy in Figure 3.5. Solvation enthalpy, instead of entropy, is the factor controls solubility.

Table 3.1: Solubility, solvation enthalpy and entropy data for selected solutes in water at 298K. Data listed here are used to generate Figure 3.2, 3.3 and 3.4. Solubilities (*lnB*) are experimental data.[39] VDW radii are from Bondi[36] VDW surface area are calculated using Van Krevelen's method.[37] Bond length are from the CRC Handbook.[38]

	VDW Surface Area ($\bullet^2$)	Solvation Enthalpy $\Delta h_p / kT$	Solvation Entropy $\Delta s_p / k$	Solubility $\ln B$
Hydrophobic Solutes				
$C(CH_3)_4$	359	-11.3	-15.8	-4.5
Ne	29.8	-1.5	-6.0	-4.5
N_2	58.4	-4.4	-8.5	-4.1
$n\text{-}C_4H_{10}$	290	-10.3	-13.9	-3.5
O_2	54.2	-5.3	-8.8	-3.5
Ar	44.4	-5.0	-8.4	-3.4
CH_4	101	-5.7	-9.1	-3.4
C_3H_8	230	-9.0	-12.3	-3.3
C_2H_6	166	-7.7	-10.7	-3.1
Kr	51.3	-6.3	-9.1	-2.8
Xe	58.6	-7.3	-9.6	-2.3
Rn	72	-8.7	-10.2	-1.5
CCl_4	171	-13.7	-13.8	-0.1
Hydrophilic Solutes				
Cl_2	71.0	-10.7	-10.3	0.4
CH_3Cl	118	-11.0	-10.0	1.0
$CHCl_3$	154	-13.3	-11.5	1.8

CH_2Cl_2	136	-13.0	-10.7	2.3
Br_2	76.9	-13.3	-10.4	2.9
CH_3OCH_3	190			3.2
I_2	83.7	-14.7	-10.8	3.9
C_2H_5CHO	231	-19.0	-13.2	5.8
CH_3CHO	163	-19.0	-13.1	5.9
$n\text{-}C_3H_7OH$	263	-24.0	-15.8	8.2
C_2H_5OH	195	-21.0	-12.6	8.4
HCHO	94.3	-22.7	-11.5	11.2

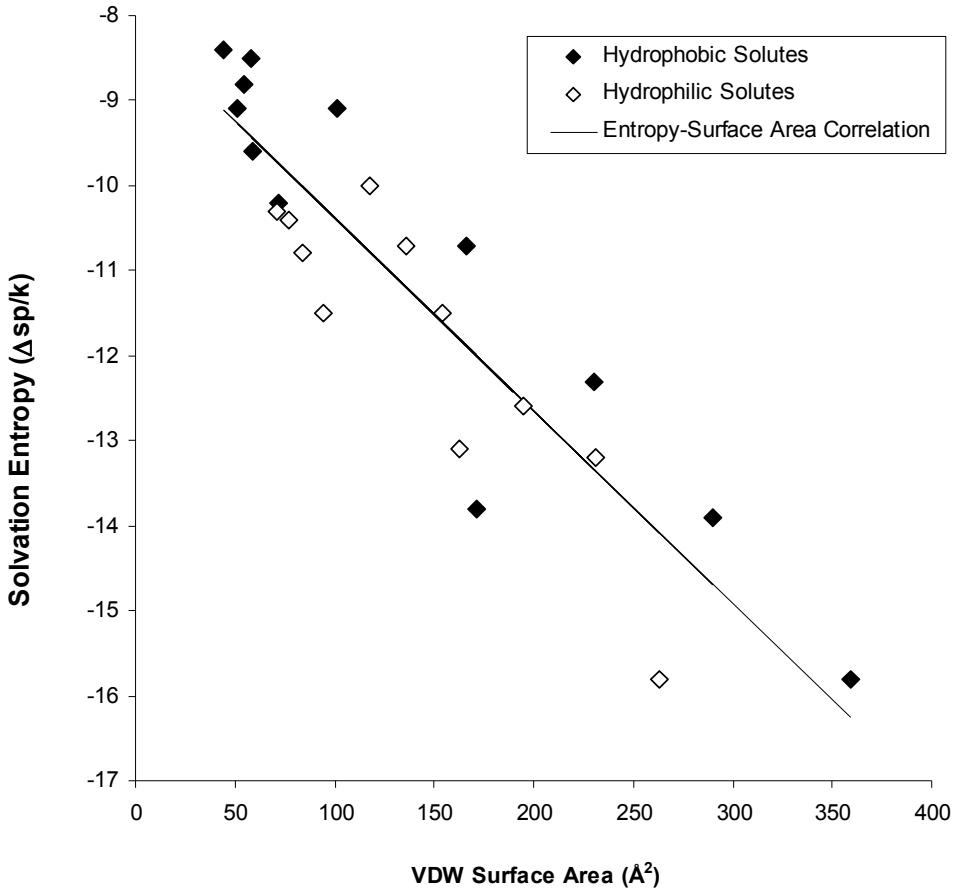

Figure 3.4: Solvation entropy vs. van der Waals surface area. The solvation entropy scales with solute size.

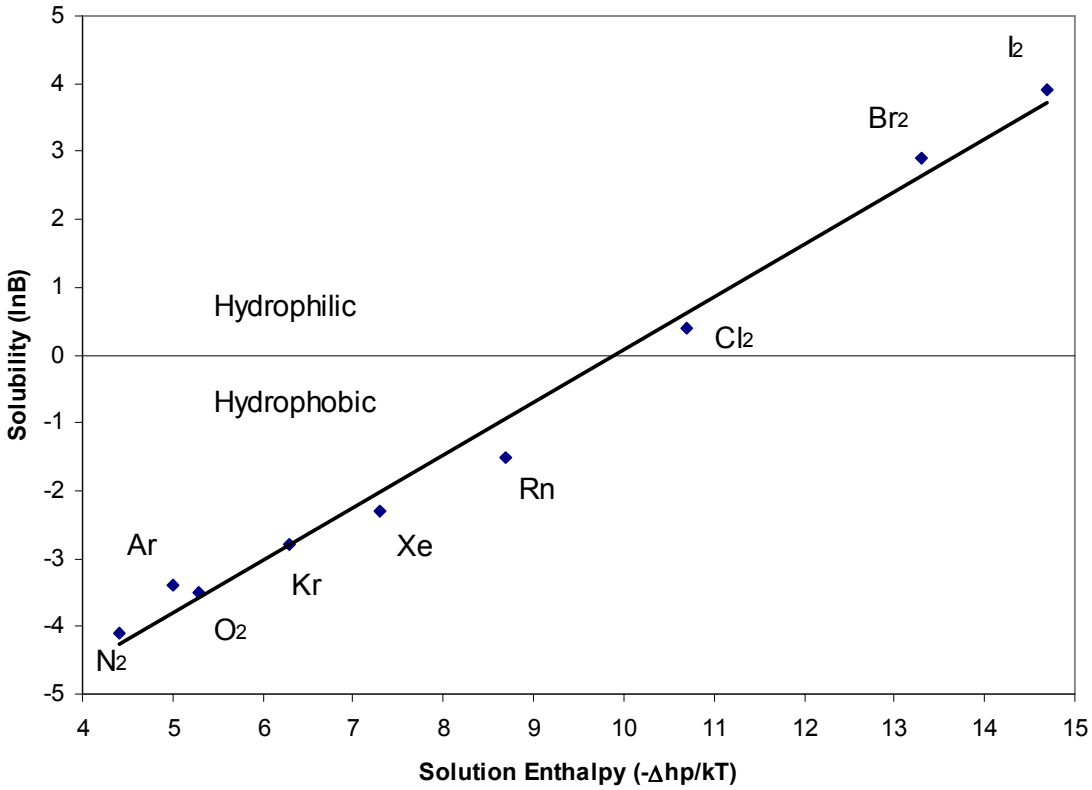

Figure 3.5: Solubilities of inert gases, hydrophobic diatomic gases and halogens in water at 298K. From N_2 to I_2 as the solute size increases the probability of finding solute size-cavities decreases and so does the solvation entropy. On other hand, as the solutes size increases more electrons bring more favorable interactions with water, so the solvation enthalpy ($-\Delta h_p/kT$) increases. Solubilities rise with enthalpy, and solvation enthalpy is the controlling factor in solubility.

Based on the discussions above, these points exist for gas solubilities in water:

1) Solubility of inert and diatomic gases increases with size.

2) Solubility of inert and diatomic gases correlates with solvation energy and not entropy.

3) Even for the normal alkanes, the solubilities of the alkanes increase with size beyond C_{11}.

4) Both hydrophobic and hydrophilic solutes have similar solvation entropies.

5) Below the normal boiling point of water, solubility increases with decreasing temperature.

Gas solubilities in water consist of an enthalpy term and an entropy term. The enthalpy term, or the energetic term, is the dominant factor.

3.3.3 Solubility minimum

In the previous section, as a proof that solvation entropy is not the controlling factor in solubility, we mentioned that gas solubility increases as temperature decreases when temperature is below the normal boiling point of water. Given the data are along the water coexistence curve, the coexistence density increases as temperature decreases. However, as shown in Figure 3.6, the trend changes at higher temperatures. The solubility vs. temperature curve has a minimum. Figure 3.6 compares simulation and experimental data for xenon in water along the water coexistence curve. Our simulation captures the solubility minimum.

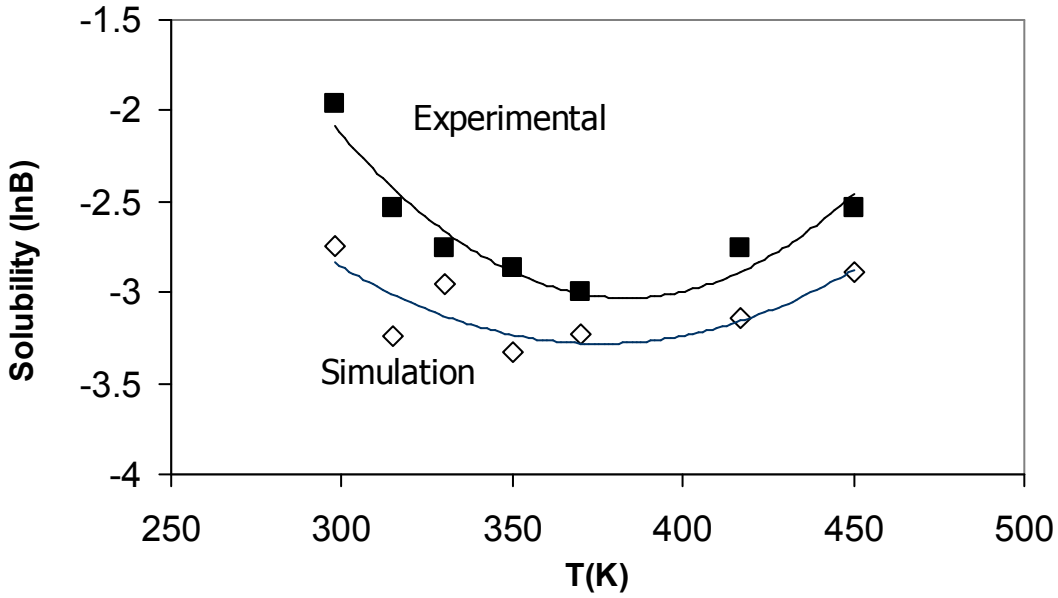

Figure 3.6: Xenon solubility in water along the water coexistence curve. Both experimental and simulation data show the solubility minimum near the normal boiling point of water.

The solubility minimum is not only observed for hydrophobic gases in water, our simulation predicted it for hydrophilic solute dimethyl ether (DME). DME is slightly soluble in water at room temperature. Figure 3.7 shows a minimum that is deeper than it in the Xe-water system.

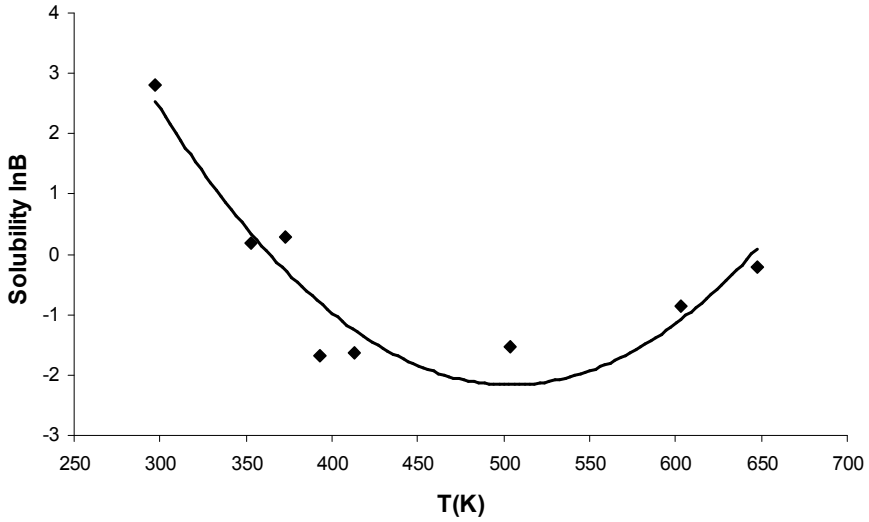

Figure 3.7: DME (dimethyl ether) solubility in water along the water coexistence curve. Monte Carlo simulations on expanded ensemble of one DME and 512 water molecules were done to get these results. The experimental data for solubility is 3.2 at 298 K.[39]

Solubility minimum is not unique in aqueous solutions. For example, it has been observed in methane and n heptane solution (see Figure 3.8).

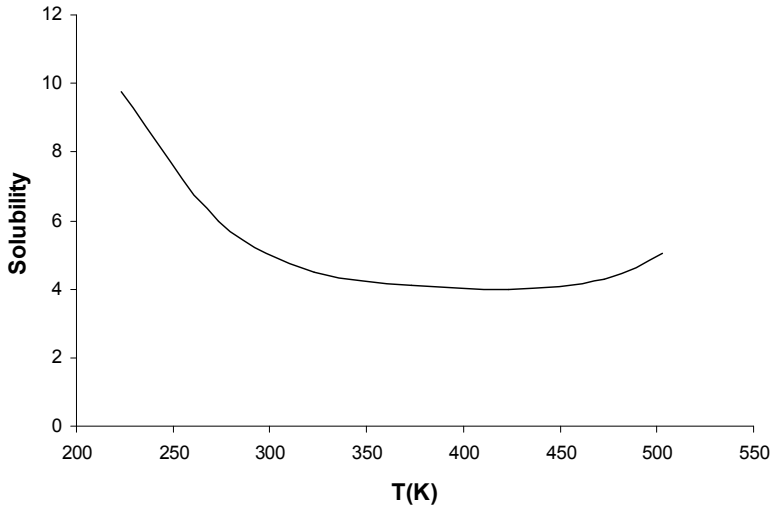

Figure 3.8: Solubility of methane in n-heptane[40]. A minimum exists at around 400K.

To find the origin of the solubility minimum, it is natural to first look at the molecular interaction between solute and solvent. Shown in Figure 3.9 are the solubilities of xenon in water, and of a hard sphere which has the same size as xenon in water. The latter does not have a minimum. The lack of attractive solute-solvent interaction makes the solubility a linear relation with the solvent density. As the density of water decreases as the temperature increases along the water coexistence curve, the probability of locating a cavity which is big enough to accommodate the hard sphere increases.

This behavior can be explained by looking at the two terms contribute to the solubility[6].

$$\ln B = -\beta\langle\psi\rangle + \Delta s_{\text{int}} / k \tag{3.14}$$

where B is called the insertion factor, which represents the solubility, and it can be directly related to the Henry's Law constant. ψ is the solute-solvent interaction, and $\langle\psi\rangle$ is the ensemble average of it. Δs_{int} is the interaction entropy and β is $1/kT$. In aqueous solutions, the hydrophobic solute such as inert gases and hydrocarbons interacts with water through dispersion, which can be well modeled by LJ interaction. Because of the attractive tail, the average ensemble average $\langle\psi\rangle$ is always negative, and the energetic contribution to the solubility ($-\beta\langle\psi\rangle$) is always positive, or favorable. The interaction entropy term is always negative, or unfavorable, in the solution because the attractive solute-solvent interaction lessen the freedom of movement of this system

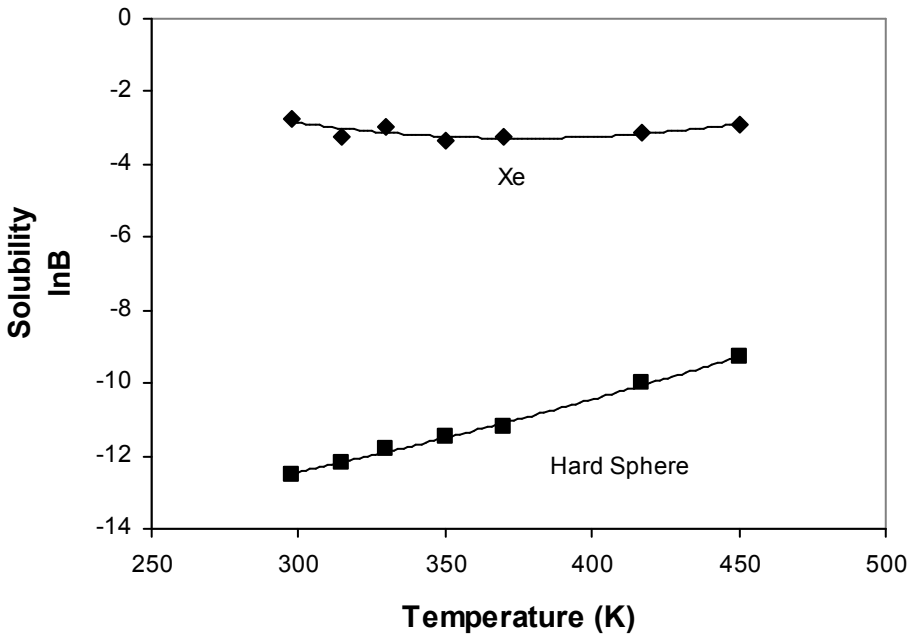

Figure 3.9: Comparing solubilities of xenon and hard sphere in water. Both are MC simulation results. The hard sphere has been assigned the size of xenon. Simulations have been done along the water coexistence curve, and the density of the solvent decreases as temperature increases. Unlike xenon, the hard sphere does not have a solubility minimum.

Figure 3.10 shows the solubility of xenon in water, and the two terms contributed to it: energy and entropy. As temperature goes up, the energy term decreases due to two reasons: the system has become less dense and the reciprocal temperature embedded in the β term makes the energy term less effective as temperature goes up. The entropy increases because the reducing density allows more free space in the solvent and more cavities large enough to accommodate the solute can be found. The competition is won by the energy at low temperature, but at high temperature the entropy term dominates.

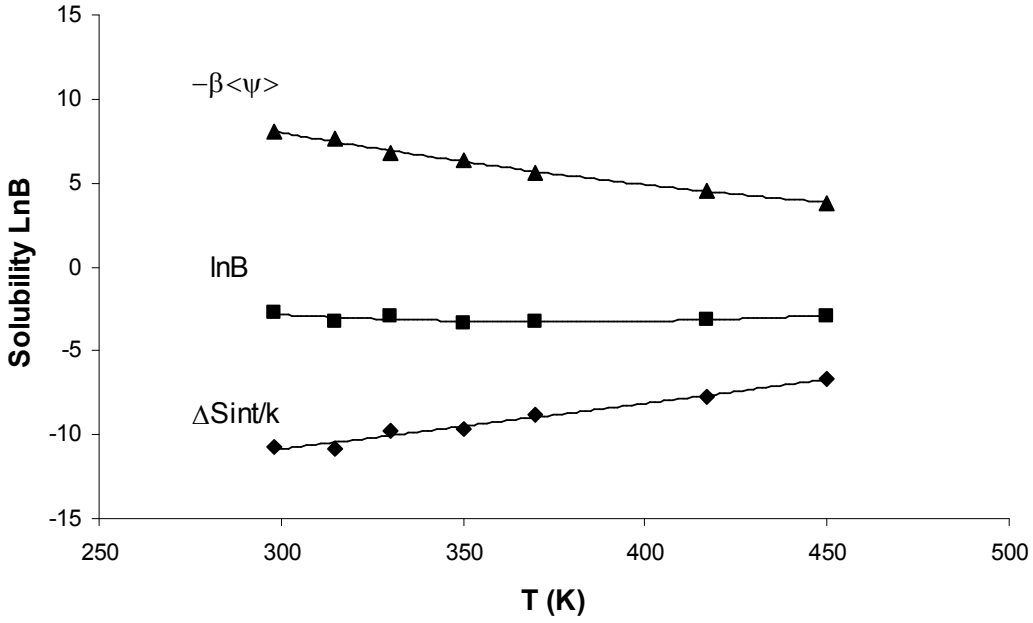

Figure 3.10: The solubility of xenon in water along the water coexistence curve. Data from MC simulation in expanded NVT ensemble. The solubility consists of a favorable energy term and an unfavorable entropy term. The minimum is the result of the competition between these two factors.

Similarly the solubility of dimethyl ether (see Figure 3.11) can be represented as the sum of an energetic term and an entropic term. The hydrophilic solute has solubility minimum that is deeper than those hydrophilic solutes. The solute-solvent interaction is larger in the hydrophilic system due to the existence of columbic interaction between the solute and water, both with charges on the molecules. If we plot both LJ and columbic interaction, the latter is much larger in absolute value.

Xe solubility in water at constant water density as temperature increases is shown in Figure 3.12. The water density is fixed to 995.61kg/m^3. The interaction entropy term $\Delta s_{\text{int}}/k$ almost keeps constant as temperature changes, and the energy term $-\beta\langle\psi\rangle$ decreases as temperature increases because of the reciprocal temperature effect.

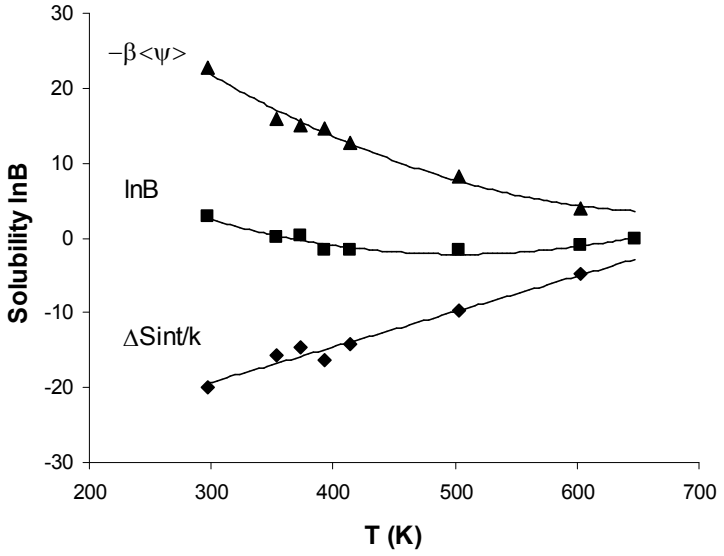

Figure 3.11: The solubility of DME (dimethyl ether) in water along the water coexistence curve. Data from MC simulation on expanded NVT ensemble. Hydrophilic solute has a solubility minimum just as the hydrophobic solute does.

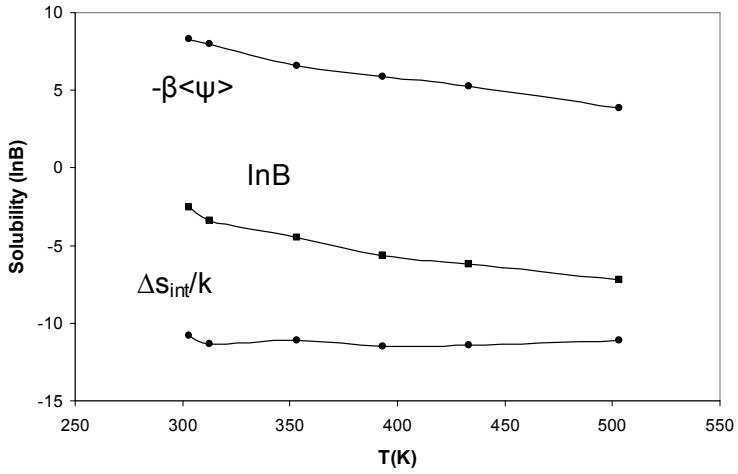

Figure 3.12: The solubility of Xe in water at constant water density (995.61kg/m^3). The solubility does not show any minimum in this case. Since the density is fixed the interaction entropy almost keeps constant, and the interaction energy term decreases as temperature increases because of the reciprocal temperature effect ($\beta = \frac{1}{kT}$).

3.4 Conclusions

At low temperature, gas solubility is primarily controlled by solvation energetics, not entropy.

Solubility minima are the result of favorable energetic interactions competing with a unfavorable entropic penalty.

[1] W. Kauzmann, Adv. Protein Chem. 14, 1 (1959).
[2] K. Dill, Biochemistry 29, 7133 (1990).
[3] K. P. Murphy, P. L. Privalov and S. J. Gill, Science 247, 559 (1990).
[4] P. L. Privalov and S. J. Gill, Pure & Appl. Chem. 61, 1097 (1989).
[5] H. S. Frank and M. W. Evans, J. Chem. Phys. 13, 507 (1945).
[6] Matthew T. Stone, Pieter J. in't veld, Ying Lu and Isaac C. Sanchez, Molecular Physics, 100, 2773 (2002).
[7] R. A. Pierotti, J. Phys. CHem. 69, 281 (1965),
[8] G. Graziano, J. Chem. Soc. Faraday Trans, 94, 3345 (1998).
[9] B. Lee, Biopolymers, 24, 813 (1985).
[10] Giuseppe Graziano, Chemical Physics Letters, 396, 226 (2004).
[11] F. H. Stillinger, J. Sol. Chem. 2, 141 (1973).
[12] A. Ben-Naim, H. L. Friedman, J. Phys. Chem. 71, 448 (1967).
[13] Isabel Tomas-Oliveira and Shoshana J. Wodak, J. Chem. Phys. 111, 8576 (1999).
[14] A. Pohorille, L. R. Pratt, J. Am. Chem. Soc. 112, 5066 (1990).
[15] K. Tang, V. Bloomfield, Biophys. J. 79, 2222 (2000).
[16] Lawrence R. Pratt, Annu. Rev. Phys. CHem. 52 (2002).
[17] L. R. Pratt and D. Chandler, J. Chem. Phys. 67, 3683 (1977).
[18] L. R. Pratt, Annu. Rev. Phys. Chem. 36, 433 (1985).
[19] G. Hummer, S. Garde, A. E. Garcia, M. E. Paulaitis, and L. R. Pratt, J. Phys. Chem. B. 102, 10469 (1998).
[20] G. Hummer, S. Garde, A.E. Garcia, and M. E. Paulaitis, Proc. Natl Acad. Sci. U.S.A. 95, 1552 (1998).
[21] B. Widom, J. Chem. Phys. 39, 2808 (1963).
[22] B. Widom, J. Phys. Chem. 86, 869 (1982).
[23] H. J. C. Berendsen, J.R. Grigera, and T. P. Straatsma, J. Phys. Chem., 91, 6269 (1987).
[24] B. Guillot and Y. Guissani, J. Chem. Phys. 99, 8075 (1993).
[25] B. Lin and J. W. Halley, J. Phys. Chem. 99, 16474 (1995).
[26] Matthew T. Stone, Mente Carlo Approaches to the Protein Folding Problem, The University of Texas at Austin, 2002
[27] Y. V. Vorobjrv and J. Hermans, J. Phys. Chem. B 103, 10234 (1999).
[28] G. C. Boulougouris, I. G. Economou, and D. N. Theodorou, J. Phys. Chem. B, 102, 1029 (1998).
[29] A. P. Lyubartsev, A. A. Martsinovski, S. V. Shevkunov, and P. M. Vorontsov-Velyaminov, J. Chem. Phys. 96, 1776 (1992).
[30] A. P. Lyubartsev, O. K. Forrisdahl, and A. Laaksonen, J. Chem. Phys. 108, 227 (1998).
[31] P. A. Egelstaff, An Introduction to the Liquid State, Academic Press, London (1967).
[32] Harry R. Allcock and Frederick W. Lampe, Contemporary Polymer Chemistry, Second Edition, Pretentice Hall, Englewood Cliffs, New Jersey (1990).
[33] A. Striolo and J. M. Prausnitz, Polymer 42, 4773 (2001).
[34] A. Ben Naim, Water and Aqueous Solutions, Plenum, New York, 1974.
[35] B. Guillot, Y. Guissani, and S. Bratos, J. Chem. Phys. 95, 5 (1991).
[36] A. Bondi, J. Phys. Chem. 68, 441 (1964).
[37] D. W. Van Krevelen, Properties of Polymers, 3rd Edition, Elsevier, Amsterdam (1990).

[38] D. R. Lide, CRC Handbook of Chemistry and Physics, 75th Edition, CRC Press, Boca Raton, Florida (1994).
[39] R. Sander, in "Henry's Law Constants" in NIST Chemistry WebBook, NIST Standard Reference Database Number 69, edited by W. G. Mallard and P. J. Linstrom (National Institute of Standards and Technology, Gaithersburg, MD, 20899, 2000), (url: http://webbook.nist.gov).
[40] J. M. Prasunitz, R. N. Lichtenthaler and E. G. de Azevedo, Molecular Thermodynamics of Fluid Phase Equilibria, Prentice Hall, Upper Saddle River, NJ, 3rd Edition (1999).

Chapter 4 Monte Carlo Studies of Polymer Chain in Aqueous Solutions

4.1 Introduction

Protein folding is a very important problem in biology and it has attracted many research interests in the past decades.[1] Research on the solubility behaviors of hydrophobic entities can shed some light on protein folding problem. Previous simulations have been done to study alkanes[4,5,6] and aqueous solutions of alkanes.[2]

Figure 3.2 shows the anomalous behavior of normal alkane solubilities in water. At room temperature, as carbon number increases, the chain solubility in water first decreases, then increases. It has a minimum at undecane (C_{11}). The solubility of eicosane (C_{20}) in water is larger than methane, and it is positive, which means the concentration of the alkane in water is larger than in the vapor phase.

For infinite dilute solutions, the Henry's Law constant governs solubility. It is well studied and there have abundant resource, both experimental and theoretical, on this data. At low pressure where the vapor phase can be considered ideal, the dimensionless Henry's Law constant B is defined as,

$$B = \frac{c_l}{P/RT} = \frac{c_l}{c_{ig}} \tag{4.1}$$

where c_l is the concentration of solute in the solvent phase, and c_{ig} is the concentration of solute in vapor phase (which can be considered as ideal gas phase). The ratio of c_l and c_{ig} equals to the ratio of the insertion factor of solute in solvent phase (B_l), and it in vapor phase (B_{ig}),

$$\frac{c_l}{c_{ig}} = \frac{B_l}{B_{ig}} = \exp(-\beta(\mu_{ex} - \mu_{ex}^{ig})) \tag{4.2}$$

in which $\beta = 1/k_B T$ is the reciprocal temperature where k_B is the Boltzmann constant, μ_{ex} is the excess chemical potential in the solvent phase, and μ_{ex}^{ig} is the excess chemical

potential in the vapor phase. Therefore, the Henry's Law constant B (or the solubility in this chapter) is,

$$B = \exp(-\beta(\mu_{ex} - \mu_{ex}^{ig})) \tag{4.3}$$

or,

$$\ln B = \ln B_l - \ln B_{ig} = -\beta\mu_{ex} + \beta\mu_{ex}^{ig} \tag{4.4}$$

So it is possible that the solubility can be calculated from chemical potentials in solvent and ideal gas phase, and our Monte Carlo simulations performed on chain models in water and vacuum measured these chemical potentials. For chain molecules, ideal gas phase actually is modeled by an ideal gas chain in vacuum, and an ideal gas chain is a chain with only intra-molecular interactions.

Worth noting here is for both ideal gas phase and aqueous phase, the contribution to the solubility is the free energy difference term between the state with chain in the phase and the state with an ideal chain in that same phase:

$$\ln B_l = -\beta\mu_{ex} = -\beta\left(\mu - \mu^{ic}\right) \tag{4.5}$$

$$\ln B_{ig} = -\beta\mu_{ex}^{ig} = -\beta(\mu^{ig} - \mu^{ic}) \tag{4.6}$$

where μ^{ic} is the chemical potential of an ideal or unperturbed chain which means no intra-chain interaction will be considered.

A freely jointed Lennard-Jones chain (bond length is fixed to be equal to the LJ particle size) was used to model the hydrophobic alkanes and Figure 4.1 shows the calculated solubilities[2] of n-alkanes in SPC/E water. The simulation results qualitatively reproduced a solubility minimum at around C_{12}, but it is not a sharp one as shown in the experimental value. As have been mentioned earlier in this section, the solubility (*lnB*) in Figure 4.1 is the sum of $\beta\mu_{ex}^{ig}$ and $-\beta\mu_{ex}$, which represents contributions from the ideal gas phase and the aqueous phase.

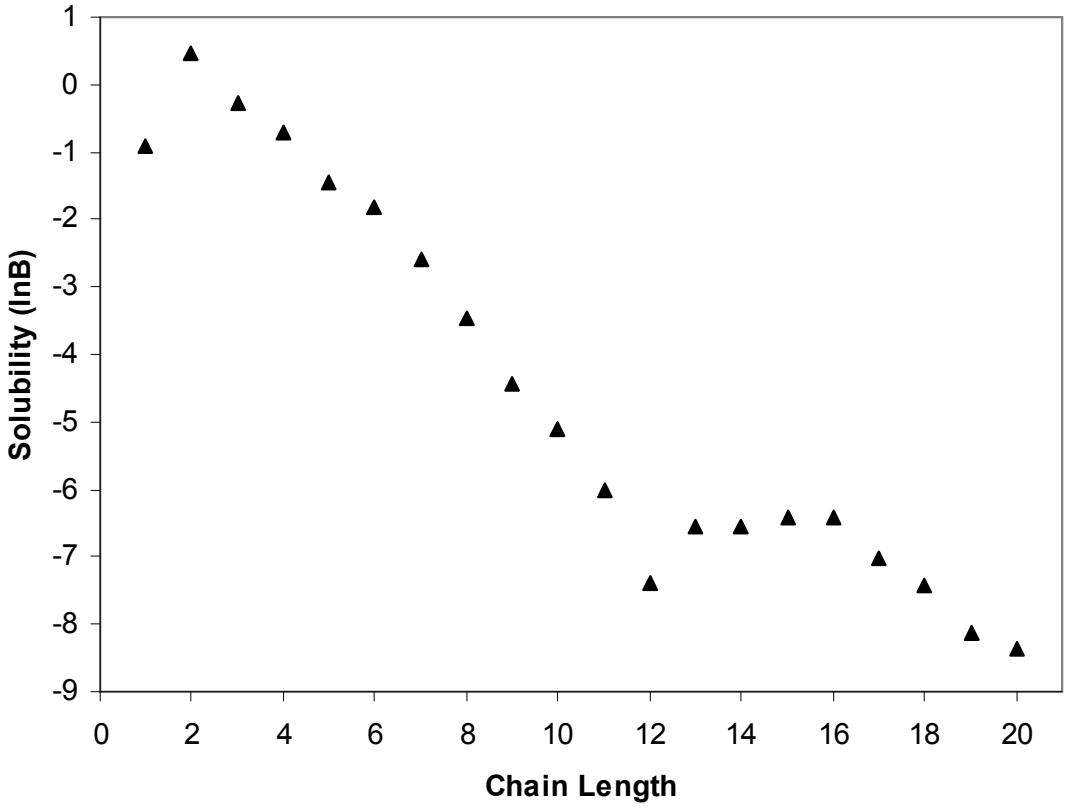

Figure 4.1: Aqueous solubility of n-alkanes at 298 K vs chain length from Monte Carlo simulations.[2] Comparing with the experimental data in Figure 3.2, the shorter chains (with carbon number from 2 to 12) the solubility behavior is captured by simulation quantitatively. The solubilities of the longer chains (carbon number above 12) in contrast are not increasing in the way shown in the experimental data.

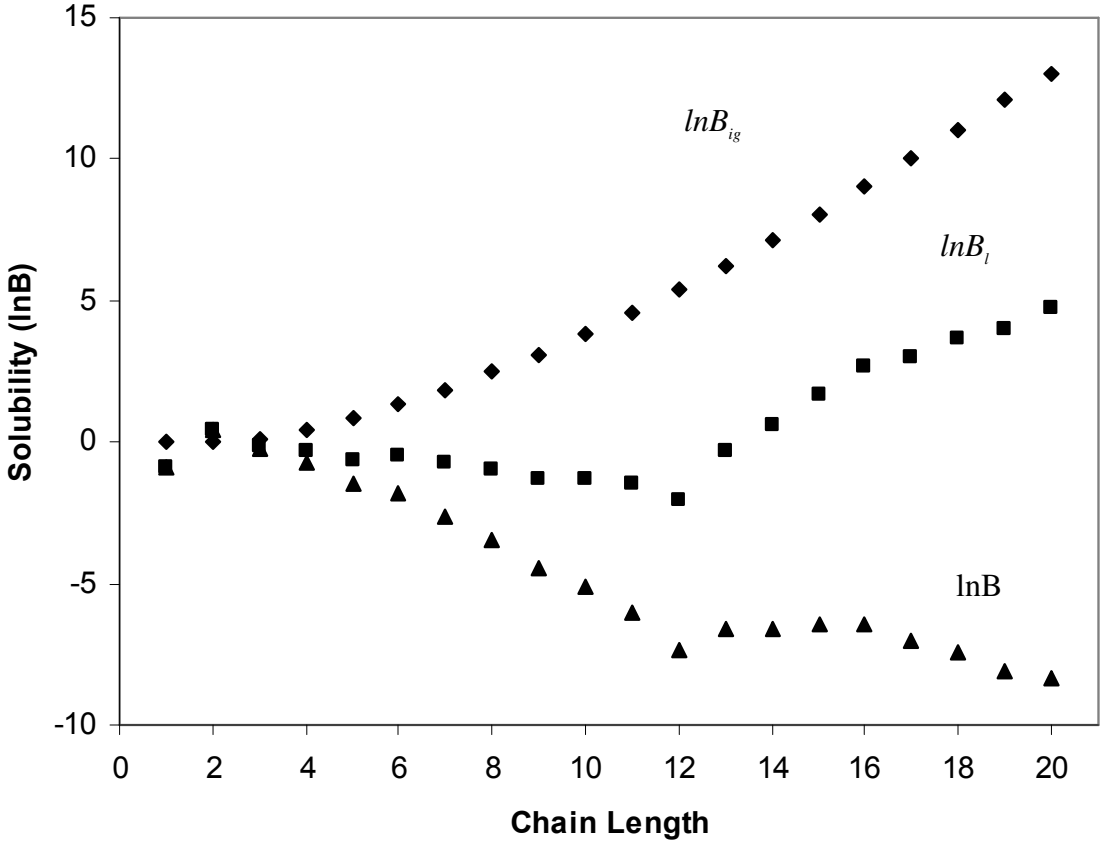

Figure 4.2: Chemical potential contributions to the solubility.[2] The solubility (triangles) decomposed into the ideal gas phase contribution (diamonds) and the aqueous phase contribution (squares).

In Figure 4.2, the free energy difference of inserting the alkane chain in water phase ($\ln B_l$) first decrease with chain size, then increase, and has a minimum at C_{12}. The curve shape is similar to the experimental data shown in Figure 3.2. The second branch (from C_{12} to C_{20}) flattens out as the ideal gas phase contribution ($\ln B_{ig}$) is added to get the solubility $\ln B$. Since a freely jointed chain with fixed bond length was used to model alkane to calculate the solubilities, it has been conjectured that by using a chain model with bond angle constraints and restricted rotation,[2] we may have a better chance to

capture the alkane solubility minimum in aqueous solution. In this work hydrophobic normal alkane chain solubility was calculated by simulations and the effects of chain flexibility and intra-chain interaction on the solubility were assessed.

4.2 Methodology

SPC/E water is chosen to model water[3]. This non-polarizable three site water model has been described in chapter 2 of this dissertation. The alkane chain is represented by some united atom models, which includes a freely jointed LJ chain, a freely rotating LJ chain, and a chain with torsion interaction. To make our results comparable with previous work,[2] the LJ parameter σ of the freely jointed LJ chain has been assigned the value of the σ of the oxygen of SPC/E water model, and the parameter ε has been set to be 4 times of the value of ε of the oxygen of SPC/E water. The freely jointed chain fixes bond length to its particle size σ, and it doesn't have any other constraint. The freely rotating chain has the same σ, ε, and bond length as the freely jointed chain, but it also has bond angles (θ) fixed to be 109.5º.

Torsional interaction (which applies on every 4 consecutive particles along a chain) is added to freely rotating chain to examine its effect on intra-molecular interaction. The torsion interaction has the form[4,5,6]:

$$U_{tor}(\phi)/k_B = c_1(1+\cos\phi) + c_2(1-\cos 2\phi) + c_3(1+\cos 3\phi) \qquad (4.7)$$

where ϕ is the dihedral angle , and the parameters c_1, c_2 and c_3 can be found in Table 4.1. Torsion interaction is plotted in Figure 4.3. As shown in the plot, the torsion energy is large in magnitude compared to the LJ interaction.

Table 4.1: Molecular model parameters for n-alkanes. Non-bonded interaction refers only to LJ interaction for freely jointed or freely rotating chains. For the torsional interaction, ϕ is the dihedral or torsion angle.

Non-bonded Interaction	Torsion Interaction
$U_{lj}(r) = 4\varepsilon[(\sigma/r)^{12} - (\sigma/r)^{6}]$	$U_{tor}(\phi)/k_B = c_1(1+\cos\phi) + c_2(1-\cos 2\phi) + c_3(1+\cos 3\phi)$
$\sigma = 3.2\text{A}, \varepsilon/k_B = 312.8K$	$c_1 = 355.0K, c_2 = -68.2K, c_3 = 791.3K$

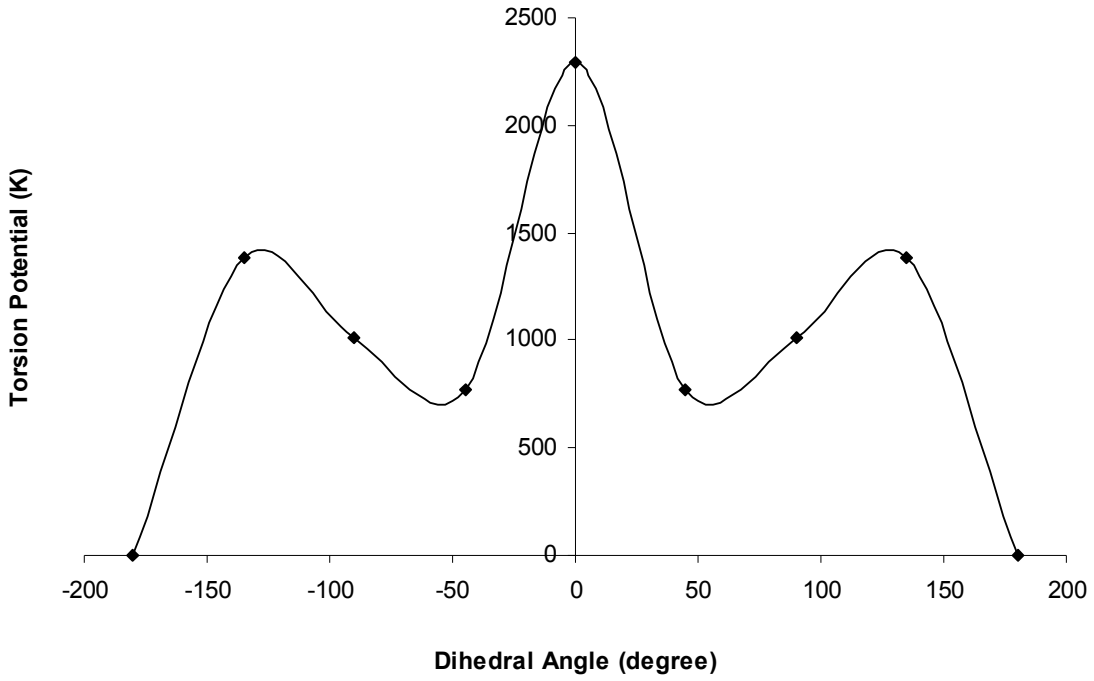

Figure 4.3: Torsion interactions vs. dihedral angle. Parameters are from literature4.

CCB (Continuum Configurational Bias)[7,8] Monte Carlo technique was used to assist chain movement. To calculate solubilities in aqueous solution, expanded ensemble method[9] was used instead of the traditional Widom insertion method since the possibility

of inserting a chain successful in room temperature water is vanishingly small due to the high density of water.

4.3 Results and Discussion

Comparing to the freely jointed chain, the freely rotating chain has one more constraint: bond angle. At room temperature a freely rotating chain was used as a model for alkane and in the ideal gas state it gave free energy results (lnB_{ig}) very close to those of a freely jointed chain model (See Figure 4.4). As the chain length increases, lnB_{ig} of the freely rotating chain becomes less than the freely jointed chain since the chain angle constraint has decreased the compactness of chain in water relative to the ideal chain state, so as to generate less favorable intra-molecular interaction energy.

For LJ chain in LJ solvent, our simulation data for freely rotating chain is compared with Frenkel and Smit's data for freely jointed chain as shown in Figure 4.5. The solvent is modeled by the same particle as the LJ chain monomer. These two results are very close. It proves that fixed chain angle does not affect the solubility much in non-polar solvent.

With the slight difference in the intra-chain interaction between these two models, we would expect the free energy contribution to the solubility from water phase, or the lnB_l term, of a freely rotating chain to be very close to that of a freely jointed chain, so it seems the fixed bond angle constraint alone will not help in the reproduce of the solubility minimum of normal alkanes in water.

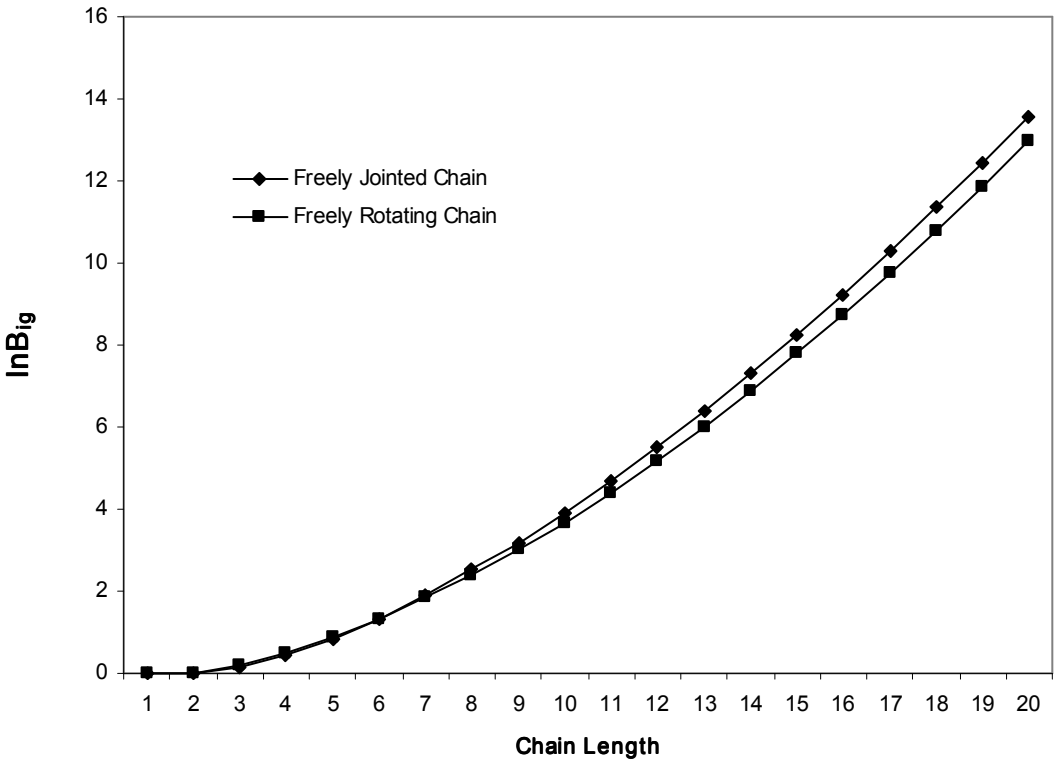

Figure 4.4:. The free energy contribution to the chain solubility from the ideal gas phase (lnB_{ig}) vs. chain length for a freely jointed chain and a freely rotating chain in vacuum at 298 K. A freely rotating chain model produces results very similar to a freely jointed chain.

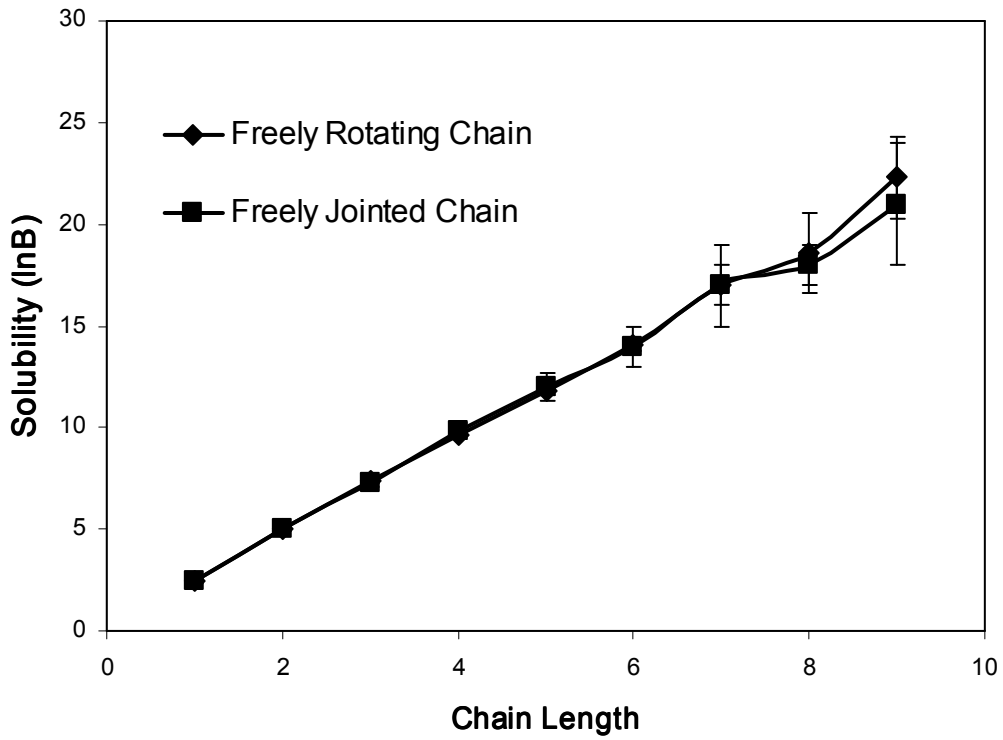

Figure 4.5: Solubility of an LJ chain in LJ solvent at reduced temperature T*=1.2, reduced density r = 0.6. Freely jointed chain data are from Frenkel and Smit's work.[10]

When torsion interaction is implemented on the chain, the free energy contribution to the solubility from the ideal gas phase (lnB_{ig}) behaves totally different. lnB_{ig} decreases very quickly as chain length increase, and unlike the previous chain models which are lack of torsion, lnB_{ig} results are negative as shown in Figure 4.6. As we have seen earlier in Figure 4.3, the torsion interaction is very strong and unfavorable. This repulsive torsion interaction on chain keeps chain from reaching a highly collapsed state, so the favorable non-bonded LJ interaction is relatively small in value, and as a result the total intra-chain interaction is still very unfavorable. If the contribution from the

water phase is similar for the torsion chain model as for the freely jointed chain model, the solubility minimum of normal alkane chain in water as shown in Figure 3.2 will be captured, because as shown in Figure 4.2, the *lnB* curve will have a sharp mimimum if the lnB_l curve keeps the same shape but the lnB_{ig} curve now goes down as shown in Figure 4.6 for the torsion chain model. Whether our assumption about the lnB_l curve of the torsion chain in water is valid will depend on the torsion interaction. It is known that a LJ chain is at its collapsed state in water at room temperature[2], but the torsion interaction we used made the intra-chain interaction unfavorable and it will work to prevent chain from collapsing. How the lnB_l change with chain length will be affected by the competition between the chain-water interaction and intra-chain interaction.

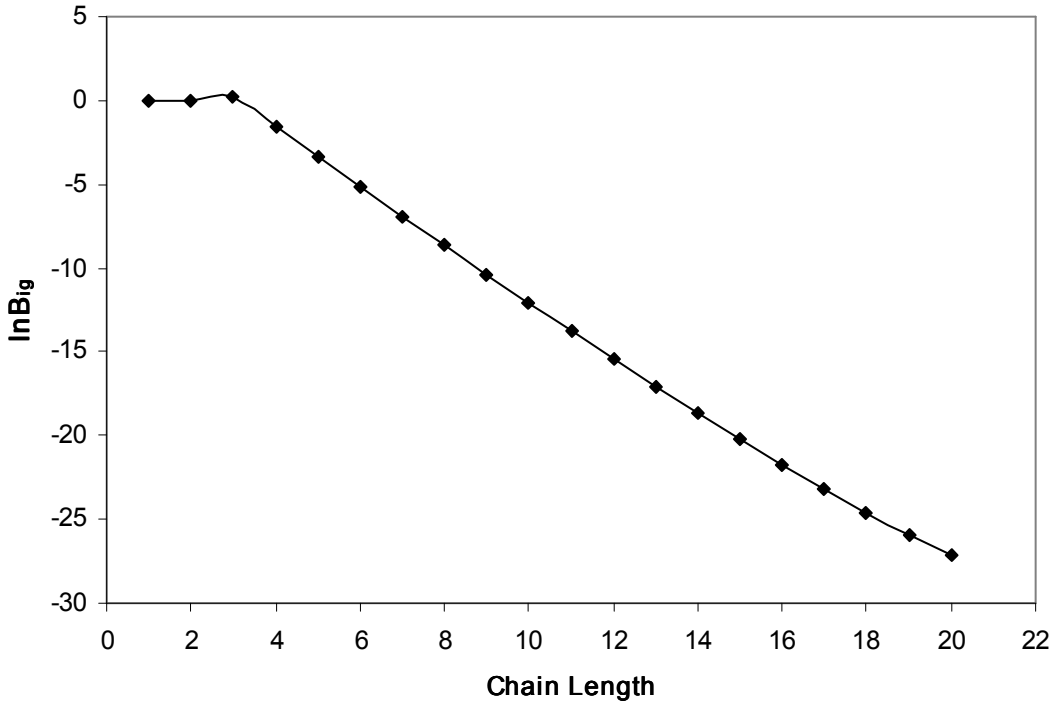

Figure 4.6: The free energy term (lnB_{ig}) vs. chain length of a LJ chain with torsion potential in vacuum at 298K. As the chain length increases, the torsion interaction makes lnB_{ig} decreases quickly.

How the lnB_{ig} term changes with chain length depends on temperature, too. The correlation is given in Figure 4.7. At low temperatures, lnB_{ig} has a minimum, but this minimum disappears as the temperature goes up. At room temperature it keeps decreasing as chain size grows. At extremely high temperature, for example, 3136 K for this model, the lnB_{ig} vs. chain length plot approaches a straight line, and lnB_{ig} only drops slightly as the chain size increases.

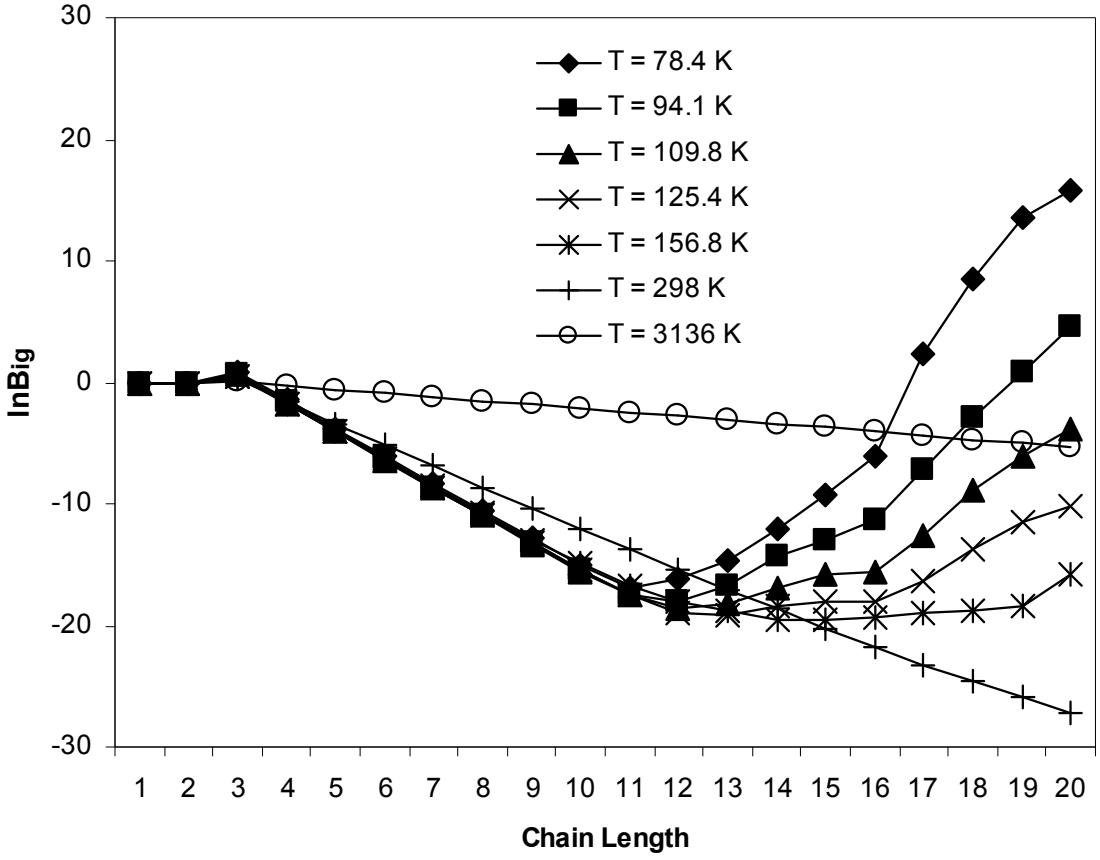

Figure 4.7: The free energy term (lnB_{ig}) vs. chain length of a LJ chain with torsion potential in vacuum. At low temperatures, e.g. 78.4 K, lnB_{ig} has a minimum. The minimum doesn't hold as temperature goes up to around room temperature.

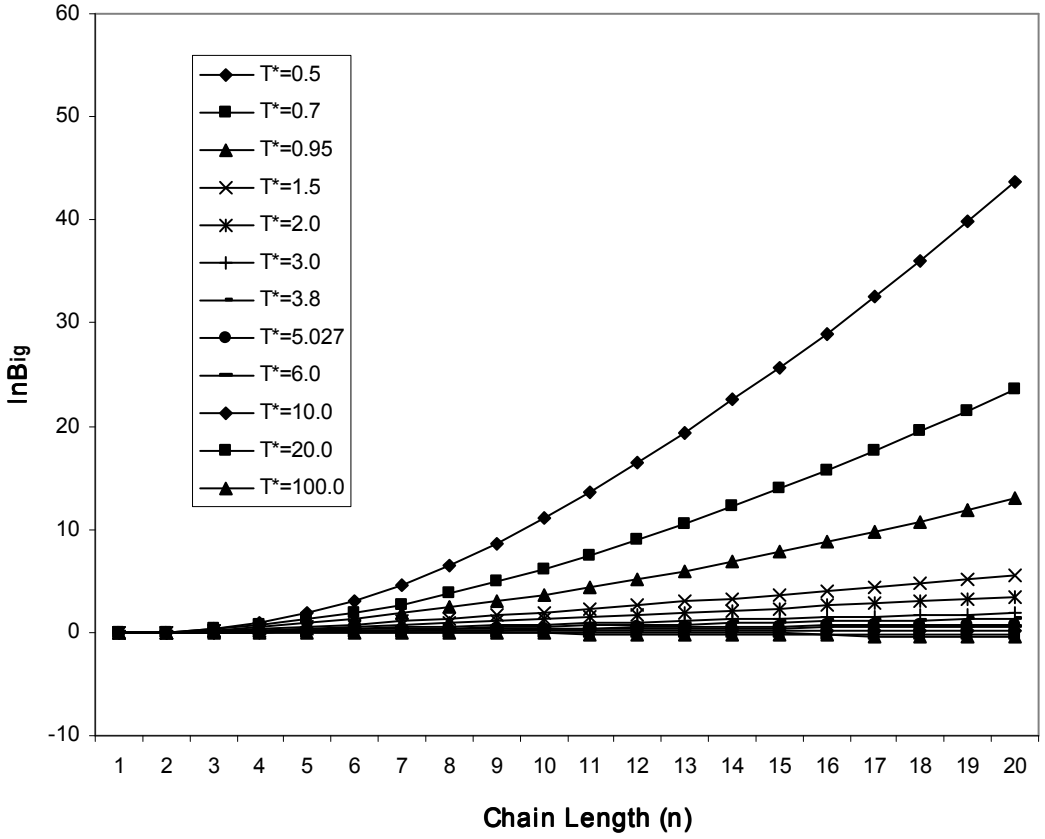

. Figure 4.8: The free energy term (lnB_{ig}) vs. chain length of a freely rotating LJ chain in vacuum. lnB_{ig} increases with chain length except at very high temperatures. At fixed chain length, the solubility decreases as the temperature increases.

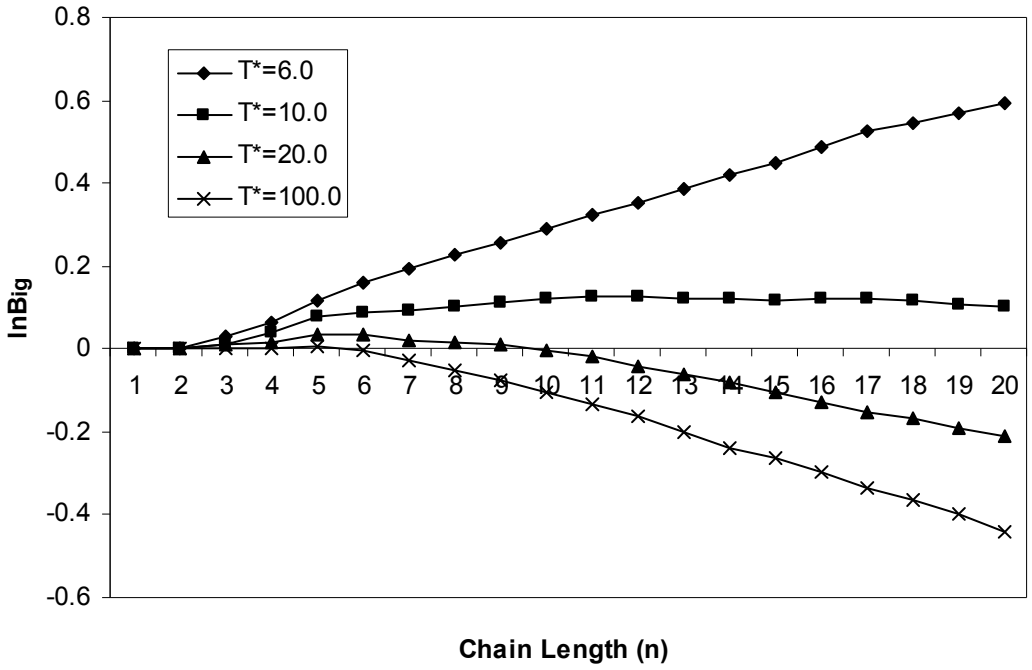

Figure 4.9: The free energy term (lnB_{ig}) vs. chain length of a freely rotating LJ chain in vacuum. To show that lnB_{ig} change from positive to negative at high temperatures, the date from figure 4.8 at T*=6.0, 10.0, 20.0, and 100.0 are shown on a larger scale.

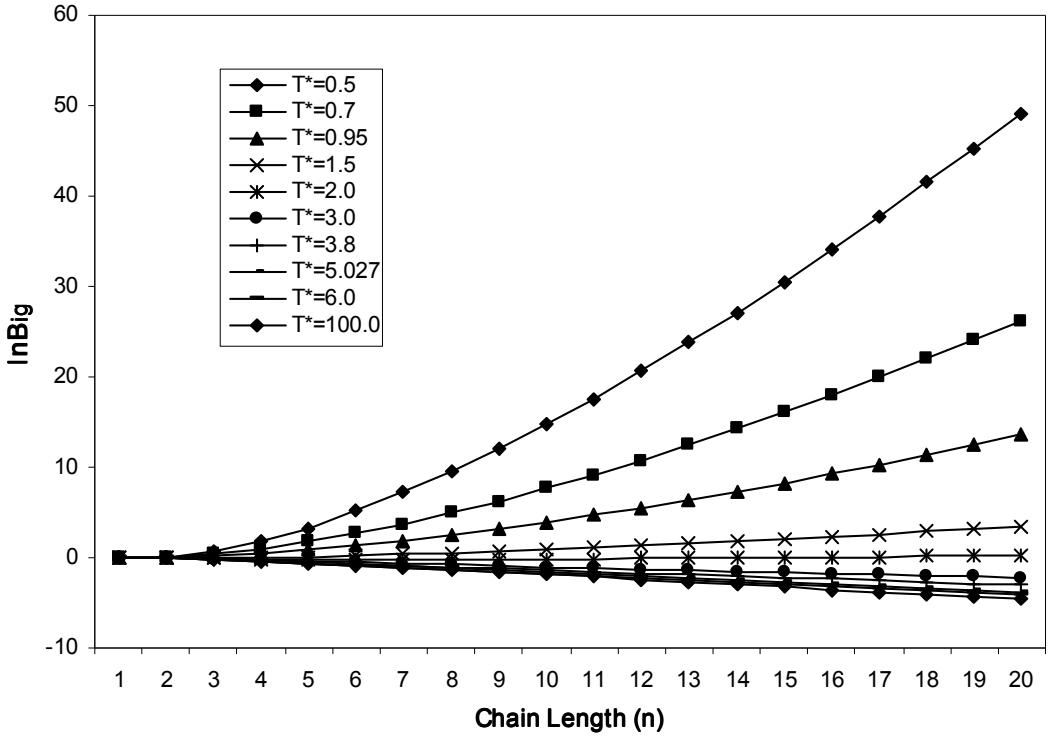

Figure 4.10: The free energy term (lnB_{ig}) vs. chain length of a freely jointed chain in vacuum. Solubility (lnB) increases with chain length when T*<2.0, but decreases with chain length when T*>2.0; the solubility-chain length curve has a minimum when T*=2.0. At fixed temperature, the solubility decreases as the chain length increases.

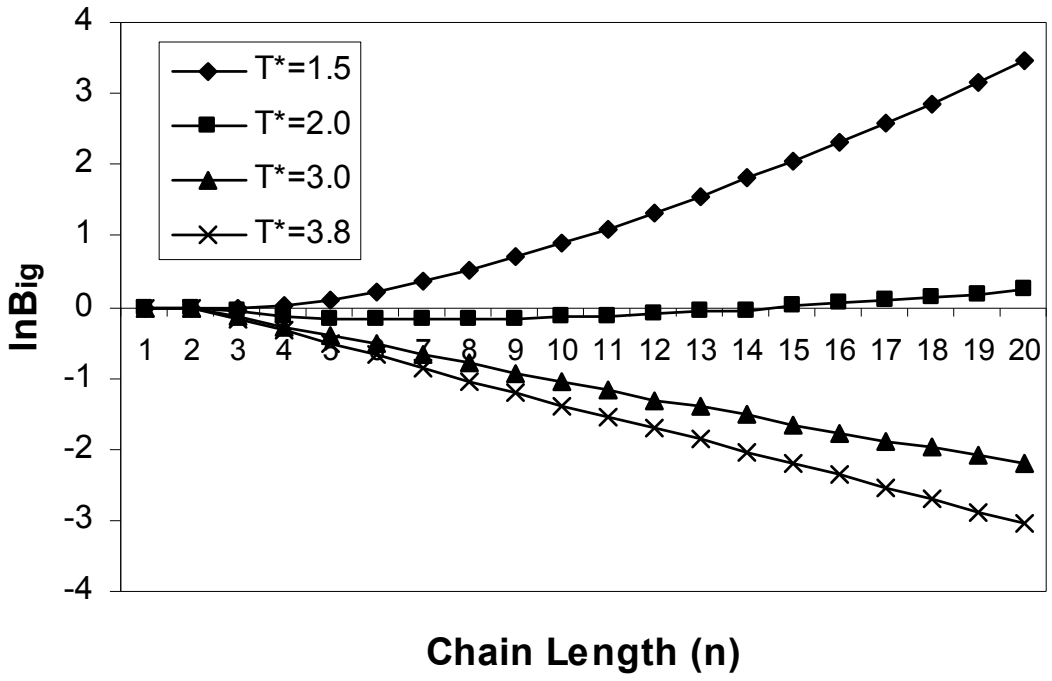

Figure 4.11: The free energy term (lnB_{ig}) vs. chain length of a freely jointed LJ chain in vacuum. To show that lnB_{ig} change from positive to negative at high temperatures, the date from figure 4.10 at T*=1.5, 2.0, 3.0, and 3.8 are shown on a larger scale.

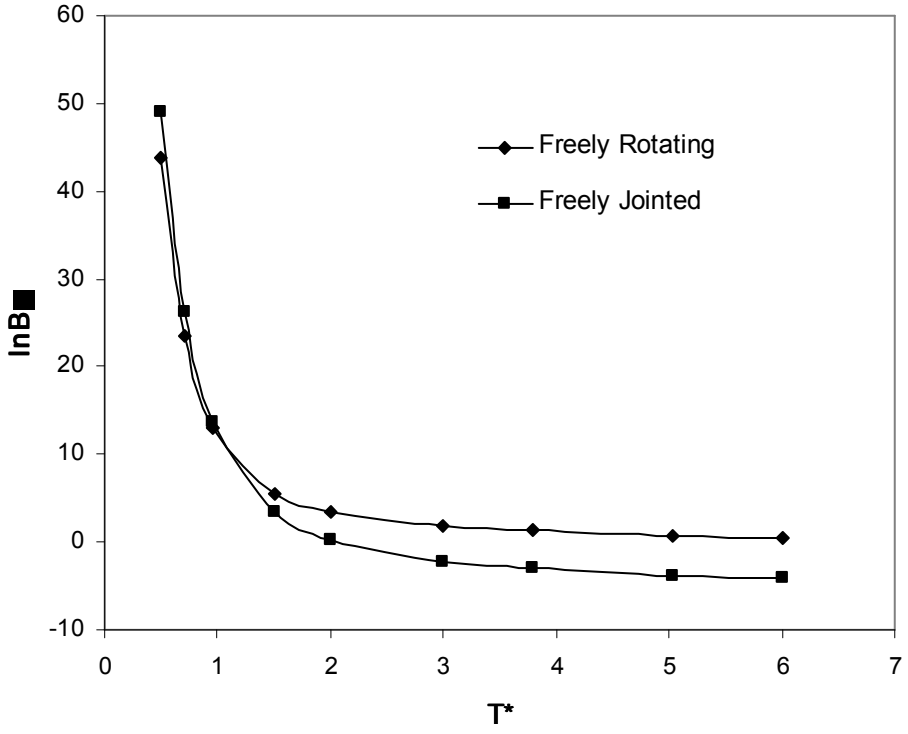

Figure 4.12: The free energy term (lnB_{ig}) vs. reduced temperature for freely rotating chain and freely jointed chain. Chain length equals to 20 for both chains. At low temperatures lnB_{ig} of freely jointed chain is higher than freely rotating chain, but it changes at around T*=1 and lnB_{ig} of freely rotating chain becomes higher at elevated temperatures.

To compare with a chain with torsion potential, the temperature dependence of lnB_{ig} for freely jointed LJ chain and freely rotating LJ chain are shown in Figure 4.8, 4.9, 4.10, 4.11 and 4.12. For both models, lnB_{ig} increases with chain length at low temperatures, but the trend gradually changes as temperature goes up, and it becomes negative and decreasing at very high temperatures. For these two LJ chain models in vacuum, the temperature dependence of lnB_{ig} –chain length relation can be easily transferred to interaction parameter effect dependence. Increasing interaction has the same effect as reducing temperature. For example as shown in Figure 4.10, the curve at reduced temperature 0.95 (the real temperature is 298K for the LJ interaction parameter

we used =312.8K) is positive and increasing, but at the same real temperature, if we decrease the by 4 times, that curve will move to where the T*=3.8 current is and lnB_{ig} now is negative and decreasing. Although for the lnB_l shown in Figure 4.1, a decreasing lnB_{ig} will be critical in reproducing the minimum in *lnB*-chain length curve, we do not believe that decreasing the LJ interaction parameter of a freely jointed or freely rotating model will success in capturing this minimum because a strong enough interaction is very important in the minimum forming in the lnB_l-chain length curve in water phase[2].

The interaction parameter we choose for torsion interaction has similar effect on lnB_{ig}-chain length relation, and by choosing the right interactions for a LJ chain with torsion potential we may be able to accomplish our goal of reproducing the experimental results shown in Figure 3.2. Again, simulation work of chain in water phase will be critical to review this problem.

The temperature dependence shown above for the three LJ chain models can be explained if we examine the free energy term. As shown in equation (4.8), free energy is consisting of a competing energy-entropy pair, of which the energy term always contributes favorably, and the entropy term contributes unfavorably.

$$\ln B = -\beta \Delta u_{\text{int}} + \Delta s_{\text{int}} / k \tag{4.8}$$

For freely jointed and freely rotating chain, the chain is collapsed so that the LJ interaction between non-bonded particles can overcome the unfavorable entropy term, so *lnB* will still be positive. Although the entropy term increases with chain length, *lnB* still increases, since the intra-chain interaction gets stronger, or more favorable as the chain gets longer. This is also evidence that energy dominates in chain solubility at room

temperatures[11]. At high temperatures the contribution from the energy term becomes trivial and the entropy term shows its effect so *lnB* becomes negative at all chain lengths.

The minimum of the chain with torsion potential shows the competing effect. The torsion potential itself is unfavorable, and it adds stiffness to the chain and made the chain less collapsed. At low temperature, the entropic factor prevails first, since the entropy term gets larger as chain length gets larger, but as chain length increases, so does the non-bonded LJ interaction, and the energy finally won the competition. At higher temperature this turnover does not happen anymore. Our simulation results show the total intra-chain interaction energy is negative at low temperature, and it changes sign at around 250K, which is also the temperature at which the free energy term vs. temperature plot stop having minima. Again this is because energy term is related to temperature by reciprocal temperature β, so the energy term always loses its power at high temperature.

4.4 Conclusions

In this work, we add constraints such as bond angle, torsion potential, to the LJ chain model to observe how these factors alter the ideal gas phase contribution to solubility. Fixed bond angle alone does not play an important role in solubility. The results are very close for united atom model of alkane chain between freely jointed chain model and freely rotating chain model. Torsional potential dramatically affects the free energy contribution from ideal gas phase to solubility of the chain and this free energy contribution (lnB_{ig}) decreases with chain length at room temperature. It is to our belief that by choosing the right interaction parameters for the LJ chain model with torsion potential, we may be able to capture the anomalous behavior of normal alkane solubilities in water at room temperature. Our simulation shows the torsion interaction also brings a

minimum to this lnB_{ig}-chain length relationship at lower temperatures. The intra-molecular interaction energy is the dominant factor for this minimum.

Future work need to study the chain constraints effect on the aqueous phase contribution to the solubility.

---

[1] K. A. Dill , Biochemistry 29, 7133 (1990).
[2] Matthew T. Stone, Monte Carlo Approaches to the Protein Folding Problem, The University of Texas at Austin (2002)
[3] H. J. C. Berendsen, J. R. Grigera, and T. P. Straatsma, J. Phys. Chem. 91, 6269 (1987).
[4] Theodora Spyriouni, Ioannis G. Economou and Doros N. Theodorou, Macromolecules, 30, 4744 (1997)
[5] B. Smit, S. Karaborni, and J.I. Sieppmann, J. Chem. Phys. 102, 2126 (1995)
[6] J.J. de Pablo, M. Laso and U.W. Suter, J. Phys. Chem., 96, 6157 (1992)
[7] J.I. Siepmann and D. Frenkel, Mol. Phys. 75, 59 (1992)
[8] J.J. de Pablo, M. Laso and U.W. Suter, J. Chem. Phys., 96, 2395 (1992)
[9] Fernando A. Escobedo and Juan J. de Pablo, J. Chem. Phys. 103, 2703 (1995)
[10] D. Frenkel and B. Smit, Molecular Physics 75, 983 (1992).
[11] Matthew T. Stone, Pieter J. in 't Veld, Ying Lu, Isaac C. Sanchez, Molecular Physics 100, 2773 (2002)

Chapter 5 Monte Carlo Studies of Aqueous Solutions of Poly Ethylene Oxide (PEO)

5.1 Introduction

Poly (ethylene oxide) (PEO) is one of the most important hydrophilic polymers. It has a simple structure, $(CH_2\text{-}CH_2\text{-}O)n$. Polyethylene glycol (PEG) has the identical main chain backbone. The differences between PEO and PEG are the molecular weight and end groups. Usually PEG refers to polymers made from condensation of ethylene glycol monomer and it has two hydroxyl groups, while PEO is the product of addition of ethylene oxide and it has one hydroxyl end group and an initiator fragment (such as t-butyl) at the other end.[1] It is difficult to get monodisperse polymer of high molecular weights from ethylene glycol so the molecular weight of PEG is usually below 20,000 g/mol, but it can be way above that for PEO. Because it is always the chain backbone that solution behavior of the long linear polyether chains are mainly related to, most of the time PEO and PEG are used to refer to the same chain structure. We chose to use PEO in this paper.

Despite its simple chemical structure, PEO has some extraordinary solubility behavior. It is completely miscible with water at room temperature over a very wide molecular weight range, while other polymers which have similar structure, for example, poly(methylene oxide) (PMO) is insoluble in water, and only very short poly(propylene oxide) (PPO) oligomers are soluble in water[2,3]. PEO is also soluble in many small molecule organic solvents. This amphiphilicity gives PEO extremely wide application in biomedical, pharmaceutical, cosmetics, and separation industries.

Through the past decades, many researchers have been trying to work on the problem of PEO solubility in water and discover the mechanism that makes PEO unique.

In aqueous solutions of PEO, the oxygen-oxygen distance in the PEO chain has been measured to be 2.85 • which matches the hydrogen bond length in bulk water. It has been thought that the solubility of PEO in water is mainly due to its ability of fitting itself into an unperturbed water structure.[4] The solubility of PEO in water has also been attributed to hydrogen bonding between water molecules and oxygen atoms on PEO chain.[5, 6] Branca et al found that PEO has a more ordered structure in H_2O than in D_2O, and also in aqueous phase than in melted phase[7,8,9].

One of the popular explanations is: in the crystalline state, PEO assumes a 7-2 helix conformation. (PEO is semi-crystalline, as are many synthetic polymers) The 7-2 helix means every 7 repeat units complete 2 turns. In aqueous solution, PEO chain retains some helical character[10]. The oxygen-oxygen distance along the chain is 2.9 Å which is close to the oxygen-oxygen distance in room temperature water. This allows a water molecule to easily form 2 hydrogen bonds with 2 ether nearest neighbor oxygens.

Many experimentalists claimed that PEO has helical structure in aqueous solutions[11.12] However, Brown and Stilbs measured (through self-diffusion coefficients) frictional coefficients for short chain PEO by spin-echo N.M.R. in chloroform, benzene, and water. Their result showed PEO has a common structure in all three solvents. In other words, water does not present any special feature compared with non-aqueous liquids.[13] Other researchers, e.g. Tanner, Liu and Anderson[14], and Molyneaux[15], came to similar conclusions that PEO is relatively insensitive to solvents.

5.2 Methodology

Monte Carlo Simulations have been performed in the canonical ensemble for PEO chains of 10 repeat units $(CH_2\text{-}CH_2\text{-}O)_{10}$ both in vacuum and in water. For the PEO chain, Bin Lin's model was used[16]. This is a united atom model, and a three unit chain is shown

in Figure 5.1. Each group (CH_2, CH_3, O) is represented by a LJ particle with according parameters. At the center of these LJ particles locate point charges, which add coulombic interaction. This model also considers torsion interaction, which has the form

$$V = \sum_i \frac{1}{2} V_2 (1 - \cos 2\phi_i) + \frac{1}{2} V_3 (1 + \cos 3\phi_i) \qquad (5.1)$$

where ϕ_i is a torsion angle, which is the dihedral angle between the plane formed by the (i-2)th, (i-1)th, ith particle, and the plane formed by (i-1)th, ith, and (i+1)th particle. The parameters are shown below in Table 5.1.

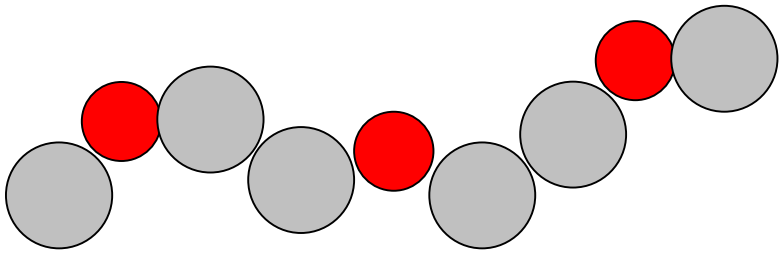

Figure 5.1: A united atom model for PEO chain (shown here is a 3 unit chain)

Table 5.1: Parameters for the PEO model[16]

$_{O}$ = 2.851 Å	$_{O}/k_b$ = 47.75 K
$_{CH2}$ = 3.43 Å	$_{CH2}/k_b$ = 60.38 K
$_{CH3}$ = 3.564 Å	$_{CH3}/k_b$ = 75.4 K
q_O = -0.326 e	q_C = 0.163 e
V_2(OC) = 0	V_2(CC) = -2.10254 kJ/mol
V_3(OC) = 12.03 kJ/mol	V_3(CC) = 12.03 kJ/mol
r_{OC} = 1.423 Å	r_{CC} = 1.538 Å
$_{COC}$ = 111.9	$_{CCO}$ = 109.0

Simple point charge (SPC/E) model was used to represent water molecule. In addition to CCB move, concerted rotation move was applied on chains to help the system reach equilibrium. This method is necessary in simulation with aqueous solutions of chains.

The Materials Studio package[17] was used to investigate PEO chains. Chains were built up with Amorphous Cell module and Molecular Dynamics and Energy Minimization were applied on chains by the Discover module. With this package it is possible to "watch" water molecules move around the PEO chain and PEO chain alter its intra-chain configuration to find the energy minimum. The energy profile can be easily obtained.

5.3 Result and Discussions

Our Monte Carlo simulation shows the histogram of distance between nearest oxygen on a PEO chain in vacuum. Since there is only one PEO chain present and no solvent is in the system, only intra-molecular interaction is considered. It is shown in Fig. 5.2, nearest oxygen distance peaks at 2.85 Å, which is close to the hydrogen bond length (2.82 Å[18].) in room temperature water. Next nearest oxygen distance has a maximum at 5.25 Å, and the maximum is much less steep.

Fig. 5.3 shows the histogram of distance between PEO oxygen when water is present. With water being added to the system, the shape of the curves is retained. Next nearest oxygen distance still has its maximum at 5.25 Å, and nearest oxygen distance has a maximum at slightly lower value (2.72 Å).

In both cases (PEO chains with/without water as solvent), the nearest oxygen distance is very close to where the first maximum of the oxygen-oxygen radial distribution function g(R) occurs in bulk water. The simulation result of g(R) of SPC/E

water at 298 K is shown in Fig. 5.4. Its first peak is at 2.8 Å, which represents the hydrogen bond length.

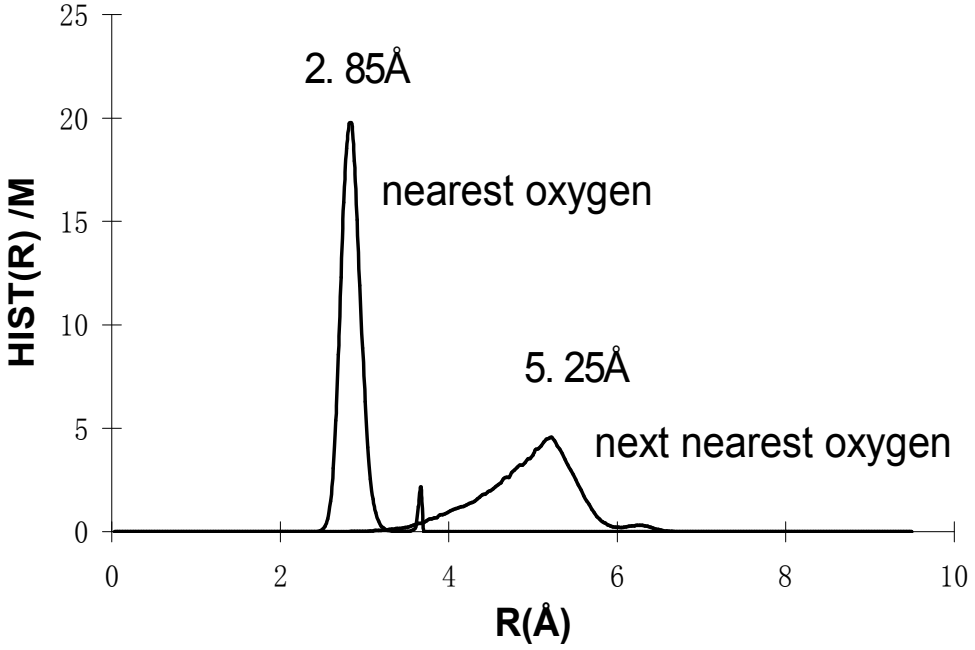

Figure 5.2: PEO chain in vacuum. The distance between two nearest oxygen atoms on PEO chain has a sharp peak at 2.85 •.

Our simulation results agree with the theory that PEO in aqueous solution has a nearest oxygen distance that matches the hydrogen bond lengthin room temperature water and this distance is very close to its value in PEO at its crystalline state. The next nearest oxygen distance issomewhat bigger (5.25Å) than the crystalline state data (4.7Å).

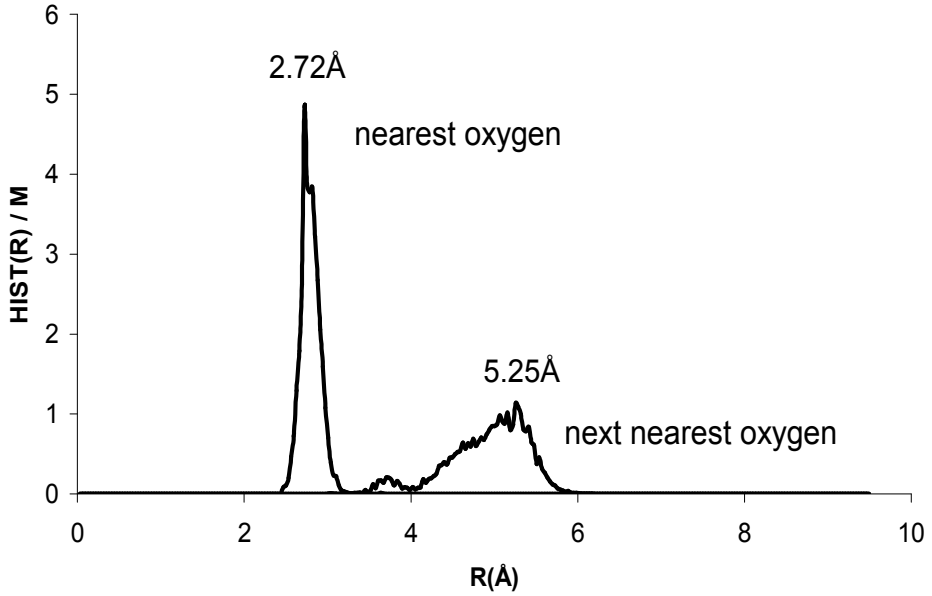

Figure 5.3: PEO chain in water at 298K. The distance between two nearest oxygen atoms on PEO chain has a sharp peak at 2.72 •

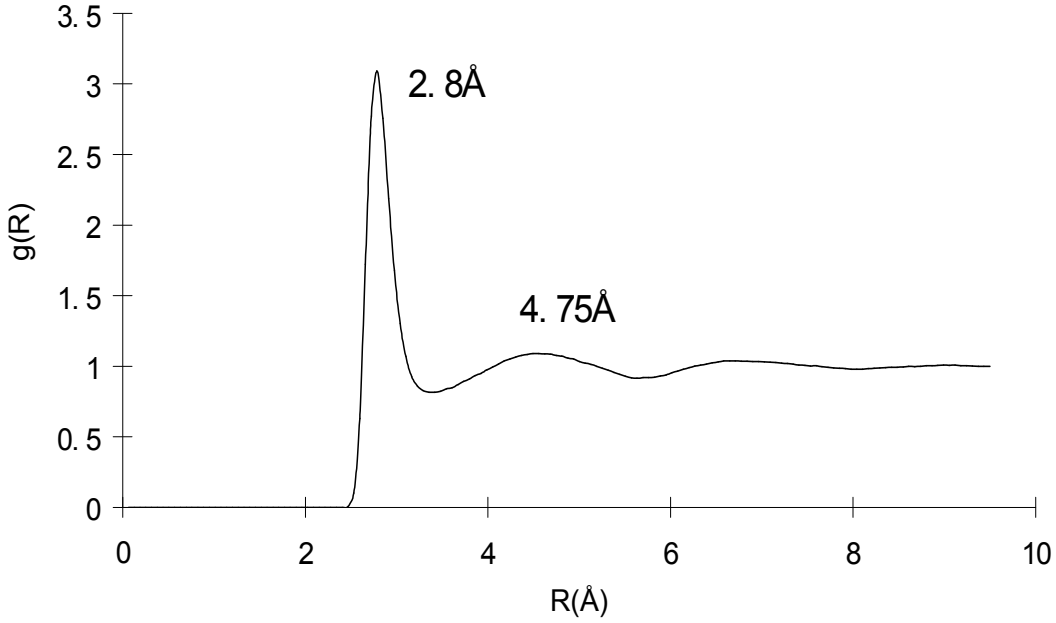

Figure 5.4: SPC/E water at room temperature (298K)To take a closer look at the interaction between water and PEO chain and decide whether the helical structure is critical in PEO-water solubility, small system with short PEO chains (2 or 4 repeat unit) and one water molecule was studied using Discover and Amorphous Builder in MSI package. Figure 5.5 shows the conformation of a 2 unit chain at its energy minimum while one water molecule is present. The two hydrogen atoms of the water molecule point to the two oxygen atoms on the chain, and the distance between water oxygen and ether oxygen is 2.7 Å. Two hydrogen bonds are formed between the water oxygen and ether oxygens, and this lowers the energy of the system.

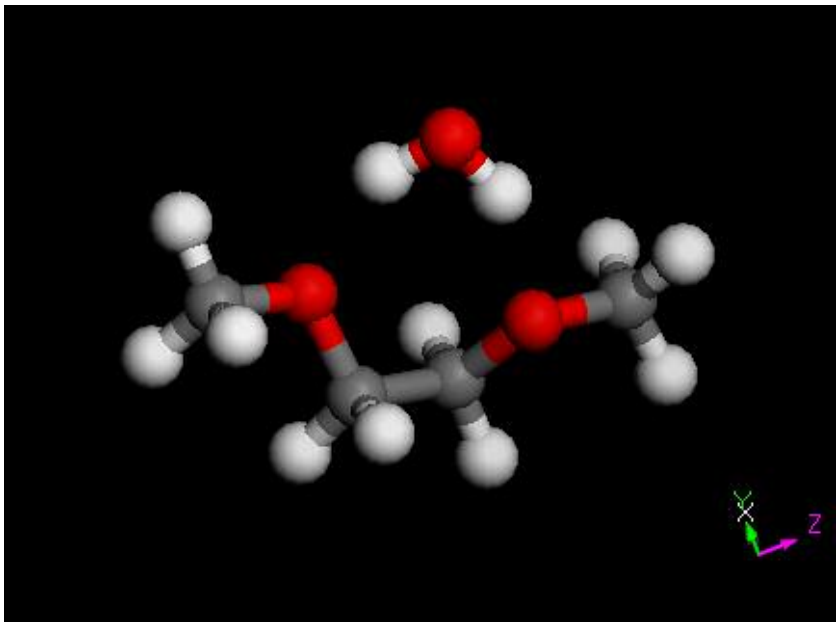

Figure 5.5: PEO chain and water at 298K. The water molecule forms two hydrogen bonds with the two ether oxygen.

The chain-water interaction energy profile was obtained by changing the torsion angle on the C-C bond on the chain while keeping the rest of its intra-structure of the chain fixed. Water moves are allowed to find the most favorable position with respect to the current

chain conformation. In Figure 5.6 the chain has a 180º of torsion angle on C-C bond, and the two ether oxygens are at their furthest position away from each other. In this state water can only form one hydrogen bond with one of the ether oxygens.

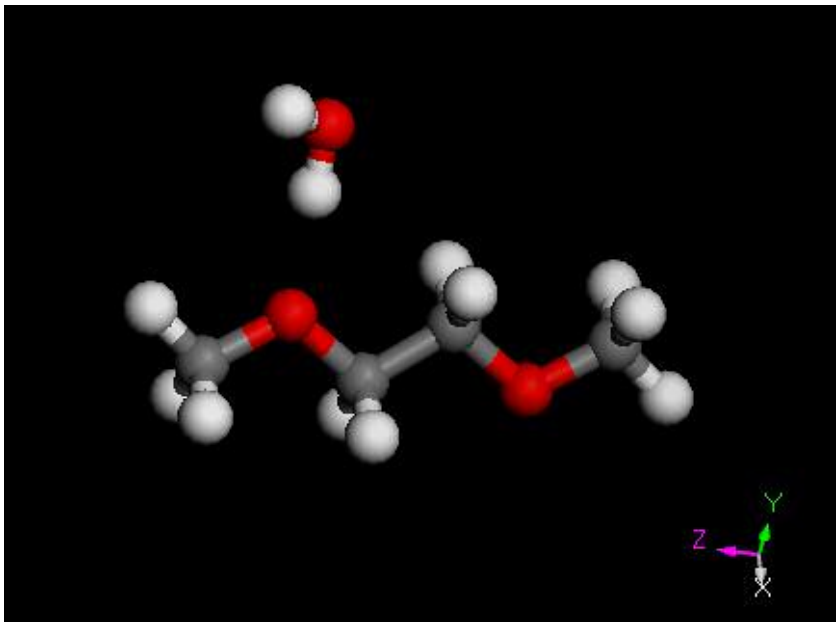

Figure 5.6: PEO chain and water at 298K while the torsion angle on O-C-C-O bond is fixed to 180º

In Figure 5.7 the PEO chain-water interaction is at its lowest energy state near where torsion angle is between about -60º to 60º, which means the O-C-C-O bonds are in a gauche conformation. In this conformation, a water molecule can always form two hydrogen bonds with the two nearest ether oxygen atoms.

If the intra-chain interaction is included in addition to the chain-water interaction, the total interaction can be plotted vs. torsion angle as in Figure 5.8. While the torsion angle is close to 0º, the chain-water interaction is favorable and the intra-chain interaction is unfavorable because of the obstructions effect between the nearest ether oxygen atoms. The latter brings the total interaction up to a maximum. The total interaction has minima

at about -60º and 60º, in which water can still form two hydrogen bonds with two nearest ether oxygen, yet these two ether oxygen atoms are not in the way of each other to create a big unfavorable intra-chain interaction. When the torsion angle on O-C-C-O bond is 60º it is a g^+ conformation and while it is -60º it is a g^- conformation. For both conformations, the total interaction is favorable.

In crystalline state PEO chain forms a 7-2 helix. The helical structure of PEO can be generated using the same parameters as for chain in crystalline state (torsion angle of 68.4º on every O-C-C-O bond and 186º on every C-C-O-C bond.[19]) The helix is shown in Figure 5.9 and 5.10. Any change to the torsion angle will disturb the helical structure. However, our result on the PEO chain and water interactions indicates the torsion angle on O-C-C-O bond can be either positive (at about 60º) or negative (at about -60º) for the system to reach low energy state. By having both positive and negative torsion angles on O-C-C-O bond, a PEO chain will not be the ordered helix as shown in Figure 5.9. This implies the helical structure is not required for PEO solubility in water, although it is possible to have some helical structure on some segments.

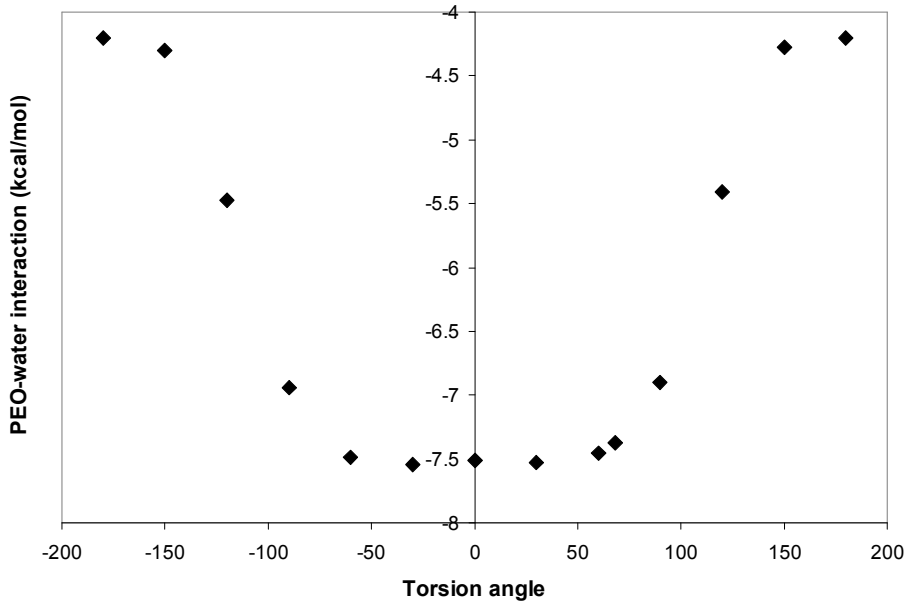

Figure 5.7: PEO chain-water interaction vs. torsion angle on O-C-C-O bond

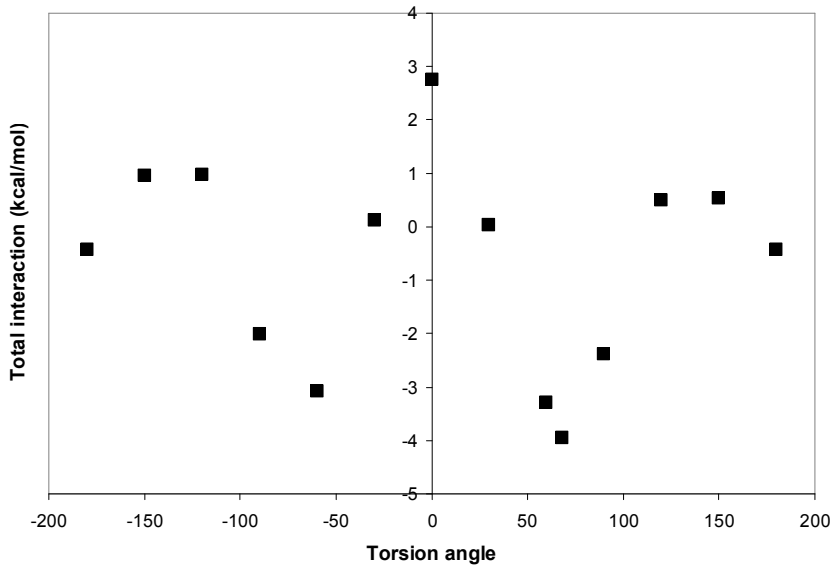

Figure 5.8: Total interaction vs. torsion angle on O-C-C-O bond

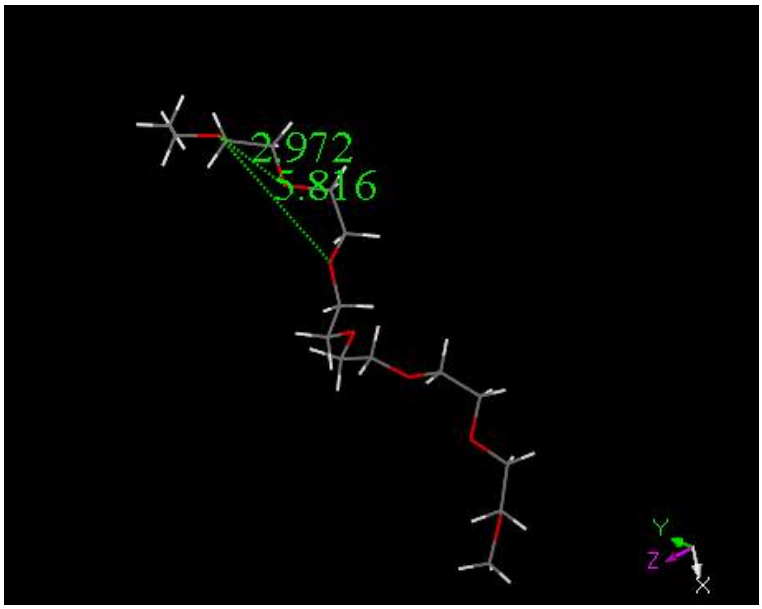

Figure 5.9: A PEO chain at its 7-2 helix conformation .Parameters is from[19], the torsion angle on C-C bond is 68.4º, and on C-O bond is 186º

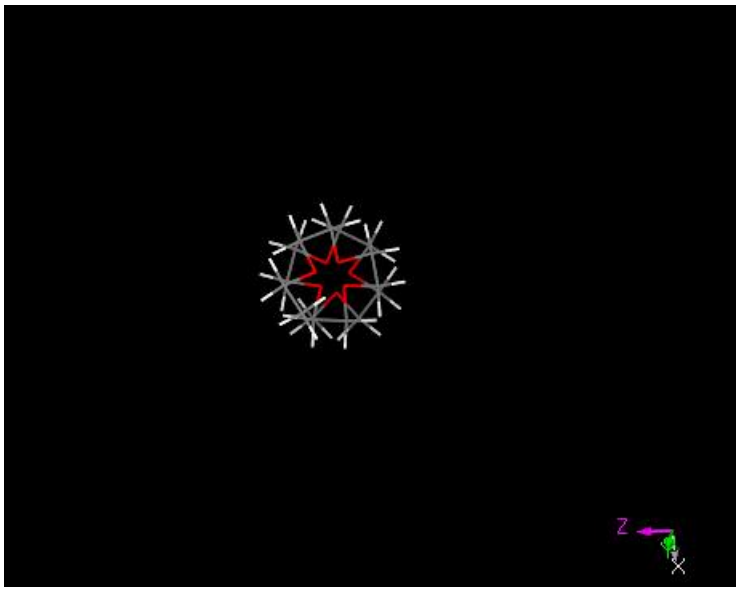

Figure 5.10: A PEO chain at its 7-2 helix conformation. View along helix axis.

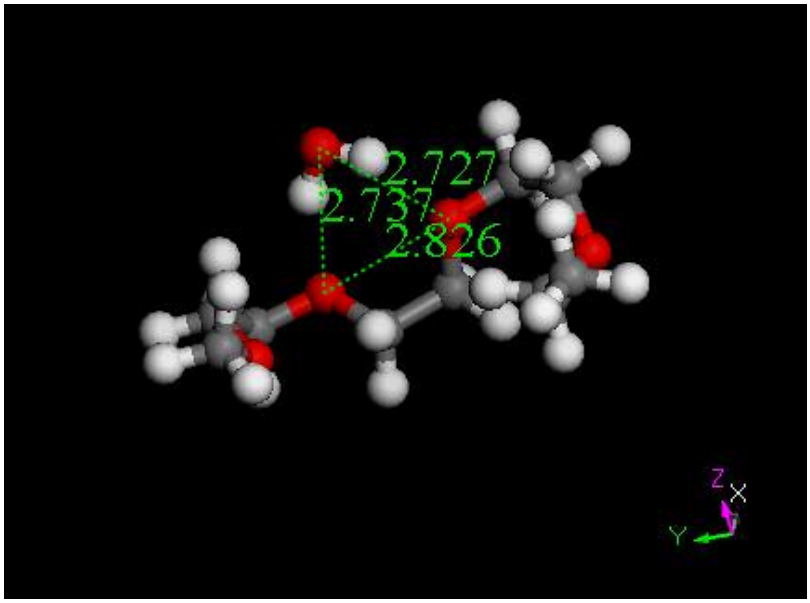

Figure 5.11: PEO chain and water at its lowest energy state. Chain-water interaction is -7.9kcal/mol and total interaction (include chain-water and intra-chain interaction) is -10.3kcal/mol. Torsion Angles on O-C-C-O bonds closest to water are 176.6°, 66.7°, and 173.3°, and it is a tgt conformation.

At the system's most favorable energy state, a four unit PEO chain and one water molecule has a similar chain-water interaction (-7.9kcal/mol) with the two unit PEO chain-water interaction(-7.4kcal/mol). The interaction between the PEO chain and water is mainly the interaction energy between the water molecule and the two units that form hydrogen bonding with it. The Total energy is different since the energy includes intra-chain interaction, so of course, the total interaction of a 4-unit chain (-10.3kcal/mol) is bigger in absolute value than that of a dimer (-3.96kcal/mol).

It is possible that a water molecule to form two hydrogen bonds with two next nearest ether oxygen atoms (as shown in Figure 5.12), instead of two nearest ether oxygen. This kind of chain conformation gives even lower chain-water interactions and total interactions.

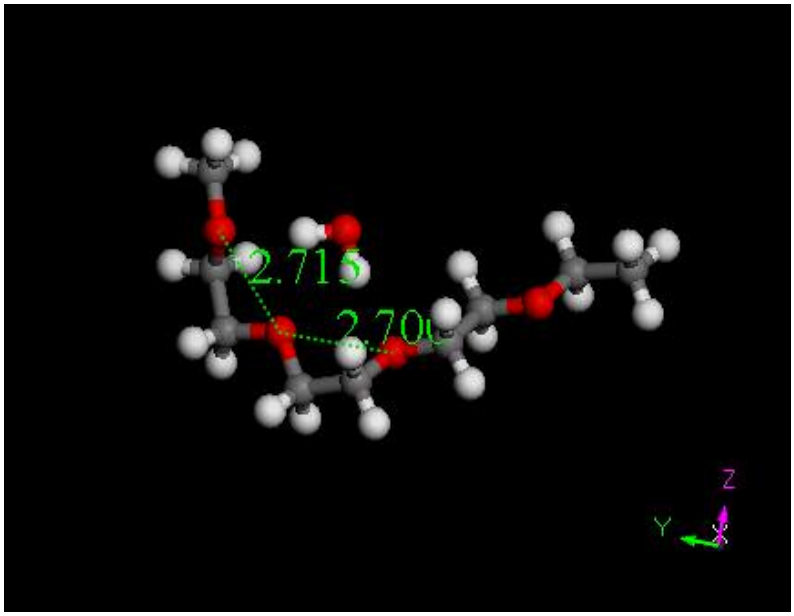

Figure 5.12: PEO chain and water at its lowest energy state. Chain-water interaction is -9.6kcal/mol and the total interaction is -13.6kcal/mol.

Poly methylene oxide (PMO) and Poly propylene oxide (PPO), which have similar chemical structures to PEO and are insoluble in water, were also constructed and simulated with water present.

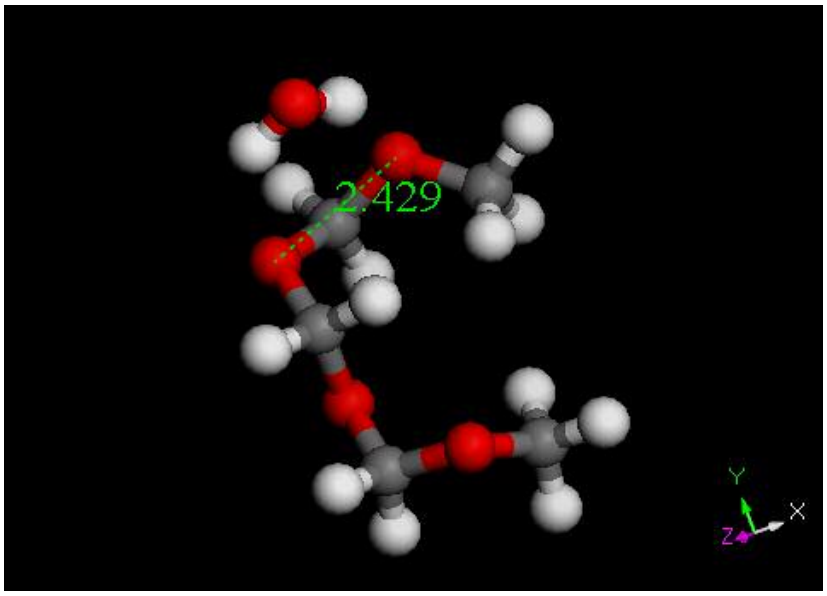

Figure 5.13: PMO (poly methylene oxide) and water at its lowest energy state. Chain-water interaction is -5.0kcal/mol.

In Figure 5.13, the two hydrogen atoms of the water molecule point toward the two nearest ether oxygens on PMO chain. It looks like the hydrogen bonding formation in the PEO-water system. However, the PMO chain-water interaction (-5.0kcal/mol) is less favorable than PEO chain-water interaction (-7.9kcal/mol). The distance between the two nearest oxygens on PMO chain is 2.4 Å, and it is less than the hydrogen bond length (2.8Å). Since there is only one CH_2 group between two ether oxygens and the tension on the water-2 ether oxygens ring prevent the formation of two hydrogen bonds.

PPO has very similar structure as PEO except the CH_3 group attached to a CH_2 group between 2 nearest ether oxygens. Although water can still form two hydrogen bonds with two nearest ether oxygens as shown in Figure 5.14 and the PPO chain-water

interaction (-7.8kcal/mol) is very close to PEO chain-water interaction (-7.9kcal/mol), the extra methyl group has brought in obstruction effect and that limits the lower energy state that the chain can explore.

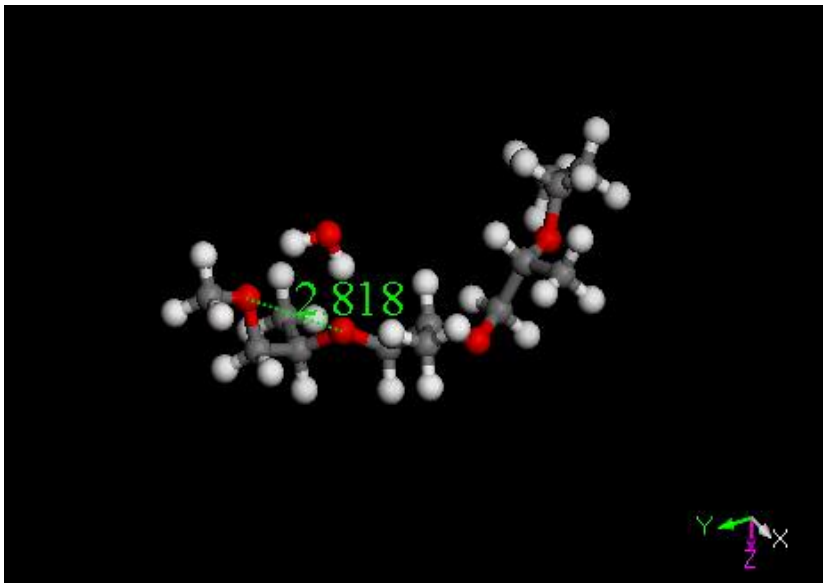

Figure 5.14: PPO (poly propylene oxide) and water at its lowest energy state. Chain-water interaction is -7.8kcal/mol

Figure 5.15 gives the relation between PPO chain-water interaction and the torsion angle on O-C-C-O bond. This figure can be compared with Figure 5.7, to see the effect of the extra methyl group of PPO. The interaction has a minimum when the torsion angle is near 60º (the configuration is shown in Figure 5.16). The water molecule forms two hydrogen bonds with the two nearest ether oxygen atoms on PPO chain, which is similar to PEO-water system. As shown in Figure 5.7, the PEO chain-water interaction has a minimum where double hydrogen bonds can be formed, but unlike the case in PEO, this PPO chain does not have the other minimum at around -60º to be symmetric with this one. The chain-water interaction at all negative torsion angles is more unfavorable since no double hydrogen bonds can form between water and the two ether oxygen because of the

existence of the methyl group. Water can only form one hydrogen bond with one of the ether oxygen, as shown in Figure 5.17. The total interaction of this PPO-water solution is shown in Figure 5.18.

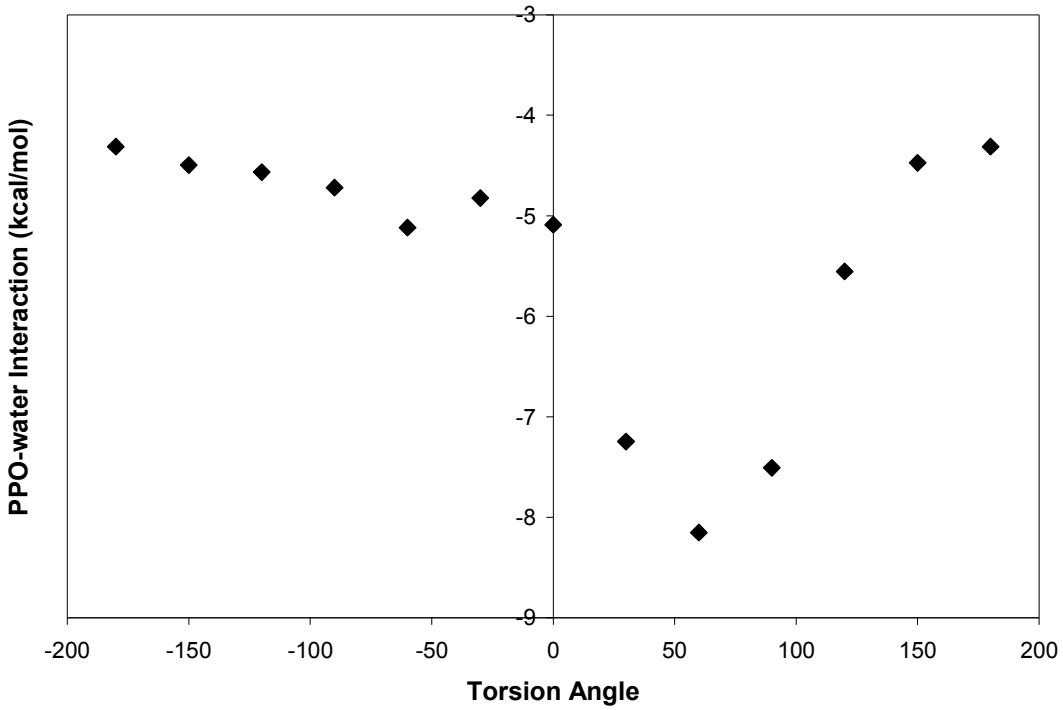

Figure 5.15: PPO chain-water interaction vs. the torsion angle on backbone O-C-C-O bond. There is an energy minimum at around 60°.

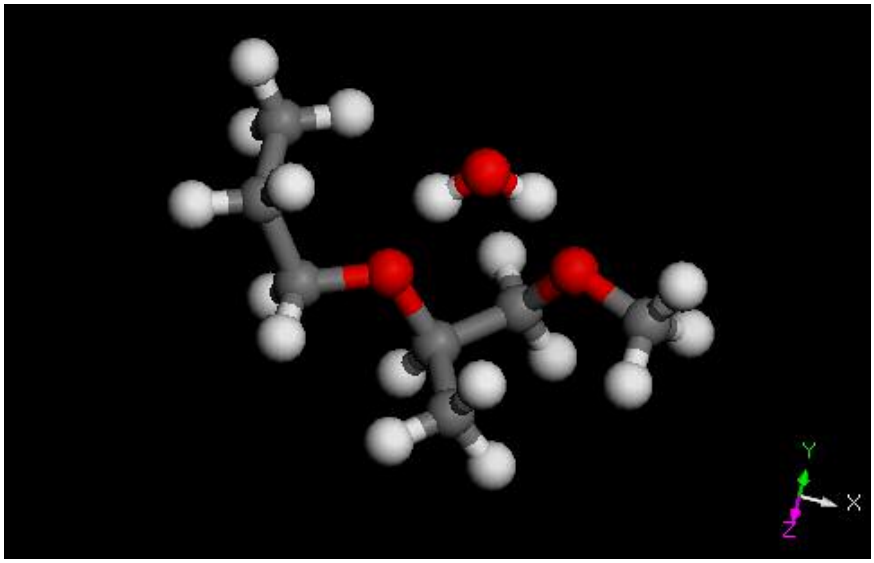

Figure 5.16: PPO chain and water at 298K. The water molecule forms two hydrogen bonds with the two ether oxygen. The torsion angle on the backbone O-C-C-O bond is 65.1º.

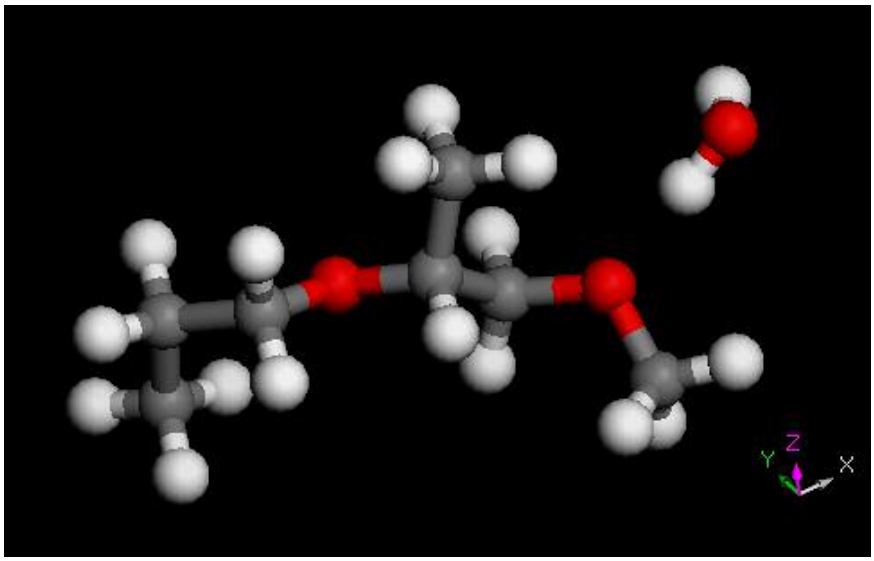

Figure 5.17: PPO chain and water at 298K while the torsion angle on O-C-C-O bond is fixed to 180º

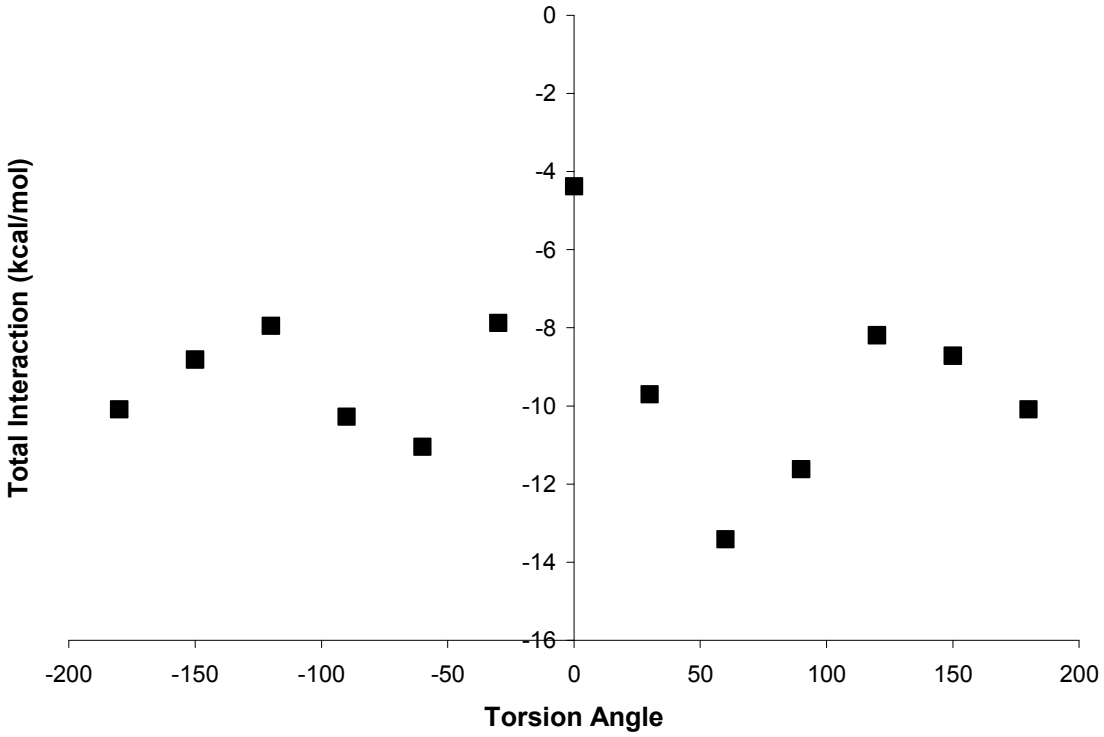

Figure 5.18: PPO chain and water system total interaction vs. torsion angle on O-C-C-O bond. The total interaction includes intra-chain interaction and chain-water interaction.

The comparison between PEO and two kinds of polyether (PMO and PPO) implies the interaction is the key point of the PEO solubility in aqueous solution.

5.4 Conclusions

1. Favorable interaction of water with PEO does not require the helical structure.
2. Along PEO chain, the nearest ether O-O distance matches the nearest neighbor O-O distance in bulk water.
3. In bulk water, the 2 H's on a water molecule form less than 2 H bonds with other water molecules. Thus, there is a favorable change in energy when water forms 2

hydrogen bonds with 2 nearest neighbor ether oxygens along the PEO backbone. The water-PEO interaction effectively increases the number of H bonds.

4. PMO and PPO have been studied for comparison. Their difference in structure from PEO, though slight, reduces the chance of hydrogen bond formation between water and chains.

---

[1] Webpage http://www.polymerlabs.com/gpc/gpcfaqs.htm#middle3
[2] G. N. Malcolm, J. S. ROwlinson, Trans. Faraday Soc. 53, 921 (1957).
[3] Yasushi Maeda, Langmuir 17, 1737 (2001).
[4] R. Kjellander and E. J. Florin, J. Chem. Soc. , Faraday Trans. 1 77, 2053 (1981).
[5] S. Bekiranov, R. Bruinsma and P. Pincus, Europhys. Lett., 24, 183 (1993).
[6] Stefan Bekiranov, Robijn Bruinsma and Philip Pincus, Physical Review E, 55, 577 (1997).
[7] C Branca, S Magazu, G Maisano, P Migliardo and V Villari, J. Phys.: Condens. Matter, 10, 10141 (1998)
[8] C Branca, A Faraone, G Maisano, S Magazu, P Migliardo, A Triolo, RTriolo and V Villari, J. Phys.: Condens. Matter, 11, 6079 (1999)
[9] C. Branca, A. Faraone, S. Magazu, etc., Physica B, 276-278, 332 (2000)
[10] Kenzabu Tasaki, J. Am. Chem. Soc. 118, 8459 (1996).
[11] Roksana Begum and Hiroatsu Matsuura, J. Chem. Soc., Faraday Trans., 93, 3839(1997)
[12] F Oesterhelt, M Rief and H E Gaub, New J. Phys. 1, 6 (1999)
[13] Wyn Brown and Peter Stilbs, Polymer, 23, 1780 (1982)
[14] Tanner, J.E., Liu, K.J. and Anderson, J.E., Macromolecules 4, 586 (1971)
[15] Molyneaux, P. in 'Water, A Comprehensive Treatise' (Ed. Felix Franks, Plenum Press, New York, 1974)
[16] Bin Lin, P. T. Boinske, and J. W. Halley, J. Chem. Phys., 105, 1668(1996)
[17] Materials Studio is a commercial software package developed by Accelrys, San Diego, CA.
[18] Martin Chaplin, Hydrogen Bonding in Water, http://www.martin.chaplin.btinternet.co.uk/hbond.html
[19] Hiroyuki Tadokoro, Structure of Crystalline Polymers, New York, (1979).

Chapter 6 Summary

6.1 Conclusions

Solubility behavior of PEO in water has been studied in our work via computer simulations. While approaching this problem, aqueous solutions of non-polar gases, ethers, and alkane chains have also become some major topics of interest. The following conclusions have been reached:

1. Gas solubility in water consists of an enthalpy (or energy) term and an entropy term. The energy term contributes favorably to the solubility while the entropy term contributes unfavorably. Contrary to the belief of entropy dominating solubility, it is actually the energetics that dominates solubility.
2. At room temperatures (below the water boiling temperature), hydrophobic and hydrophilic solutes both present solubility minima at heating/cooling along the water coexistence curve. This solubility minimum is the result of competition between the favorable energetic term and the unfavorable entropic penalty.
3. LJ chains were used to model normal alkanes (from C_1 methane to C_{20} eicosane) and to study the aqueous solutions of alkanes. To the previous freely jointed LJ chain, various chain constraints were tested to research their effects on the solubility of ideal gas phase. The freely rotating chain which only possesses one more constraint (fixed bond angle) yields similar solubilities as the freely jointed chain. Since the freely rotating chain doesn't collapse as much as the freely jointed chain as the temperature rises, a slight difference between their solubility results can be observed.
4. Torsion interactions affect the alkane solubilities dramatically. The intra-molecular interaction becomes so unfavorable that it produces very low chain

solubilities at room temperature. By choosing the right interaction parameters for the LJ chain model with torsion potential, we may be able to capture the anomalous behavior of normal alkane solubilities in water at room temperature. At low temperatures the solubility first decreases as the chain length increases, then pass through a minimum and increases again when the chain is long enough to bend back and have more intra-chain interaction balancing the entropy penalty.

5. PEO was modeled by a united atom chain. The most probable distance between two nearest ether oxygens in both vacuum and aqueous solutions matches the hydrogen bond length in bulk water. Hydrogen bonding plays an important role in the unique water solubility behavior of PEO.
6. Although trans-gauche-trans conformation along the O-C-C-O bonds does enable hydrogen bond forming between one water molecule and two nearest or next nearest ether oxygens, a helix structure is not required for the PEO to have favorable interactions with water.
7. In bulk water, the 2 H's on a water molecule form less than 2 hydrogen bonds with other water molecules. In the aqueous solutions of PEO, the water-PEO interaction effectively increases the total number of hydrogen bonds because some water molecules form two hydrogen bonds with ether oxygen along the PEO chain. This results in a favorable change in energy.
8. PMO and PPO have also been studied to compare with PEO. Their difference in structure from PEO, though slight, reduces the chance of hydrogen bond formation between water and chains.

6.2 Future work

Future work would be on the solubility of alkane chains in aqueous phase. Various conformational/energetic constraints can also be added to the model and observe their effect on the solubility in aqueous phase as well as the final results (the combination of aqueous phase and ideal gas phase).

More work can be expected on the insoluble polymers including PMO, PPO, poly (trimethylene oxide), which are similar in structure as PEO, and also another polymer soluble in water, poly (vinyl methyl ether) (PVMA).

Bibliography

F. E. Bailey, Jr., and R. W. Callard, Journal of Applied Polymer Science, 1, 56 (1959).

N. B. Bikales, editor, Water-Soluble Polymers, New York, Plenum Press (1973).

J. A. Johnson, M. L. Saboungi, D. L. Price, S. Ansell, T. P. Russell, J. W. Halley and B. Nielsen, J. Chem. Phys. 109, 7005 (1998).

J. L. Lumley, Ann. Rev. Fluid Mech., 367 (1969).

J. M. Harris, editor. Poly(ethylene glycol) Chemistry: Biotechnical and Biomedical applications. New York, Plenum Press (1992).

H. L. Cox and L. H. Cretcher, J. Am. Chem. Soc. 48, 451 (1926).

G. N. Malcolm and J. S. Rowlinson, Trans. Faraday Soc. 53, 921 (1957).

S. Saeki, N. Kuwahara, M. Nakata, and M. Kaneko, Polymer 17, 685 (1976).

Y. C. Bae, J. J. Shim, D. S. Soane, and J. M. Prausnitz, J. Appl. Polym. Sci. 47, 1193 (1993).

V. Kuppa and E. Manias, J. Chem. Phys. 118, 3421 (2003).

H. Tadokoro, Y. Chatani, T. Yoshihara, S. Tahara and S. Murahashi, Makromol. Chem. 73, 109 (1964).

J. L. Koenig and A. C. Angood, J. Polym. Sci. A 8, 1787 (1970).

F. E. Bailey and J. V. Koleske, Poly(Ethylene Oxide), Academic Press, New York (1976).

R. Kjellander and E. Florin, J. Chem. Soc. Faraday Trans. l. 77, 2053, (1981).

Kenzabu Tasaki, J. Am. Chem. Soc. 118, 8459 (1996).

Roksana Begum and Hiroatsu Matsuura, J. Chem. Soc., Faraday Trans., 93, 3839(1997).

F Oesterhelt, M Rief and H E Gaub, New J. Phys. 1, 6 (1999).

Susumu Saeki, Nobuhiro Kuwahara, Mitsuo Nakata, and Motoxo Kaneko, Polymer 17, 685 (1976).

Wyn Brown and Peter Stilbs, Polymer, 23, 1780 (1982).

Seigou Kawaguchi, Genji Imai, Junto Suzuki, Akira Miyahara, Toshiaki Kitano and Kiochi Ito, Polymer 38, 2885 (1997).

Tanner, J.E., Liu, K.J. and Anderson, J.E., Macromolecules 4, 586 (1971).

Molyneaux, P. in 'Water, A Comprehensive Treatise' (Ed. Felix Franks, Plenum Press, New York, 1974).

J. L. Koenig and A. C. Angood, Journal of Polymer Science: Part A-2 8, 1787 (1970).

C Branca, S Magazu, G Maisano, P Migliardo and V Villari, J. Phys.: Condens. Matter, 10, 10141 (1998).

C Branca, A Faraone, G Maisano, S Magazu, P Migliardo, A Triolo, RTriolo and V Villari, J. Phys.: Condens. Matter, 11, 6079 (1999)

C. Branca, A. Faraone, S. Magazu, etc., Physica B, 276-278, 332 (2000)

K. Liu and J. L. Parsons, Macromolecules 2, 529 (1969).

Elena E. Dormidontova, Macromolecules 35, 987 (2002).

Stefan Bekiranov, Robijn Bruinsma and Philip Pincus, Physical Review E 55, 577 (1997).

A. Matsuyama and F. Tanaka, Phys. Rev. Lett. 65, 341 (1990).

John G. Curro and Amalie L. Frischknecht, Polymer 46, 6500 (2005).

Bin Lin, P. T. Bionske, and J. W. Halley, J. Chem. Phys. 105, 1668 (1996).

Grant D. Smith, R. L. Jaffe, D. Y. Yoon, J. Phys. Chem. 97, 12752 (1993).

P. Ahlstrom, O. Borodin, G. Wahnstrom, E. J. W. Wensink, P. Carlsson and G. D. Smith, J. Chem. Phys. 112, 10669 (2000).

G. D. Smith, O. Borodin,and D. Bedrov, J. Comp. Chem. 23, 1480 (2002).

Sylvie Neyertz and David Brown, J. Chem. Phys. 102, 9725 (1995).

T. W. N. Bieze, A.C. Barnes, C. J. M. Huige, J. E. Enderby and J. C. Leyte, J. Phys. Chem. 98, 6568 (1994).

Dmitry Bedrov, Oleg Borodin and Grant D. Smith, J. Phys. Chem. B. 5683 (1998).

Akihiro Abe, Kenzabu Tasaki and J. E. Mark, Polym. J. 17, 883 (1985).

Kenzabu Tasaki and Akihiro Abe, Polym. J. 17, 641 (1985).

H. Matsuura and K. Fukuhara, J. Polym. Sci. Part B: Polym. Phys. 24, 1383 (1986).

Ola Engkvist and Gunnar Karlstrom, J. Phys. Chem. B 101, 1631 (1997).

S. Bekiranov, R. Bruinsma and P. Pincus, Europhys. Lett., 24, 183 (1993).

Stefan Bekiranov, Robijn Bruinsma and Philip Pincus, Physical Review E, 55, 577 (1997).

W. W. Wood. Early history of computer simulation in statistical mechanics. In G. Ciccotti and W. G. Hoover, editors, Molecular Dynamics Simulations of Statistical Mechanics Systems, pages 2-14. Proceedings of the 97th Int. "Enrico Fermi" School of Physics, North Holland, Amsterdam, (1986).

N. Metropolis, A. W. Rosenbluth, M. N. Rosenbluth, A. N. Teller, and E. Teller, J. Chem. Phys. 21, 1087 (1953)

M. P. Allen, D. J. Tildesley, Computer Simulation of Liquids (Oxford Science Publications, 1987).

Marvin Bishop and Sharon Frinks, J. Chem. Phys. 87, 3675 (1987).

Matthew T. Stone, Pieter J. In 'T Veld, Ying Lu and Isaac C. Sanchez, Mol. Phys. 100, 27733 (2002).

Y. V. Vorobjrv and J. Hermans, J. Phys. Chem. B 103, 10234 (1999).

Frank H. Stillinger, Aneesur Rahman, J. Chem. Phys. 60,1545 (1974).

H. J. C. Berendsen, J. P. M. Postma, W. F. van Gunsteren, and J. Hermans, Intermolecular Forces, edited by B. Pullmannn (Reidel, Dordrecht, 1981), pp331-8.

W. L. Jorgensen, J. Chandrasekhar, J. D. Madura, R. W. Impey, and M. L. Klein, J. CHem. Phys. 79, 926 (1983).

M. W. Mahoney and W. L. Jorgensen, J. Chem. Phys. 112, 8910 (2000).

H. J. C. Berendsen, J. R. Grigera and T. P. Straastsma, J. Phys. Chem. 91, 6269(1987).

B. Guillot and Y. Guissani, J. Chem. Phys. 99, 8075(1993).

D. van der Spoel, P. J. van Maaren, and H. J. C. Berendsen, J. Chem. Phys. 108, 10220 (1998).

B. Lin and J. W. Halley, J. Phys. Chem. 99, 16474 (1995).

Daan Frenkel and Berend Smit, Understanding Molecular Simulation (Academic Press, 1996)

I. C. Sanchez and M. T. Stone, Statistical Thermodynamics of Polymer Solutions and Blends. Polymer Blends, Vol. 1. D. R. Paul, C. Bucknall (John Wiley and Sons, Inc.; New York, 2000) Chapter 1, pages 15-53.

Kenneth Michael Lee, Exploring Solvent Properties of High Pressure Carbon Dioxide via Computer Simulation, The University of Texas at Austin, 2003.

B. Widom, J. Chem. Phys., 39, 2802 (1963).

A. P. Lyubartsev, A. A. Martsinovskii, S. V. Shevkunov and others, J. Chem. Phys. 96, 1776 (1992).

P. N. Vorontsov-Velyaminov, A. V. Broukhno, T. V. Kuznetsova and A. P. Lyubartsev, J. Phys. Chem. 100, 1153 (1996).

Matthew T. Stone, Mente Carlo Approaches to the Protein Folding Problem, The University of Texas at Austin, (2002).

Aberg K. Magnus, Alexander P. Lyubartsev, Sven P. Jacobsson and Aatto Laaksonen, J. Chem. Phys. 120, 3770 (2004).

George Kaminski, William L. Jorgensen, J. Phys. Chem., 100, 18010 (1996).

Erin M. Duffy, William J. Jorgensen, Journal of the American Chemical Society, 122, 2878 (2000).

William L. Jorgensen, Jokob P. Ulmschneider, Julian Tirado-Rives, J. Phys. Chem. B, 108. 16264 (2004).

H. Sun, J. Phys. Chem. B, 102. 7338 (1998).

Paul J. Flory, Statistical mechanics of chain molecules (Interscience Publishers, New York, 1969).

M.N. Rosenbluth and A.W. Rosenbluth, J. Chem. Phys., 23, 356 (1955).

J.I. Siepmann and Frenkel, Mol. Phys., 75, 59 (1992).

J.J. de Pablo, M. Laso, and U.W. Suter, J. Chem. Phys., 96, 2395 (1992).

F.A. Escobedo and J.J. de Pablo, J. Chem. Phys., 102, 2636 (1995).

L. R. Dodd, T. D. Boone, and D. N. Theodorou, Molecular Physics, 78, 961 (1993).

P. V. K. Pant, D. N. Theodorou, Macromolecules 28, 7224 (1995).

Vlasis G. Mavrantzas, Travis D. Boone, Evangelia Zervopoulou, and Doros N. Theodorou, Macromolecules 32, 5072 (1999).

W. Kauzmann, Adv. Protein Chem. 14, 1 (1959).

K. Dill, Biochemistry 29, 7133 (1990).

K. P. Murphy, P. L. Privalov and S. J. Gill, Science 247, 559 (1990).

P. L. Privalov and Stanley J. Gill, Pure & Appl. Chem. 61, 1097 (1989).

H. S. Frank and M. W. Evans, J. Chem. Phys. 13, 507 (1945).

R. A. Pierotti, J. Phys. CHem. 69, 281 (1965),

G. Graziano, J. Chem. Soc. Faraday Trans, 94, 3345 (1998).

B. Lee, Biopolymers, 24, 813 (1985).

Giuseppe Graziano, Chemical Physics Letters, 396, 226 (2004).

F. H. Stillinger, J. Sol. Chem. 2, 141 (1973).

A. Ben-Naim, H. L. Friedman, J. Phys. Chem. 71, 448 (1967).

Isabel Tomas-Oliveira and Shoshana J. Wodak, J. Chem. Phys. 111, 8576 (1999).

A. Pohorille, L. R. Pratt, J. Am. Chem. Soc. 112, 5066 (1990).

K. Tang, V. Bloomfield, Biophys. J. 79, 2222 (2000).

Lawrence R. Pratt, Annu. Rev. Phys. CHem. 52 (2002).

L. R. Pratt and D. Chandler, J. Chem. Phys. 67, 3683 (1977).

L. R. Pratt, Annu. Rev. Phys. Chem. 36, 433 (1985).

G. Hummer, S. Garde, A. E. Garcia, M. E. Paulaitis, and L. R. Pratt, J. Phys. Chem. B. 102, 10469 (1998).

G. Hummer, S. Garde, A.E. Garcia, and M. E. Paulaitis, Proc. Natl Acad. Sci. U.S.A. 95, 1552 (1998).

B. Widom, J. Chem. Phys. 39, 2808 (1963).

B. Widom, J. Phys. Chem. 86, 869 (1982).

H. J. C. Berendsen, J.R. Grigera, and T. P. Straatsma, J. Phys. Chem., 91, 6269 (1987).

B. Guillot and Y. Guissani, J. Chem. Phys. 99, 8075 (1993).

Y. V. Vorobjrv and J. Hermans, J. Phys. Chem. B 103, 10234 (1999).

G. C. Boulougouris, I. G. Economou, and D. N. Theodorou, J. Phys. Chem. B, 102, 1029 (1998).

A. P. Lyubartsev, A. A. Martsinovski, S. V. Shevkunov, and P. M. Vorontsov-Velyaminov, J. Chem. Phys. 96, 1776 (1992).

A. P. Lyubartsev, O. K. Forrisdahl, and A. Laaksonen, J. Chem. Phys. 108, 227 (1998).

P. A. Egelstaff, An Introduction to the Liquid State, Academic Press, London (1967).

Harry R. Allcock and Frederick W. Lampe, Contemporary Polymer Chemistry, Second Edition, Pretentice Hall, Englewood Cliffs, New Jersey (1990).

A. Striolo and J. M. Prausnitz, Polymer 42, 4773 (2001).

A. Ben Naim, Water and Aqueous Solutions, Plenum, New York, 1974.

B. Guillot, Y. Guissani, and S. Bratos, J. Chem. Phys. 95, 5 (1991).

R. Sander, in "Henry's Law Constants" in NIST Chemistry WebBook, NIST Standard Reference Database Number 69, edited by W. G. Mallard and P. J. Linstrom (National Institute of Standards and Technology, Gaithersburg, MD, 20899, 2000), (url: http://webbook.nist.gov).

J. M. Prasunitz, R. N. Lichtenthaler and E. G. de Azevedo, Molecular Thermodynamics of Fluid Phase Equilibria, Prentice Hall, Upper Saddle River, NJ, 3rd Edition (1999).

R. Sander, in "Henry's Law Constants" in NIST Chemistry WebBook, NIST Standard Reference Database Number 69, edited by W. G. Mallard and P. J. Linstrom (National Institute of Standards and Technology, Gaithersburg, MD, 20899, 2000), (url: http://webbook.nist.gov).

H. J. C. Berendsen, J. R. Grigera, and T. P. Straatsma, J. Phys. Chem. 91, 6269 (1987).

Theodora Spyriouni, Ioannis G. Economou and Doros N. Theodorou, Macromolecules, 30, 4744 (1997)

B. Smit, S. Karaborni, and J.I. Sieppmann, J. Chem. Phys. 102, 2126 (1995)

J.J. de Pablo, M. Laso and U.W. Suter, J. Phys. Chem., 96, 6157 (1992)

J.I. Siepmann and D. Frenkel, Mol. Phys. 75, 59 (1992)

J.J. de Pablo, M. Laso and U.W. Suter, J. Chem. Phys., 96, 2395 (1992)

Fernando A. Escobedo and Juan J. de Pablo, J. Chem. Phys. 103, 2703 (1995)

D. Frenkel and B. Smit, Molecular Physics 75, 983 (1992).

Webpage http://www.polymerlabs.com/gpc/gpcfaqs.htm#middle3

Yasushi Maeda, Langmuir 17, 1737 (2001).

S. Bekiranov, R. Bruinsma and P. Pincus, Europhys. Lett., 24, 183 (1993).

Martin Chaplin, Hydrogen Bonding in Water, http://www.martin.chaplin.btinternet.co.uk/hbond.html

Hiroyuki Tadokoro, Structure of Crystalline Polymers, New York, (1979).

Vita

Ying Lu, daughter of Laiying Luo and Mingqing Lu, was born on Dec. 24th, 1972 in Nanchang, Jiangxi Province, P. R. China. She attended Northwestern Polytechnical University in Xi'an, China and got her Bachelor of Science degree in Polymer Materials Science & Engineering in 1993. After that she went to Beijing University of Chemical Technology and got her Master of Science degree in Polymer Science & Engineering in 1996. Ms. Lu was admitted to graduate school at the University of Texas at Austin in 1997.

Permanent address: 11584 Cedarcliffe Dr., Austin, TX78750

This dissertation was typed by the author.